

UNIVERSITY OF NAPLES FEDERICO II



Department of Chemical, Materials and Industrial Production Engineering

Ph.D COURSE IN MATERIALS ENGINEERING AND STRUCTURES

XXV CYCLE

“ENGINEERING PATTERNED SURFACES TO CONTROL CELL BEHAVIOUR”

Tutor:

Prof. Paolo Antonio Netti

Prof. Maurizio Ventre

Coordinator:

Prof. Giuseppe Mensitieri

Candidate:

Carlo Fortunato Natale

March 2010 - March 2013

TABLE OF CONTENTS

Chapter 1	5
Introduction.....	5
1.1 Tissue engineering.....	5
1.2 Cell Instructive Materials	7
1.3 The Focal Adhesion.....	8
1.4 Cell Cytoskeleton	10
1.5 Mechanosensing	12
1.6 Substrate Topography.....	13
1.7 Aims and outcomes	14
1.8 References	16
Chapter 2	21
Molding Micropatterns of Elasticity on Peg-Based Hydrogels to Control Cell Adhesion and Migration.....	21
2.1 Experimental	23
Hydrogel Preparation and Characterization.....	23
Micrometer Hydrogel Stamp Fabrication.....	24
2D Microelasticity Pattern Fabrication by the FIMIC Process	25
Atomic Force Microscopy (AFM).....	26
Fibroblast Cell Culture	26
Immunological Staining.....	27
Optical and Fluorescent Microscopy	27
Field Emission Scanning Electron Microscopy (FESEM)	27
Cell Migration Experiments	27
2.3 Results and Discussion.....	28
2.4 Conclusions	35
2.5 References	37
Chapter 3	39
Influence of nanotopography on focal adhesions, cytoskeleton assembly and nuclear shape.....	39
3.1 Experimental	41
Preparation of nanopatterned substrates	41

Cell Culture.....	42
Immunofluorescence.....	42
Drug treatment.....	42
Live-cell confocal microscopy	43
Image analysis	43
3.2 Results	44
Topography alters cell shape and FA clustering	44
Nanopattern affects actin dynamics and cell polarization	48
Basal stress fibres do not affect nuclear polarization.	51
3.3 Discussion and conclusions.....	53
3.4 References	57
Chapter 4	59
Microtopographies to control cell migration by interfering with surface probing and focal adhesion assembly.....	59
4.1 Experimental	61
Preparation of micropatterned substrates.....	61
Cell Culture.....	62
Spreading Area and Immunofluorescence analysis	62
Time Lapse experiments	63
4.2 Results	64
Early events in cell adhesion	64
Long times cell migration analysis	66
Adhesion and Cytoskeleton assemblies.....	68
4.3 Discussion	71
4.4 Conclusions	75
4.5 References	77
Chapter 5	80
Build up order tissue	80
5.1 Experimental	81
Preparation of nanopatterned substrates	81
Cell Culture.....	81
ECM characterization and Confocal microscopy	82

Time Lapse experiments	82
5.2 Results	83
Nanogrooved substrate effects on cell migration	83
Nanograted PDMS substrate influences collagen deposition	84
Multilayered cell sheet as a guidance for cell migration	85
5.3 Discussion	87
5.4 Conclusion.....	89
5.5 References	90
Chapter 6	92
Conclusions.....	92
6.1 References	94

Chapter 1

Introduction

Tissues injury can often result in a reduction or loss of tissue functions. This is mainly due to the formation of scar tissue at the site of injury with a modification of local mechanical and structural properties. A great number of pathological conditions require replacement therapies involving the use of medical implants [1-2]. During the past several years a large variety of materials have been used for the fabrication of these medical implants leading to the development of a new discipline named Tissue Engineering.

Tissue Engineering is defined as the interdisciplinary field applying the principles and methods of engineering and life sciences to fundamentally understand and develop biological substitutes to restore, maintain or improve tissue functions [3]. This field combines the unique properties of cells and biomaterials to repair or regenerate damaged and injured tissues, obtaining the potential to provide a revolutionary method for helping to treat such injuries and the many currently incurable degenerative diseases [3-4-5]. More specifically, any tissue engineered end product attempts to mimic the function of natural tissue. Implant material induce a tissue response and a control of this physiological response plays a critical role for the long term function of a medical device when implanted in the body. So the natural circumstances of the specific tissue have to be fundamentally understood, in order to optimize the development of function biological substitute.

1.1 Tissue engineering

Tissue Engineering approaches are based on the paradigm that using three basic ‘tools’, cell, scaffold and soluble factors, it is possible to induce the re-generation of a new tissue. The purpose of tissue engineering research is very clear: establishing a new clinical technology that makes possible medical treatments for diseases that have been too difficult to be cured by existing methods.

Biological tissues basically consist of cells, signaling systems and extracellular matrix (ECM) [4]. The cells are the core of the tissue, however, in the absence of signaling systems and/or of the ECM can't explicate their functions. ECM represents the substances produced by cells and excreted to the extracellular space that supports attachment and proliferation processes. In particular, cells have to

synthesize new tissue but without a three dimensional guide, isolated cells are not able to reproduce a tissue with its whole complex architecture and therefore functions. Cell proliferation is not sufficient for the generation of large-sized tissues and organs which require a proper support to generate 3D complex structures. The support is called scaffold. The major function of scaffold is to assist proliferation, differentiation and biosynthesis. Third key factor of tissue engineering are soluble molecules like proteins and growth factors that promote and support cells in the regeneration of neotissues. A wide range of proteins play a key role in cells proliferation and differentiation. These proteins are endogenously secreted in the body by cells themselves (autocrine) or as a result of communication with surrounding cells (paracrine). The practical use of growth factors in tissue engineering or clinical settings is very delicate. Indeed many studies demonstrated the limits of the direct application of growth factor in site of regeneration owing to rapid denaturation of the growth factors or by rapid enzymatic digestion. The earliest clinical application of human cell in tissue engineering started around 1980 concerning skin tissue. Just some year later, a membrane was used to attempt the regeneration of periodontal and alveolar bone. This membrane prevented fibroblast invasion and guided bone regeneration. In 1988 Vacanti et al. studied cell transplantation using bioadsorbable synthetic polymer as scaffold.

Successful clinical trials of tissue engineering constructs have been reported in literature. Nowadays, skin, cardiovascular, bone and cartilage are the major areas of tissue-engineered replacements in clinical trials and applications [7-8-9-10]. Matsumura et al. [11] reported the application of tissue-engineered systems in cardiovascular surgery on children with various complex heart diseases. In this work they described a treatment with autogenic cells were isolated, cultured and subsequently seeded on a biodegradable polymer scaffold of poly(glycolic acid) combined with poly(lactic acid- ϵ -caprolactone). The first operation was performed in May 1999, and over 40 patients were treated the following years. Post-operative analysis revealed no complications related to the tissue engineering autograft.

Macchiarini et al. designed and implanted a tissue-engineered airway [12]. In this case, all donor cells and antigens of an allogenic donor trachea were removed to prevent an immune reaction of the host towards the donor material. Subsequently, they cultivated the matrix with autogenic cells and transplanted the cell-seeded scaffold into the patients. Immediately, the tissue engineered trachea became functional and after 4 months, the scaffold still showed normal appearance and good mechanical properties.

However biomedical devices applications were not always successful both for inflammatory response activation and defective interaction between cell and devices itself.

Improvement of cell material interaction assumes a relevant role in integration of exogenous material in an attempt to minimize non functional tissue encapsulation [13-14].

1.2 Cell Instructive Materials

A decrease in cellular adhesion may be the origin of reduced biomedical devices biocompatibility. A mild adhesion induces both a destabilization of the implant and an inhibition of tissue regeneration [15]. The mechanism of cell-material interactions is crucial for the successful outcome of tissue engineered implants. Therefore, they need to be thoroughly understood in order to achieve all the desired and regulated cellular responses.

A combination of biochemical and biophysical signals, including interfacial presentation of molecular, topographic and mechanical cues occurs when cell interact with material surfaces. Adhesion, migration, proliferation and differentiation are the cell activities mostly influenced by material properties.

Specifically engineered surfaces displaying selected biofunctional groups or micrometer-scale patterns have been used in order to study signal interactions and control cell responses in a systematic way.

Advancements in chemistry, material science and nanotechnologies greatly improved the possibility to imprint many different signals, according to predefined spatial patterns. In particular, patterns of biochemical signals, topographies on different length scales and mechanical cues clearly revealed cells' ability to 'sense' and 'react' to external stimuli.

The potential to pattern material properties with nanometric accuracy has lead to the development of the next generation of biomaterials with extended functionalities and bioactivity [16]. Cell Instructive Materials (CIMs) are designed to control and to direct cell fate making use of complex commands or instructions of nanofeatures exhibited on the top of material surface. Realization of these attractive materials will lead to a deep understanding of the mechanisms that regulate cell-material interactions unravelling the unknown events that occurs on the boundary between cell membrane and material surface.

Adherent cells are complex, self-sustaining units [17] that require ECM anchorage in order to proliferate [18]. Chemical and topographical substrate modifications constitute a tool to facilitate cellular adhesion [19] and tissue deposition. After implantation a cascade of biological events occurs following adhesive protein adsorption to a material surface.

First of all, cells probe extracellular environment, forming protrusion termed “lamellipodia” with which cells move and sense their surroundings. Lamellipodia are associated with thin actin-rich plasma- membrane protrusion, filopodia, that function as antennae for cell to probe extracellular environment [20]. Once cell locates a site suitable for adhesion a signaling feedback pathway initiates integrin receptor clustering at the plasma membrane and adhesion plaque protein recruitment [21]. Initial cell-substrate contact and filopodia exploration is followed by lamellipodia-mediated ruffling [22], membrane activity and cellular flattening and spreading [23] all mediated by the development of cell-substrate contacts termed “Focal Adhesions” (FAs).

1.3 The Focal Adhesion

Cell interacts with substrate and communicates intracellularly via transmembrane proteins termed integrins. These adhesion receptors are recognized as the central regulators of cell–biomaterial interactions, which mediate adhesion to the extra cellular matrix [24].

Integrin receptors are composed of 2 subunit alfa-beta, non-covalently linked. 18 α and 8 β subunit have been found, which combine to form 24 distinct dimers that can interact specifically to peptide motifs (most notably the RGD tripeptide) in ECM adhesive proteins such as fibronectin, vitronectin and laminin [25]. Integrin-RGD link transmits information in a bi-directional manner from the extracellular environment to the machinery of intracellular transcription.

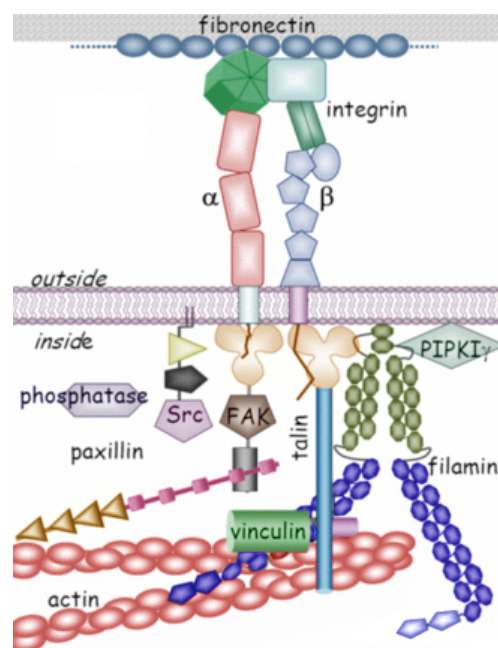


Figure 1.1: The proteins of the focal adhesion plaque (Campbell, 2008)

After recognition of RGD domain integrin rapidly associate and clusterize at binding site connecting actin microfilaments the via adaptor proteins as talin, vinculin, paxillin, a-actinin and focal adhesion kinase (FAK) (fig 1.1).

Nascent adhesion may mature into larger molecular structure. This requires clustering of additional integrins dimmers which increases nascent adhesion dimension by recruitment of more cytoplasmatic adhesion protein. In particular the binding of vinculin to talin triggers the clustering of activated integrin and through vinculin tail this complex associates with actin filament.

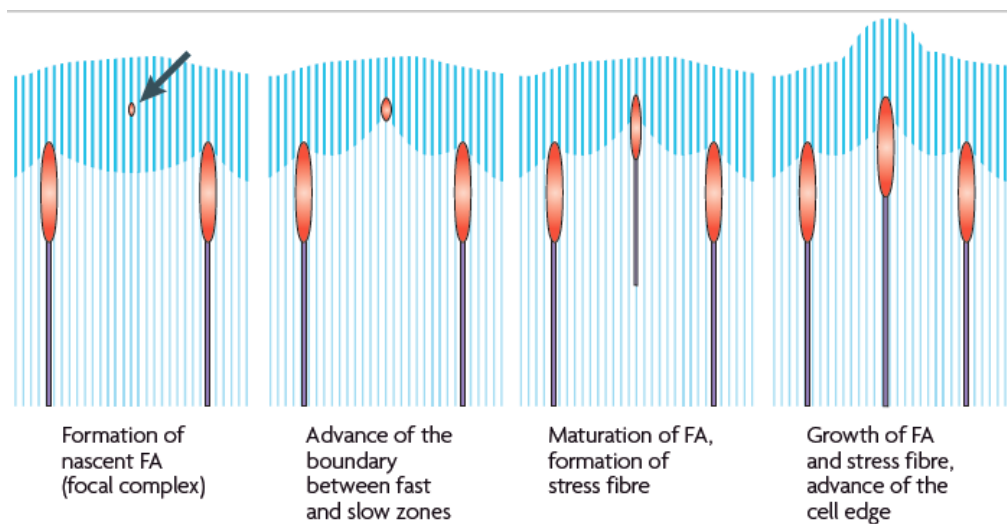


Figure 1.2: Model of Focal Adhesion formation (Geiger B., 2009)

Figure 1.2 summarizes FA formation and maturation process. Focal complex originates as spot of $0,5 \mu\text{m}^2$ regulated by the GTPase Rac pathway [26]. Formation of focal complex occurs underneath lamellipodium [27]. Focal complex gradually matures into focal adhesion during lamellipodium retrograde flow, a local retraction of actin branched network. In turn formation of newly focal complexes is followed by the advance of lamellipodium during cell ruffling. Experimental data suggest that those FA that originates from micron sized focal complex undergo maturation. FAs emerge as diverse protein networks that provide actin cytoskeleton structural integrity and the dynamic association with the ECM to facilitating cell migration and spreading through continuous regulation and the dynamic interaction with actin.

1.4 Cell Cytoskeleton

The interactions between integrin-mediated adhesions and the actin cytoskeleton are bidirectional: cytoskeletal forces regulate the assembly and maturation of adhesions (see above), and at the same time, the growing adhesions can regulate the assembly of the actin system [27].

Actin assembles into a wide variety of structures (fig. 1.3) which are able to support cellular integrity. It can be subdivided into five categories:

- (1) lamellipodial networks at the leading edge of the cell,
- (2) filopodial bundles,
- (3) the cortical actin shell beneath the plasma membrane,
- (4) the contractile actin ring located at the division plane during cytokinesis
- (5) contractile filamentous actin.

Last category was commonly denoted as “stress fibres”, structures associated at their termini with FAs and maintain an isometric tension, which is applied to the ECM through cellular adhesions [28]. Stress fibers are the major contractile structures in many cultured animal cells like fibroblasts, smooth muscle, endothelial and some cancer cell lines.

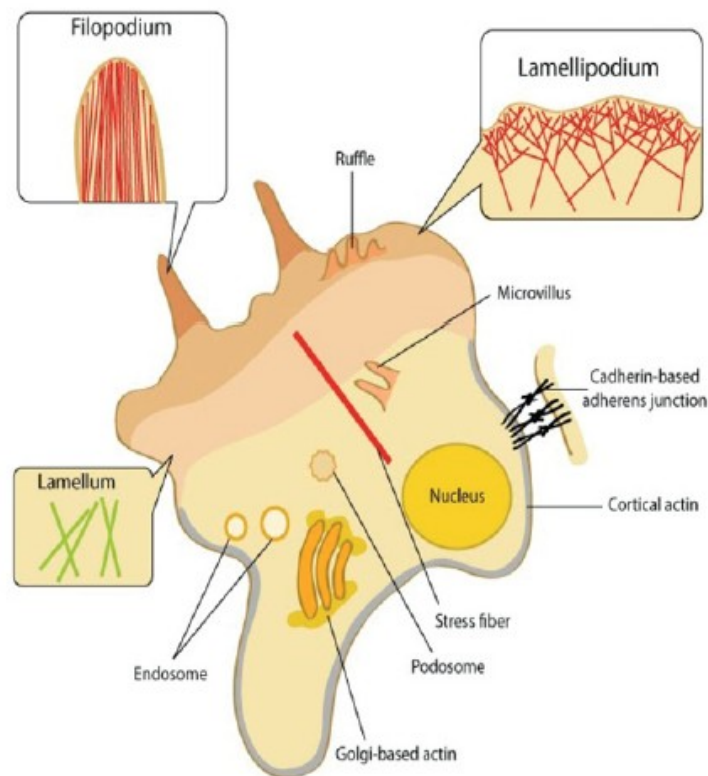


Figure 1.3: Schematic representation of the different actin cytoskeleton assemblies within cells

Actin filaments are polar helical structures, with a rapidly growing barbed end and a slowly growing pointed end [29]. Stress fibers are composed of bundles of 10–30 actin filaments, which are crosslinked together by α -actinin, typically in a bi-polar arrangement. As described before, these contractile structures are often anchored to focal adhesions.

Stress fibers can be divided into at least four different categories: dorsal and ventral stress fibers, transverse arcs and the perinuclear actin cap [30-31-32] (fig 1.4).

Dorsal stress fibers are anchored to focal adhesions at their distal ends. Unlike the other types of stress fibers, dorsal fibers are not contractile structure in fact as described in several work [32-34] dorsal SFs were defined as a platform for the assembly of other stress fibers.

Transverse arcs are contractile curved actin filament bundles, not associated with focal adhesions. They display a periodic α -actinin–myosin pattern which is typical for contractile actomyosin bundles. Retrograde flow represent a distinctive feature of these structures. This process consists in the continuous contraction of arcs from the leading edge towards the cell center [31-34].

Ventral stress fibers are mainly located at posterior part of the cell. They are contractile actomyosin bundle characterized by two focal adhesions at both end of stress fiber [30].

Recent studies elucidated the role of perinuclear actin cap in regulating nucleus shape in interphase cell, acting as mechanotransducers to transform force from cell environment to the nucleus [32]. This cap is composed of contractile actin filament bundle which form a highly organized, dynamic and oriented structure [32].

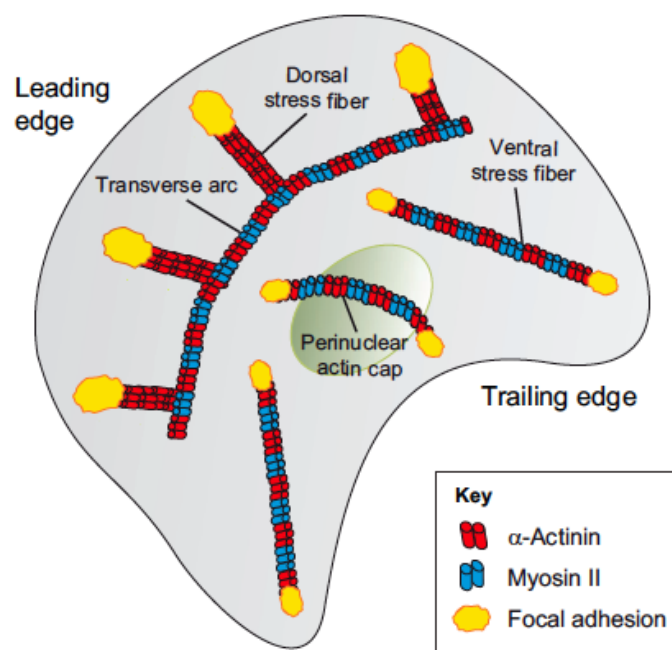


Figure 1.4 Schematic representation of stress fiber network of motile mesenchymal cells

1.5 Mechanosensing

In their surrounding environment, cells are exposed to various external forces such as stretching (muscle cells), compression (bones) or shear flows (blood cells). In the past years it has become clear that these extracellular stimuli affect cell behavior by triggering specific intracellular molecular pathways. Unfortunately, most of these intracellular events are still poorly understood. Many experimental observations revealed the existence of a regulatory mechanisms for the interplay between intracellular- generated forces and the mechanical properties of the extracellular environment. Cells' ability to react to substrate mechanical properties is referred as mechanosensing. The first experimental evidence of mechanosensing dates back more than 30 years when Harris et al. [35] reported and measured myoblasts contractile forces on flexible rubber membranes. Following this first report, other authors focused on developing systems to analyze the dynamics of cell-generated forces. Many cellular structure as integrin/FA sites, G-protein, ion channels, cytoskeleton constituents and membrane biomolecules have all been identified as potential mechanosensors [36]. These specialized biomolecules change their chemical activity state when they are mechanically distorted, converting mechanical energy into biochemical energy [37]. Single molecule force spectroscopy studies showed that individual peptide domains within protein found in the cytoskeleton underwent stepwise elongation when they were mechanically extended [38].

Physical forces can modulate the kinetics of protein-protein binding in living cells. For example integrin, as described above, are transmembrane receptors structurally connected to cytoskeleton thanks to which, cells pull on their surrounding and probe the stiffness of extracellular environment. As a consequence of the applied force, integrin signaling induces a reorganization of cytoskeleton architecture.

Moreover FAs dynamics via actomyosin contraction transmit force to substrate. So the material-cytoskeleton crosstalk involves force exchange between cells and substrate [37]. Therefore, understanding the mechanism of cell's interaction with natural or artificial surfaces should be a fundamental requirement when designing biomaterial to stimulate specific intracellular pathways. The mechanical properties of the material represent a relevant aspect of the dynamic reciprocity between adhesion plaques growth and substrate deformation. It has been reported that cells have a higher proliferation rates on stiffer material than softer. Moreover cells migrate faster on soft substrates while they are more stationary on stiff substrate. According to this view, patterning of mechanical properties may be used to control cell behaviour.

1.6 Substrate Topography

A consistent number of studies reported that cell behavior is strongly influenced by material topographic texture. In vivo contexts, extracellular environment represents a set of topographic signals, perceived by cell at different length scale. Fibrils and fiber bundles (collagen and fibrin), rough surfaces (crystal deposit in bone) and porous membranes (basement membranes) represent examples of natural topographies. So topographical signals are not to be considered in vitro artifacts but they play a relevant role in cell-material interaction through direct alteration in several cellular processes.

Recent advancements in micro and nanofabrication technologies made it possible to imprint on top of substrate surface topographic feature favoring the study of the role of topography in cell-material interaction. Soft lithography [40-41], electron beam lithography [42] and nano-imprint lithography [43] can imprint topographic patterns with huge spatial resolution (of a few nanometers).

To describe material topography-cell interactions, it is appropriate to differentiate between length scales that might elicit different responses, consequently topographic features are generally subdivided into macro-micro- and nanoscale topography

Macrotopography refers to topographies features exhibiting characteristic dimensions that surpass those of cells (tens of micrometers) providing a geometric confinement of them. Usually microtopography is related to the use of surface roughness whose feature varying from few micron to 100 micron. Fabrication process as welding or laser cutting modify devices surface in order to regulate cell attachment.

Concerning nanotopography Lamers et al. [44-45] demonstrated that 70 nm represents a limit scale dimension under which topographic signal begin to be ineffective. So within the dimensional range of 70 nm and 2-5 μm topographic features approximate those of cell's sensorial organelles such as FAs and filopodia, affecting cellular processes regulated by these structures.

Many authors reported that topographic substrate modification induced a nonuniform deposition of serum proteins on anisotropic patterned surface. Usually, fibronectin, vitronectin or collagen are adsorbed on the top surface of material. Braber et al. [46] and Recum et al. [47] thought that different surface energies on anisotropic patterned surface regions induce selective adsorption of ECM proteins on the top of substrate topography. When contacting such surfaces, cells may recognize the anisotropic protein distribution on the top surfaces of the patterns. More and more researches have proved that the topography of the surface can influence significantly not only the distribution and adsorption but also the conformation and the activity of proteins [48, 49]. However, the processes that mediate cellular reaction to nanoscale surface structures are not well understood. The most extensively studied topographies are grooves and grids, protrusions and pit arrays.

The use of micro/nanometric groove patterns is a method to mimic *in vitro* the topographical cues exposed to cell in extracellular environment in *in vivo* contexts. Cells seeded on grooved substrates usually acquire an elongated morphology and alignment to groove direction, reproducing *in vivo* tissue organization, facilitating active self assembly of ECM molecules enhancing cell attachment and polarization rate. A wide range of cell types such as fibroblasts [50], osteoblast [51], nerve cells [52] and MSCs [53] respond dramatically to grooved substrates.

Topography surface features are defined by three characteristic dimensions, namely ridge (or groove) width, inter-feature length (or pitch) and depth.

Furthermore, topographic patterns create surfaces that are readily accessible for cell lamellipodia and filopodia, such as the top of ridges or pillars, as well as impervious recesses, such as the bottom of grooves and pits. The accessibility of a given region to the cell membrane and its protrusions depends on the geometric characteristic of the pattern, i.e. the feature depth and pitch. Braber *et al.* [46], Meyle *et al.*[54] and Matsuzaka *et al.*[55] reported that on microgroove patterns, focal adhesions formation occur predominantly on the top of the ridge due to the restriction imposed by steric hindrance. Furthermore orientation of FA plaques is affected by the presence of micro-nanogrooved substrate [56]. The use of nanogroove substrates induces FAs maturation along the ridges [57] or at the groove/ridge boundaries [58] In this context many works investigate the effect of ridge/groove dimensions that are able to induce a cell alignment by FAs polarization. Teixeira *et al.* [59] observed that rearranging the FA distribution, epithelial cells switch from parallel to perpendicular alignment on grooved substrate when features decreased in pitch size from 4000 to 400 nm.

The molecular mechanism governing cell alignment is not fully characterized. In particular the crosstalk between topographic signals and cytoskeleton is not systematically described.

1.7 Aims and outcomes

The aim of this Thesis is to gain a deeper insight into the material-cytoskeleton crosstalk in order to design novel biomaterials which effectively control cell behavior in terms of cell polarization, migration and matrix deposition.

As discussed above several studies described the effects of mechanical and topographical feature on specific cellular processes. In particular cell adhesion and migration are affected by substrate surface feature. In these studies the effect of nanotopographic feature have been well characterized but the intrinsic mechanism that induce cell to response to substrate features were still unknown.

This Thesis highlights the importance to improve the knowledge on cell material crosstalk with the aim of developing third generation devices (CIMs). In particular:

- We present an innovative and simple soft UV lithographic method “Fill-Molding In Capillaries”(FIMIC) that combines soft lithography with capillary force driven filling of micro-channels to create smooth hydrogel substrates with a 2D micro-pattern on the surface. Within this study, smooth hydrogel surfaces displaying locally varied elasticity regions have been successfully achieved and applied in cell culture for cell guidance and durotaxis studies.
- We study the effect of nanograted substrates on FA dynamics-cytoskeleton assembly-nuclear shape by time lapse live imaging in order to better understand the intrinsic mechanisms that regulate cell and nuclear polarization.
- We investigated the synergistic effect of topographic signals and chemical characteristics on cell adhesion and migration. To this aim, we used micrograted polydimethylsiloxane (PDMS) substrates having feature dimension that might in principle interfere with the cell probing machinery, whereas surface chemical modifications were performed to modulate hydrophobic / hydrophilic properties by means of oxygen plasma treatment in order to affect focal adhesion formation and maturation.
- We observed an intimate correlation between cell alignment and extracellular matrix production. In particular we studied the effect of cell migration on collagenous matrix production. To this aim we used nanograted substrate in ordered to produce a cell multilayer whose collagen fibers have a predefined spatial distribution.

1.8 References

- [1] Esposito M, Worthington HV, Coulthard P. Interventions for replacing missing teeth: dental implants in zygomatic bone for the rehabilitation of the severely deficient edentulous maxilla. *Cochrane Database Syst Rev*.2005;CD004151.
- [2] Brooks KR, Capo JT, Warburton M, Tan V. Internal fixation of distal radius fractures with novel intramedullary implants. *Clin Orthop Relat Res*. 2006;445:42–50.
- [3] Langer R, Vacanti JP. Tissue Engineering. *Science* 1993;260:920-926
- [4] Bonassar LJ, Vacanti CA. Tissue engineering: the first decade and beyond. *J Cell Biochem Suppl*. 1998;30-31:297-303
- [5] Saxena AK, Marler J, Benvenuto M, Willital GH, Vacanti JP. Skeletal muscle tissue engineering using isolated myoblasts on synthetic biodegradable polymers: preliminary studies. *Tissue Eng*. 1999 Dec;5(6):525-32.
- [6] Lanza RP, Langer RS, Vacanti J. Principles of tissue engineering. 2nd ed. San Diego, CA ::Academic Press, 2000.
- [7] Saltzman WM. Tissue Engineering: principles for the design of replacement organs and tissues. 1st ed. Oxford: Oxford University Press, 2004.
- [8] Blitterswijk CA, Thomsen P. Tissue engineering. 1st ed. Amsterdam; Boston: Elsevier/Academic Press, 2008
- [9] Fong P, Shin'oka T, Lopez-Soler RI, Breuer C. The use of polymer based scaffolds in tissue engineered heart valves. *Progress in Pediatric Cardiology* 2006;21(2):193-199
- [10] Nesic D, Whiteside R, Brittberg M, Wendt D, Martin I, Mainil-Varlet P. Cartilage tissue engineering for degenerative joint disease. *Advanced Drug Delivery Reviews* 2006;58(2):300-322
- [11] Matsumura G, Hibino N, Ikada Y, Kurosawa H, Shin'oka T. Successful application of tissue engineered vascular autografts: clinical experience. *Biomaterials* 2003;24(13):2303-2308
- [12] Macchiarini P, Jungebluth P, Go T, Asnaghi MA, Rees LE, Cogan TA, et al. Clinical transplantation of a tissue-engineered airway. *The Lancet* 2008;372(9655):2023-2030
- [13] Suska, F., Emanuelsson, L., Johansson, A., Tengvall, P. & Thomsen, P. (2007). Fibrous capsule formation around titanium and copper. *J Biomed Mater Res A* 85, 888-96
- [14] Andersson, M., Suska, F., Johansson, A., Berglin, M., Emanuelsson, L., Elwing, H. & Thomsen, P. (2007). Effect of molecular mobility of polymeric implants on soft tissue reactions: An in vivo study in rats. *J Biomed Mater Res A* 84A, 652-660
- [15] Baxter, L. C., Frauchiger, V., Textor, M., ap Gwynn, I. & Richards, R. G. (2002). Fibroblast and osteoblast adhesion and morphology on calcium phosphate surfaces. *Eur Cell Mater* 4, 1-17

- [16] Ventre M, Causa F, Netti PA. Determinants of cell-material crosstalk at the interface: towards engineering of cell instructive materials *J R Soc Interface*. 2012 Sep 7;9(74):2017-32.
- [17] Schwarz, U. S., Erdmann, T. & Bischofs, I. B. (2006). Focal adhesions as mechanosensors: the two-spring model. *Biosystems* 83, 225-32
- [18] Triplett, J. W. & Pavalko, F. M. (2006). Disruption of alpha-actinin-integrin interactions at focal adhesions renders osteoblasts susceptible to apoptosis. *Am J Physiol Cell Physiol* 291, C909-21
- [19] Dettin, M., Conconi, M. T., Gambaretto, R., Bagnò, A., Di Bello, C., Menti, A. M., Grandi, C. & Parnigotto, P. P. (2005). Effect of synthetic peptides on osteoblast adhesion. *Biomaterials* 26, 4507-15
- [20] Pieta K. Mattila and Pekka Lappalainen. (2008). Filopodia: molecular architecture and cellular functions. *Nat Rev Mol Cell Biol*. 2008 Jun;9(6):446-54.
- [21] Lim, J. Y., Dreiss, A. D., Zhou, Z., Hansen, J. C., Siedlecki, C. A., Hengstebeck, R. W., Cheng, J., Winograd, N. & Donahue, H. J. (2007). The regulation of integrin-mediated osteoblast focal adhesion and focal adhesion kinase expression by nanoscale topography. *Biomaterials* 28, 1787-97
- [22] Bershadsky, A. D., Ballestrem, C., Carramusa, L., Zilberman, Y., Gilquin, B., Khochbin, S., Alexandrova, A. Y., Verkhovskiy, A. B., Shemesh, T. & Kozlov, M. M. (2006b). Assembly and mechanosensory function of focal adhesions: experiments and models. *Eur J Cell Biol* 85, 165-73
- [23] Cavalcanti-Adam, E. A., Volberg, T., Micoulet, A., Kessler, H., Geiger, B. & Spatz, J. P. (2007). Cell spreading and focal adhesion dynamics are regulated by spacing of integrin ligands. *Biophys J* 92, 2964-74.
- [24] Cohen, D. M., Chen, H., Johnson, R. P., Choudhury, B. & Craig, S. W. (2005). Two distinct head-tail interfaces cooperate to suppress activation of vinculin by talin. *J Biol Chem* 280, 17109-17
- [25] Garcia, A. J. (2005). Get a grip: integrins in cell-biomaterial interactions. *Biomaterials* 26, 7525-9
- [26] Michele A. Wozniak, Katarzyna Modzelewska, Lina Kwong, Patricia J. Keely (2004). Focal adhesion regulation of cell behavior. *Biochimica et Biophysica Acta* 1692, 103– 119
- [27] Geiger B, Spatz JP, Bershadsky AD. Environmental sensing through focal adhesions. *Nat Rev Mol Cell Biol*. 2009 Jan;10(1):21-33
- [28] Zimmerman, B., Volberg, T. & Geiger, B. (2004). Early molecular events in the assembly of the focal adhesion-stress fiber complex during fibroblast spreading. *Cell Motil Cytoskeleton* 58, 143-59
- [29] Pollard, T. D. and Cooper, J. A. (2009). Actin, a central player in cell shape and movement. *Science* 326, 1208-1212
- [30] Cramer, L. P., Siebert, M. and Mitchison, T. J. (1997). Identification of novel graded polarity actin filament bundles in locomoting heart fibroblasts: implications for the generation of motile force. *J. Cell Biol.* 136, 1287-1305

- [31] Small, J. V., Rottner, K., Kaverina, I. and Anderson, K. I. (1998). Assembling an actin cytoskeleton for cell attachment and movement. *Biochim. Biophys. Acta.* 1404, 271-281
- [32] Khatau, S. B., Hale, C. M., Stewart-Hutchinson, P. J., Patel, M. S., Stewart, C. L., Searson, P. C., Hodzic, D. and Wirtz, D. (2009). A perinuclear actin cap regulates nuclear shape. *Proc. Natl. Acad. Sci. USA* 106, 19017-19022
- [33] Tojkander, S., Gateva, G., Schevzov, G., Hotulainen, P., Naumanen, P., Martin, C., Gunning, P. W. and Lappalainen, P. (2011): A molecular pathway for myosin II recruitment to stress fibers. *Curr. Biol.* 21, 539-550
- [34] Hotulainen, P. and Lappalainen, P. (2006). Stress fibers are generated by two distinct actin assembly mechanisms in motile cells. *J. Cell Biol.* 173, 383-394.
- [35] Harris, A. K., Wild, P. & Stopak, D. 1980 Silicone rubber substrata: a new wrinkle in the study of cell locomotion. *Science* 208, 177–179.
- [36] Mack, P. J., Kaazempur-Mofrad, M. R., Karcher, H., Lee, R. T. & Kamm, R. D. (2004). Force-induced focal adhesion translocation: effects of force amplitude and frequency. *Am J Physiol Cell Physiol* 287, C954-62
- [37] Ingber DE Cellular mechanotransduction: putting all the pieces together again. *FASEB J.* 2006 May;20(7):811-27
- [38] Li, H., Linke, W. A., Oberhauser, A. F., Carrion-Vazquez, M., Kerkvliet, J. G., Lu, H., Marszalek, P. E., and Fernandez, J. M. (2002) Reverse engineering of the giant muscle protein titin. *Nature* 418, 998 –1002
- [39] Nicolas A. Physically based principles of cell adhesion mechanosensitivity in tissues. *Rep Prog Phys.* 2012 Nov;75(11):116601.
- [40] den Braber, E. T., de Ruijter, J. E., Ginsel, L. A., von Recum, A. F. & Jansen, J. A. 1998 Orientation of ECM protein deposition, fibroblast cytoskeleton, and attachment complex components on silicone microgrooved surfaces. *J. Biomed. Mater. Res.* 40, 291–300.
- [41] Yim, E. K., Reano, R. M., Pang, S. W., Yee, A. F., Chen, C. S. & Leong, K. W. 2005 Nanopattern-induced changes in morphology and motility of smooth muscle cells. *Biomaterials* 26, 5405–5413.
- [42] Dalby, M. J., Biggs, M. J., Gadegaard, N., Kalna, G., Wilkinson, C. D. & Curtis, A. S. 2007 Nanotopographical stimulation of mechanotransduction and changes in interphase centromere positioning. *J. Cell. Biochem.* 100, 326–338.
- [43] Gaubert, H. E. & Frey, W. 2007 Highly parallel fabrication of nanopatterned surfaces with nanoscale orthogonal biofunctionalization imprint lithography. *Nanotechnology* 18, 135 101–135 107.
- [44] Lamers, E., van Horssen, R., te Riet, J., van Delft, F. C., Luttge, R., Walboomers, X. F. & Jansen, J. A. 2010 The influence of nanoscale topographical cues on initial osteoblast morphology and migration. *Eur. Cell Mater.* 20, 329–343

- [45] Loesberg, W. A., te Riet, J., van Delft, F. C., Schön, P., Figdor, C. G., Speller, S., van Loon, J. J., Walboomers, X. F. & Jansen, J. A. 2007 The threshold at which substrate nanogroove dimensions may influence fibroblast alignment and adhesion. *Biomaterials* 28, 3944–3951.
- [46] den Braber E T, Ginsel L A, von Recum A F, et al. Orientation of ECM protein deposition, fibroblast cytoskeleton, and attachment complex components on silicone microgrooved surfaces. *J Biomed Mater Res*, 1998, 40: 291–300
- [47] Recum A F, van Kooten T G. The influence of micro-topography on cellular response and the implications for silicone implants. *J Biomater Sci Polym Ed* 7, 1995, 7: 181–198
- [48] Song W, Chen H. Protein adsorption on materials surfaces with nano-topography. *Chinese Sci Bull*, 2007, 52: 3169–3173
- [49] Roach P, Farrar D, Perry C C. Surface tailoring for controlled protein adsorption: effect of topography at the nanometer scale and chemistry. *J Am Chem Soc*, 2006, 128: 3939–3945
- [50] Dalby, M. J., Riehle, M. O., Yarwood, S. J., Wilkinson, C. D. & Curtis, A. S. (2003c). Nucleus alignment and cell signaling in fibroblasts: response to a micro-grooved topography. *Exp Cell Res* 284, 274-82
- [51] Lenhert, S., Meier, M. B., Meyer, U., Chi, L. & Wiesmann, H. P. (2005). Osteoblast alignment, elongation and migration on grooved polystyrene surfaces patterned by Langmuir-Blodgett lithography. *Biomaterials* 26, 563-70
- [52] Yim, E. K., Pang, S. W. & Leong, K. W. (2007). Synthetic nanostructures inducing differentiation of human mesenchymal stem cells into neuronal lineage. *Exp Cell Res* 313, 1820-9
- [53] Dalby, M. J., McCloy, D., Robertson, M., Agheli, H., Sutherland, D., Affrossman, S. & Oreffo, R. O. (2006b). Osteoprogenitor response to semi-ordered and random nanotopographies. *Biomaterials* 27, 2980-7.
- [54] Meyle J, Gultig K, Brich M, et al. Contact guidance of fibroblasts on biomaterial surfaces. *J Mater Sci Mater Med*, 1994, 5: 463–466
- [55] Matsuzaka K, Walboomers F, de Ruijter A, et al. Effect of microgrooved poly-l-lactic (PLA) surfaces on proliferation, cytoskeletal organization, and mineralized matrix formation of rat bone marrow cells. *Clin Oral Implant Res*, 2000, 11: 325–333
- [56] Teixeira, A. I., Nealey, P. F. & Murphy, C. J. (2004). Responses of human keratocytes to micro- and nanostructured substrates. *J Biomed Mater Res A* 71, 369-76.
- [57] Teixeira, A. I., Abrams, G. A., Bertics, P. J., Murphy, C. J. & Nealey, P. F. (2003). Epithelial contact guidance on well-defined micro- and nanostructured substrates. *J Cell Sci* 116, 1881-92
- [58] Wojciak-Stothard, B., Curtis, A., Monaghan, W., MacDonald, K. & Wilkinson, C. (1996). Guidance and activation of murine macrophages by nanometric scale topography. *Exp Cell Res* 223, 426-35.

[59] Teixeira, A. I., McKie, G. A., Foley, J. D., Bertics, P. J., Nealey, P. F. & Murphy, C. J. (2006). The effect of environmental factors on the response of human corneal epithelial cells to nanoscale substrate topography. *Biomaterials* 27, 3945-54.

Molding Micropatterns of Elasticity on Peg-Based Hydrogels to Control Cell Adhesion and Migration

This work arose from the collaboration with Prof. M. C. Lensen of the Technische Universität Berlin · Institut für Biotechnologie and it was published on Advanced Engineering Material in October 2011.

It is well known that surface characteristics such as biofunctionality, topography, and elasticity have a profound effect on cell adhesion, spreading, migration, and intracellular processes, which can also direct cell differentiation. [1–5]

Therefore, understanding of the mechanisms of cells' interaction with natural or artificial surfaces is a fundamental requirement when designing biomaterials for different biomedical applications, e.g. tissue engineering, drug delivery, or diagnostics. Several systems and techniques have been introduced which can be applied for a systematic in vitro study of the correlation between substrate characteristics and cell reactions. Yet, although it is the combination of several substrate properties that directs the cellular outcome, most of the in vitro studies so far have varied only one parameter at a time, e.g. employing either chemical or physical surface patterns.[1,6–8]

Lithographic techniques such as photolithography, which were developed at first for minimizing electronic devices, have emerged as powerful tool toward the engineering of biosurfaces.[9] However, and to defeat shortcomings of conventional techniques on soft materials, development has pushed fabrication techniques such as soft lithography which have rendered successful micro- and nano- structures of a wide variety of soft materials, including the one described here.[10–15] Chemical patterning to create cell responsive patterns can be achieved by controlled incorporation of cell-specific responsive ligands.[5,16–18] Lately, many successful strategies have been developed to create gradient elasticity on substrates destined to cell-based assays; photolithographic patterning, [19–22] soft lithography,[23,24] and capillary in microchannels [25] have been effectively utilized to gradient the elasticity of e.g., PDMS (polydimethylsiloxane) and PAAm (polyacrylamide) using mainly silicon and glass as base substrate.

Although there is significant evidence of the influence of mechanical and tensile properties of the substrate on the host response, e.g. cell adhesion and motility are highly dependent on the substrate's rigidity,[7,26,27] the use of chemical modification of the surfaces with specific ligands for cell recognition is normally reported to be required.[20,23,24,28]

So far, elasticity variations have been fabricated mostly in a gradual fashion, for example by employing a photomask over a UV-curable polymer. Lo and coworkers, nevertheless, have described binary patterns of stiffness and consequent “durotaxis” experiments have demonstrated the migration of cells in the direction of stiffer regions of the substrate.[29]

Such surfaces with a rigidity boundary are exceptionally interesting to elucidate cells’ mechanosensing of relatively sharp contrasts in stiffness.[30] With our surface patterning method we are able to take this concept of contrast sensing a step further and investigate cell migration on substrates with multiple boundaries of stiffness variations. As a material of choice we have employed hydrogels, which can be tailored in their mechanical properties by virtue of variations in their crosslinking density.

Over the past years, much attention has been paid to hydrogel materials as potential synthetic biomaterials due to their biocompatibility promoted by the high water content and physicochemical similarities to native extra cellular matrix.[31–33] Hydrogels have found many applications, for instance, in tissue engineering scaffolds, implantable devices, and drug delivery.[31] The ability to swell makes this kind of material eligible for use in drug delivery and immobilization of proteins, peptides, and other biological compounds.[34–39]

In the same way, the possibility of changing the inner architecture by varying crosslinking density of the network can dramatically impact polymer diffusivity and permeability, degradation rate, equilibrium water content (EWC), elasticity, and modulus.[31,40–43] encompassing the elastic moduli found in human tissue, i.e. ranging from a few kPa to a few GPa.[44,45]

As biomaterials, hydrogels provide bulk and mechanical support for cellular attachment since they can be designed as required of the construct in terms of mechanical and chemical properties.[42,46]

A wide variety of natural and synthetic chemical building blocks have been used to synthesize many different hydrogel materials with engineered surface chemistry, controlled porosity, and crosslinking density.[31] Especially poly(ethylene glycol), PEG, based hydrogels are very popular for biomedical applications. They are highly hydrated, oxygen permeable and protein absorption resistant, and also often used as coating material to render surfaces bioinert.[47–49] Nevertheless, PEG’s renown, non-adsorptive properties can be modulated by different factors, e.g. by the addition of peptide sequences, chemical, or topographical cues, etc.[50] In fact, we have recently discovered that the PEG-hydrogel surface loses its cell anti-adhesive properties when it is topographically patterned.[51] The so-called contact guidance is an outstanding example of the important role of nano- and micro scale structures in cell adhesion and migration processes.[52–60] With the development of FIMIC (Fill-Molding In Capillaries), which is a novel technique that partly relies on the soft lithography technique MIMIC (MicroMolding In Capillaries),[61] we intend to provide a versatile strategy to obtain a defined, two-dimensional elasticity pattern on an otherwise smooth

substrate in a simple, low-cost, and reproducible manner. The PEG-based biocompatible hydrogel material herein was prepared via UV photopolymerization of starPEG acrylate macromonomers in the presence of a photoinitiator and eventually a crosslinker (CL). Tuning of the elasticity of the substrate was easily done by varying crosslinking density on the final hydrogel material.

The PEG-hydrogel here presented has been reported in our group to be non adsorptive, biocompatible, and without further chemical modification or bioactivation, able to induce different cellular responses.[51] Furthermore, patterning on its surface has been proved down to a few nanometers.[62] Within this study, smooth hydrogel surfaces displaying locally varied elasticity regions have been successfully achieved and applied in cell culture, i.e. for cell guidance and durotaxis studies.

2.1 Experimental

Hydrogel Preparation and Characterization

The hydrogel material in this method was formed by UV photocrosslinking of multiacrylate starPEG macromonomers in the presence of benzoin methyl ether (BME) as photoinitiator (PI) and pentaerythritol triacrylate (PETA) as a CL as described in ref.[13,51]. Briefly, acrylate functional groups were introduced in star-shaped sP(EO-stat-PO) (Mn 12 500 Da, Dow Chemicals, The Netherlands) macromonomers which, in the presence of a photoinitiator could take part in photoinitiated crosslinking reactions to yield polymer networks. In order to fabricate different stiffness, pre-curing mixtures were prepared by mixing Acrylate terminated starPEG macromonomer (Acr- sPEG) with varying amounts of PI (0.5–1 wt%) and CL (5–10 wt%) with respect to the amount of polymer in the presence of acetone as a solvent. Once the solvent was evaporated under nitrogen stream, the pre-curing mixture could be stored in the dark at 4- 8°C for as long as 3 weeks without deterioration. UV curing was performed using 20 min of irradiation ($\lambda=365$ nm; $W=1.20\text{mW}\cdot\text{cm}^{-2}$). As a result of UV curing, a 3D transparent crosslinked hydrophilic network was obtained. Within this text the three different compositions employed will be denoted based on their elasticity as soft, medium, and stiff, respectively (see Table 1).

Mechanical analysis of the resultant hydrogels was performed on dry as well as on hydrated samples. The bulk gels were allowed to swell in seral (double-distilled) water for 24 h prior use to

ensure EWC. Swelling ratio (SR) was determined by the weight ratio of the bulk gel before and after swelling.

Rheology experiments were performed on a Dynamic Stress Rheometer DSR (Rheometrics Inc., New Jersey, USA) using rotating parallel plates at room temperature. Storage and loss moduli were measured as a function of the frequency (from 0.05 to 10 Hz) in a constant strain mode. Young's modulus (E) was then calculated from the elastic shear modulus (G) using the rubber elasticity theory $E=3G'$. [63] Dynamic Mechanical Analyzer (DMA Q800 TA Instruments) in compression mode was employed to determine the

Young's moduli from the slope in the linear region of the strain–stress curve. A stress ramp of $0.5\text{N}\cdot\text{min}^{-1}$, with initial force 0.01N was applied up to 30% strain. The experiments in swollen state were performed in similar conditions using the submersion compression clamp.

Hydrogel		
Notation	Composition	
	PI (wt%)	CL (wt%)
Soft	0.5	5
Medium	1	5
Stiff	1	10

Table 1: Notation assigned to the different hydrogel material based on the composition of the pre-curing mix

Micrometer Hydrogel Stamp Fabrication

Silicon masters were prepared from silicon wafers by conventional photolithographic techniques with trenches as relief (Amica, Aachen, Germany). For different masters, feature design consisted on diverse spacing (5, 10, 20 mm) and groove width (10, 20, 50 μm) at constant depth (10 μm) (see Table 2). Silicon wafers were rinsed with acetone, water, and isopropanol and dried under a mild stream of nitrogen before use. Within the text the notation of the silicon master will be e.g., 20_10 mm (spacing_groove width), resulting in hydrogel mold with e.g., 10_20 μm patterns.

The selected hydrogel pre-curing mixture was dispensed on the silicon master under inert atmosphere and exposed to UV light for 20 min. Following curing, the transparent polymeric film with inverse relief compared to that on the silicon master was peeled off mechanically. The replicas displayed a constant spacing of 10, 20, or 50 μm between grooves of variable width, i.e. 5, 10, or 20 μm , which were filled in the subsequent patterning step.

Spacing (s)	Width (w)	Depth (d)
[μm]	[μm]	[μm]
5	10	10
10	20, 50	
20	10	

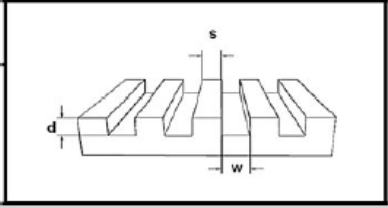


Table 2: Silicon master design and dimensions

2D Microelasticity Pattern Fabrication by the FIMIC Process

A small amount of the second hydrogel precursor of the composite was carefully dispensed at the edge of the open channels of the PEG stamp hydrogel placed upside down on a glass slide (see Fig. 3). The viscous liquid mixture was allowed to fill the capillaries, in the dark and inert atmosphere for 30 min after which the assembly was exposed to UV light for 20 min. After exposure time was complete the hybrid construct was easily detached from the glass substrate mechanically and turned upside down to proceed with surface characterization and cell culture. The resultant polymer composite was a robust, free standing, transparent film.

The surface of the hybrid hydrogel structure was investigated by several techniques, FESEM and AFM in dry state and eventually optical microscopy on the sample in water. Notation of the assembly will be done as follows, e.g. “soft (20 μm) in stiff (10 μm)”, meaning that the surface contains 20 μm wide soft lines alternated with the 10 μm wide stiff lines of the stamp. The composition and patterning dimensions of all hybrid constructs prepared in this study are listed in Table 3. The samples were handled with Teflon tweezers and cut with razor blades with no further cares. Prior to use, glass slides used as substrates were cleaned by rinsing in acetone, water, and isopropanol and dried under a mild stream of nitrogen in order to eliminate organic residues.

Si-master	Hydrogel stamp/ channels filling	Hybrid sample notation
20_10 μm	Stiff/soft	Soft (20 μm) in stiff (10 μm)
10_50 μm	Stiff/soft	Soft (10 μm) in stiff (50 μm)
10_20 μm	Stiff/soft	Soft (10 μm) in stiff (20 μm)

Table 3: Notation of the hybrid hydrogel samples

Atomic Force Microscopy (AFM)

Images were taken in tapping mode using standard silicon cantilevers ($k=40 \text{ N}\cdot\text{m}^{-1}$, $f=300 \text{ kHz}$; Nanoworld, Neuchatel, Switzerland) on a Digital Instrument Multimode equipped with a NanoScope IIIa controller (Veeco Instruments, SantaBarbara, CA) in air. Data were edited using NanoScope III v5.12r5 software (Veeco Instruments, Santa Barbara, CA). The images were flattened but not further modified.

Fibroblast Cell Culture

Mouse connective tissue fibroblast cell line NIH L929 was used for the experiments (DMSZ, Braunschweig, Germany). Cells were cultured in RPMI-1460 medium supplemented with 10% fetal bovine serum and 1% penicillin/streptomycin at 37°C in a 5% CO_2 supplied incubator. The culture medium was changed every 2 days. Cells were harvested with 0.25% trypsin/EDTA. For the cultivation experiments the inoculation density was $50\,000 \text{ cells}\cdot\text{cm}^{-2}$. (Samples were cultivated in well plates with a well area of 1 cm^2 and 1ml of a $50\,000 \text{ cells}\cdot\text{ml}^{-1}$ suspension was added to the wells on top of the samples). Samples were rinsed with sterile water and buffer prior to cell seeding. All reagents were purchased from PAA, Cölbe, Germany.

Immunological Staining

For immunological staining of the cytoskeleton, cells were fixed in 4.0% formaldehyde at pH 7 (Carl Roth, Karlsruhe, Germany), permeabilized with 0.1% Triton X-100 (Sigma–Aldrich Chemie, Munich, Germany) and blocked in 1% BSA in PBS (PBSA). To visualize cell morphology cells were labeled with tetramethylrhodamine isothiocyanate (TRITC)-conjugated phalloidin (1:500) for 30–45 min followed by DNA staining with 4'6-diamidino-2-phenylindole (DAPI) (1:1000) for 5 min (Chemicon).

Optical and Fluorescent Microscopy

Light microscopy images were taken with an inverted Axiovert 100A Imaging microscope (Carl Zeiss, Goettingen, Germany). Cell adhesion and spreading were monitored by means of fluorescent microscopy with an Axio Observer Z1, equipped with an Apo Tome system to achieve optical sectioning through the fluorescent sample. Pictures were taken using an AxioCam MRm digital camera and analyzed using the AxioVisionV4.6/V4.7 software package (Carl Zeiss, Goettingen, Germany).

Field Emission Scanning Electron Microscopy (FESEM)

Images were taken by a high resolution field emission scanning electron microscope (FESEM; S-4800, Hitachi, Krefeld, Germany). In the case of hydrogel substrates an accelerating voltage of 1.5 kV and varying working distance (6.5 to 10mm) were used. In the case of cell imaging 1.0 kV and a working distance of 8mm were the microscope parameters. Cell containing samples were prepared as follows: after a cultivation time of 24 h, the substrates with the L929 cells were rinsed three times with PBS and fixed with 4.0% formaldehyde for at least 30 min and dehydrated by incubating consecutively in 50, 70, 90, and 100% ethanol.

Cell Migration Experiments

Videos of migrating cells were obtained by acquiring images (approximately 700 μ m_600 μ m) on selected regions of the L929 populated hydrogel gel [stiff (10 μ m) in soft (20 μ m)] every 10 min during 24 h using a Olympus IX 50 optical microscope (Olympus Co., Tokio, Japan) equipped with

a mini-incubator mounted on an automated stage (PRIOR, Rockland, MA) and a CoolSnap Camera (Photometrics, Tucson, AZ). Cell tracks were reconstructed from the time lapse videos using Metamorph software (Molecular Device, Sunnyvale, CA).

2.3 Results and Discussion

To fabricate our hydrogel system we use a previously described procedure (see Experimental Part). The macromonomer of choice is a six armed Acr-SP(EO-stat-PO) (Mn 12 500 Da) which can undergo radical crosslinking initiated by UV light in the presence of a photoinitiator. Varying the amount of initiator and eventually adding a CL molecule to the pre-curing mixture results in an increase of the network density, the resulting polymer is an insoluble highly crosslinked network able to take up large amounts of water (or biological fluids), hence a hydrogel by definition.[64]

So far, hydrogels have been described ranging in elasticity from few Pa to hundreds of kPa. As several hydrogels can be fabricated with different elasticities yet the same chemistry, they represent a useful substrate to study elasticity-dependent cell behavior (mechanotransduction).

In the present study we prepare smooth hydrogel substrates which exhibit two different, tuneable elasticities on their surface, arranged in a specific pattern. Three hydrogel compositions were prepared for this purpose in order to obtain a relevant elasticity range, although mainly the combinations of softest and the stiffest gel were applied in the experiments. The fabrication of different elasticity hydrogels was done by varying the amount of PI and CL in the liquid pre-curing mixtures as specified in Table 1. In order to assess the impact of PI and CL concentration on the resulting hydrogel, the elasticity range of the bulk gels was investigated by rheology applying the rubber elasticity theory[63] and by dynamic mechanical analysis for comparison.

The swelling behavior of the materials was investigated as well and represented by the SR in Figure 1; mechanical properties in hydrated conditions were determined after 72 h in water. A graphical representation of the mechanical analysis can be seen in Figure 1, where Young's Moduli (E) is plotted against the composition of the pre-curing mixture.

From the measurements in the dry state, DMA data provided 0.24 ± 0.02 MPa and 2.50 ± 0.50 MPa for the soft and stiff hydrogel, respectively, and these results compare well to those from rheological determinations. Young's moduli increase with increasing the crosslinking density of the network, which implies formation of a denser network.

Normally, an increase in crosslinking density is associated with a decrease in the water uptake. As expected, the SR values clearly decrease with increasing crosslinking density of the gel network [Fig. 1(b)]. Further, the swelling makes the gels softer; the stiffness of the swollen hydrogel decreases to typically half of the dry hydrogel value. All samples were transparent polymers before and after swelling in water, still easy to handle as free-standing films. Those results prove the ability of this hydrogel to vary in rigidity over a quite large range, without compromising the transparency of the polymer as required for further applications, e.g. live imaging of cell culture on the samples by optical microscopy and immunological staining experiments by fluorescence microscopy using inverted microscopes.

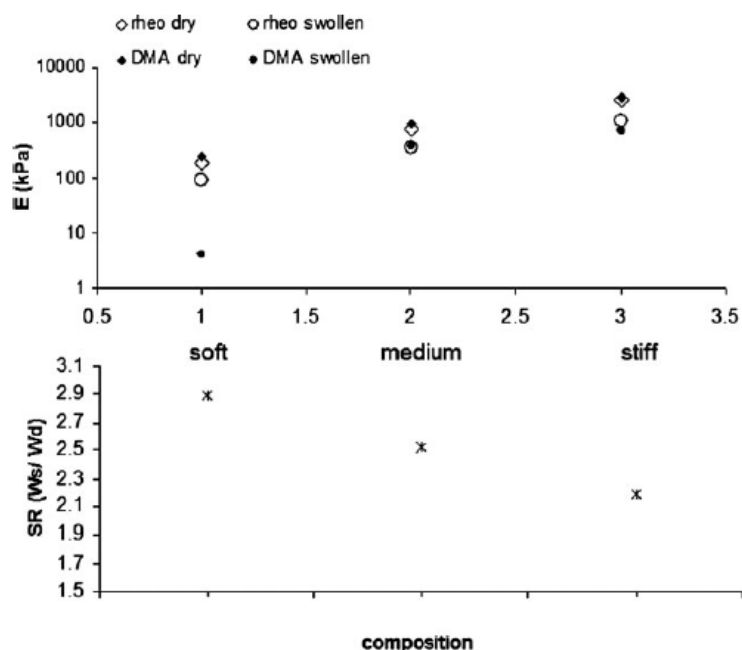


Figure 1: a) Elastic modulus as a function of gel composition as obtained from DMA (solid symbols) and rheology (open symbols); circles and diamonds represent the values for hydrated and dry hydrogels, respectively. b) SR represented as a function of the composition

For the preparation of the PEG-hydrogel mold, the Acr-sP(EO-stat-PO) mix of choice was cured under UV light for 20 min against mm-sized groove structured silicon master (e.g. 20_10 mm). As a result of the imprinting process, the micrometer design was transferred inversely into the surface of the cured polymer [Fig. 2, top].

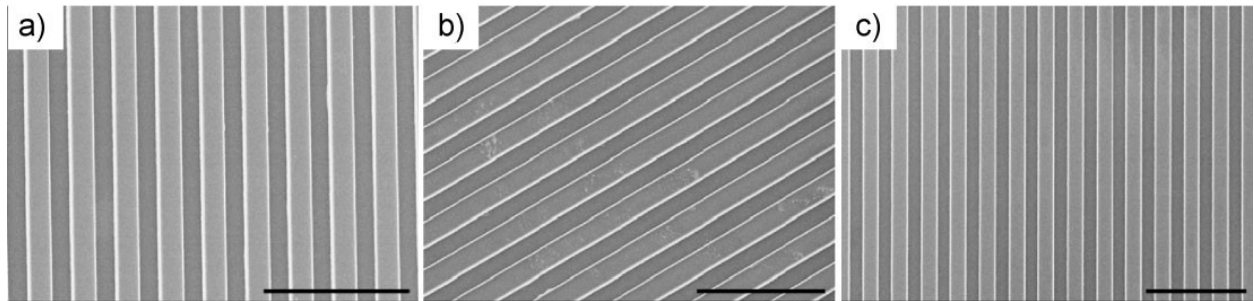
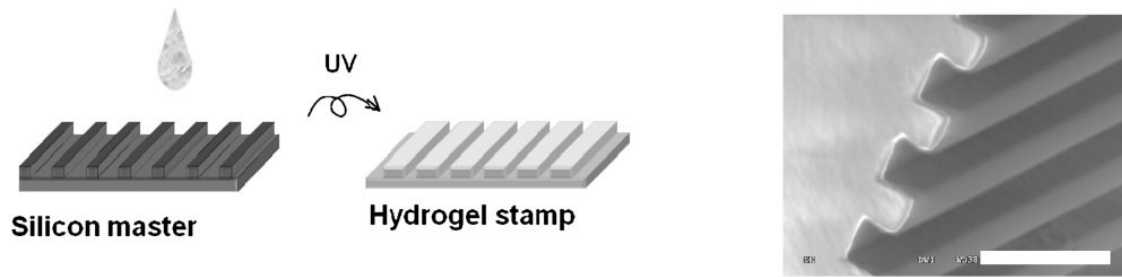


Figure 2: Top: schematic representation of the micromolding process to fabricate a hydrogel replica. The electron micrograph on the right depicts a cross-section through the material, which is a negative copy of the micropatterned silicon master (scale bar 25 mm). Electron micrographs a), b), and c) depict replicas from a 5_10 mm silicon master (thus bearing 5mm wide grooves, spaced by 10mm) using soft, medium, and stiff hydrogel, respectively. Scale bars represent 50mm.

The free-standing polymeric micropatterned mold was placed upside down on a microscopy glass using tweezers and applied subsequently as the mold for the capillary filling process. Figure 3 shows a sketch of the experimental procedure of the new FIMIC method. In the second step, the capillary filling of the open channels of the PEG-hydrogel stamp were filled within 30min under inert atmosphere and cured into a solid elastomer. The hybrid film was lifted mechanically without residual polymeric material remaining on the glass slide. Delaminating of the composite was not observed, confirming that the integrity of the hybrids was not disrupted by shear or pulling forces that can be significant during release.

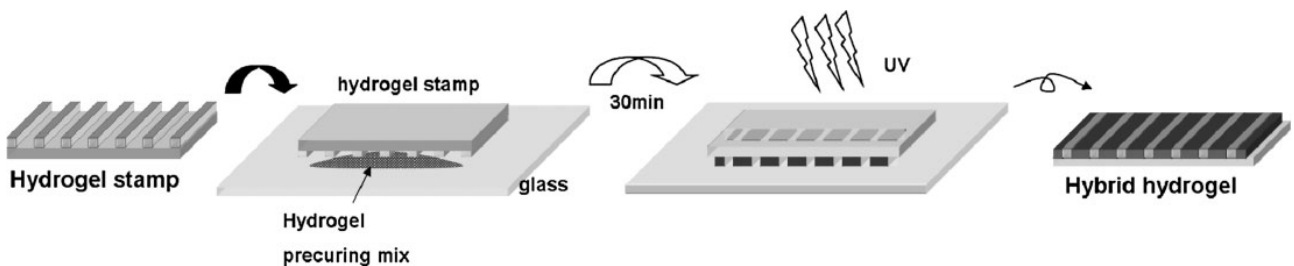


Figure 3: Schematic representation of the FIMIC method to prepare hybrid hydrogels with micropatterns of elasticity on the otherwise smooth surface

The versatility of this strategy and the material properties permitted the capillary filling process to be completed within 30 min for all dimensions tested. In all cases the resulting microfabricated substrate was a transparent freestanding polymeric film that could be easily manipulated with tweezers without further precautions. A smooth, micropatterned surface was expected provided by the set up. In Figure 4(a), the FESEM image of a hybrid structure “soft (20 μm) in stiff (10 μm)” is shown. The stripes corresponding to soft and stiff hydrogel can be recognized in the electron micrograph by their light and dark gray color, respectively. The image clearly demonstrates a binary pattern consisting of well-defined, parallel lines. An optical micrograph of the surface area is shown in Figure 4(c). The smoothness of the surface contour was verified by analyzing the cross-section profile on the AFM images (Inset in Fig. 4); on a span of 10 μm a negligible unevenness of $<0.03 \mu\text{m}$ can be perceived.

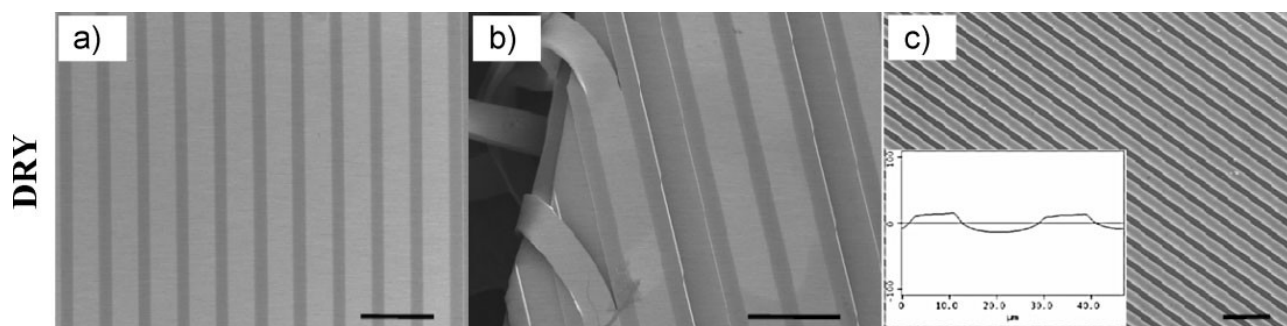


Figure 4: Micrographs of hybrid hydrogel “soft (2mm) in stiff (10mm)” measured in dry state. Scale bars represent 50 μm . Recognized in light and dark gray are soft and stiff material, respectively. a) and b) FESEM images of the micro-patterned surfaces. In b) defects at the cutting edge of the hybrid sample are shown; lines (of the soft material; light gray) that come loose from the mold (stiffer gel; dark gray) or are completely missing are clearly recognized. c) Optical micrograph. Inset: AFM cross-section profile of the smooth surface

In order to verify that the binary pattern on the image indeed corresponds to alternating hydrogel material certain considerations must be taken into account. On the one hand, the mold should provide good “sealing” to the glass slide at the protruding areas to avoid creeping of the liquid underneath the mold during the capillary filling process, which would lead to the formation of a scum layer. On the other hand, diffusion of the second hydrogel precursor into the already crosslinked mold is not desired since blending of the two components could lead to a change in gel properties at the interfaces. To acknowledge those matters, we cut the substrate with a razor blade and examined the surface profile at the cutting edge. As can be observed in Figure 4(b) no trace of scum layer was evident in the whole area of investigation. Moreover, the image reveals how the soft

lines are flexible, since 20 μm wide laminas can be separated and stand alone, apart from the stiff hydrogel frame, when they are mechanically disturbed, e.g. at the cutting edge. Nevertheless, delamination of the lines was rarely observed away from the edge. Thus it seems that the soft lines embedded in the stiff hydrogel stamp are neither chemically nor physically interconnected, however physically entrapped in the micrometer cavities, which is apparently quite adequate to keep them in place.

Since the substrates are destined to biological applications it is important to know how they respond in liquid media. We are aware that additional forces caused by e.g., the differential swelling of both materials might affect the reliability of the hybrid structure under water. Hydrogels in water are known to swell to larger size than initially in dry state showing decreasing values with stiffness (see Fig. 1 for SR depending on composition). Accordingly, one could expect that expansion forces encountered due to swelling may provoke the trapped lines to be pushed out of their initial location. To that purpose, the resultant hybrid-hydrogel substrates were hydrated for as long as 3 days in distilled water and monitored afterwards.

FESEM images of the swollen samples were taken after gently wiping off the excess water of the hydrated samples. Figure 5(a) shows the image of the largely defect-free surface in comparison to an area with a defect in Figure 5(b). A clear binary pattern can be distinguished on the hydrogel surface.

However to a more faithful analysis, optical microscopy was the method of choice in order to characterize the integrity of the structures directly in water. It can be seen how the soft hydrogel stripes, recognized by the brighter lines are stable in the frame; still, delamination was observed to occur occasionally as well. [Fig. 5(d)]. No major deformation of the assembly seemed to be initiated by swelling expansion forces at the surface. Further inspection of the surfaces by means of AFM under water is in progress in order to visualize the possible effect of differential swelling on pattern dimensions and surface smoothness.

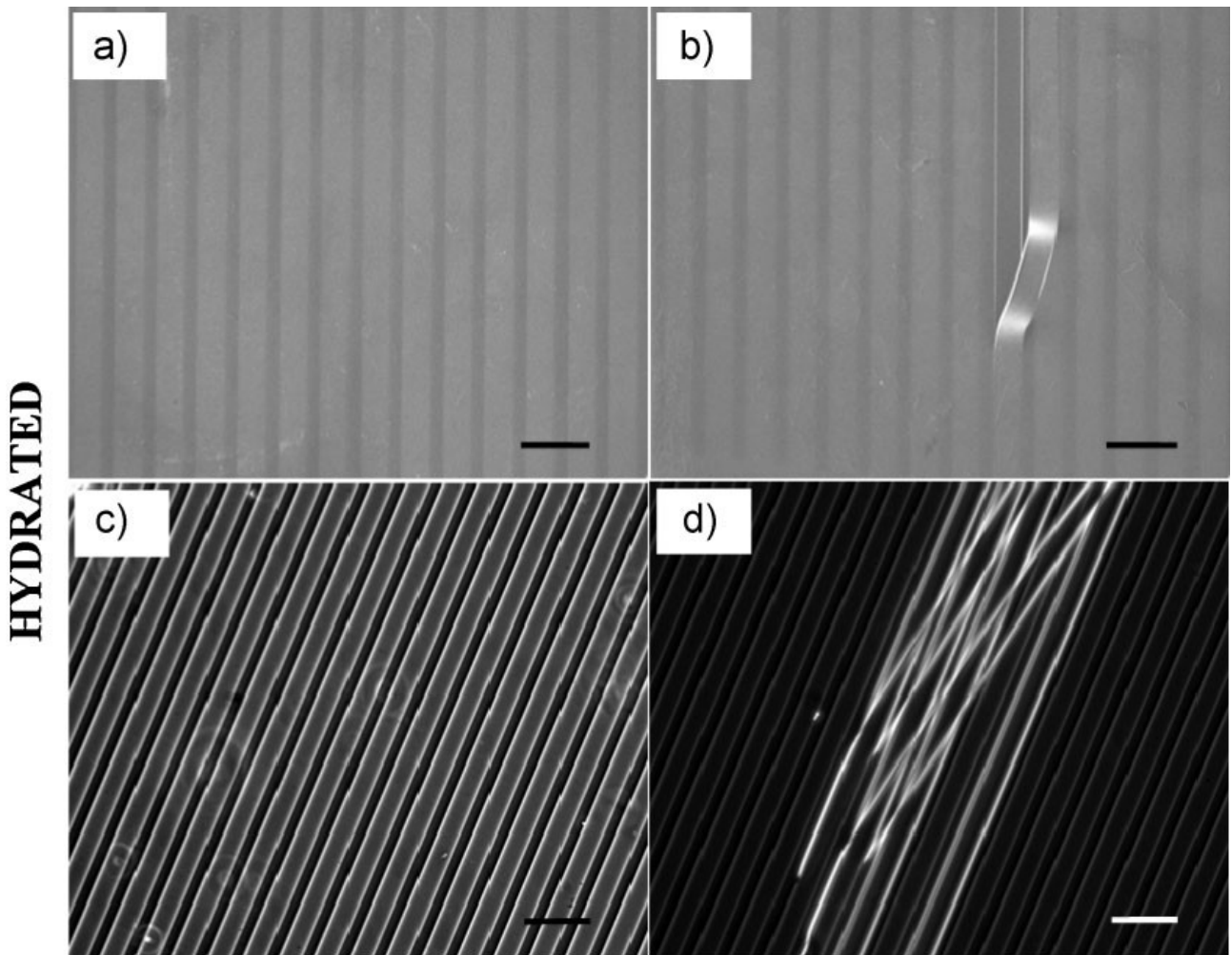


Figure 5: Hybrid hydrogel with pattern “soft (20mm) in stiff (10mm)” in hydrated state; a) and b) depict FESEM images; showing one line coming loose in image b). Light and dark gray are soft and stiff hydrogel, respectively. c) and d) depict optical micrographs, revealing a defect area on the patterned surface in d). Scale bars represent 50mm.

The described substrates have been applied for preliminary cell culture experiments with a murine fibroblast cell line (NIH L929). We wanted to assess whether the cells react in their adhesion and spreading behavior according to the pattern of elasticity, whereas they have been observed not to adhere at all on non-biofunctionalized, smooth hydrogel surfaces with uniform stiffness.[10]

Fibroblasts were cultured on the hybrid surface for 24 h and monitored by optical microscopy, electron microscopy, and fluorescent microscopy after immunological staining.

Cells were seeded on various hybrid substrates with different line patterns created by either filling “stiff in soft” (Fig. 6, top) or “soft in stiff ” (Fig. 6, bottom). Also “stiff in stiff” samples were prepared as control samples (images not shown).

From the microscopy images one can clearly distinguish how cells seeded on smooth hybrid substrates accumulate preferentially on the stiffer areas after 24 h (Fig. 6). FESEM images in Figure

6 show the clear alignment of single cells along the 10 μm stiffer lines, evident from Figure 6(b) where some stripes appear to be missing. The live optical micrograph in Figure 6(d) confirms selective cell adhesion and agglomeration on 50 μm stiffer regions, leaving the soft lines in between practically untouched. In order to visualize the cell morphology more precisely, the cell nucleus and the actin cytoskeleton were stained with DAPI (blue) and phalloidin (red), respectively. The fluorescence micrographs shown in Figure 6(c), (e), and (f) confirm the selective attachment on the stiffer regions. This cellular behavior was observed independent of the feature size; stiffer lanes as narrow as 5 μm (which is smaller than the cell's own size) were effective (images not shown) and stripes as broad as 50 μm were recognized. This also implies that the elasticity sensing mechanism is not restricted to a border effect; it stretches over several micrometers.

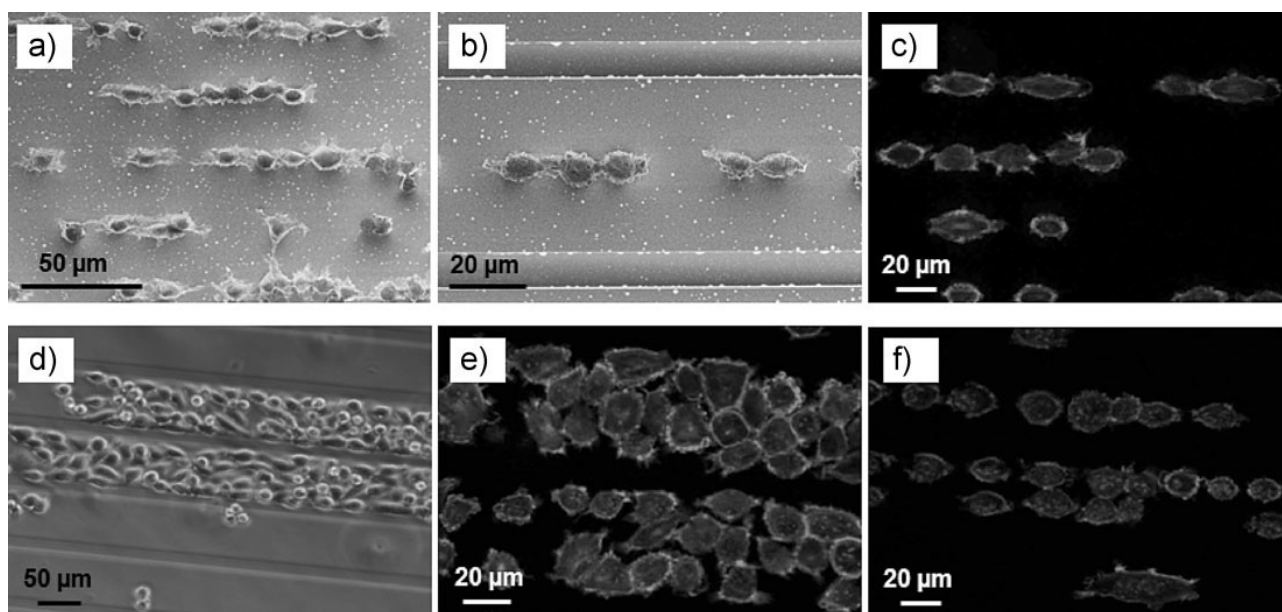


Figure 6. Fibroblast L2929 adhesion to hybrid hydrogel; cells selectively adhere to the stiffer areas of the samples. Top: “stiff in soft” samples, for example 10 μm stiff lines in soft mold with 20 μm spacing as shown in the FESEM images in a) and b). Bottom: “soft in stiff” samples, for example 10 μm soft lines in stiff mold with 50 μm spacing as shown in d) and e). c), e), and f) show fluorescence micrograph; the cells were stained with DAPI and phalloidin, which appear as dark and light grey, respectively, to highlight the nucleus and the actin filaments of the cytoskeleton, respectively.

Notwithstanding the remarkable effectiveness of directing cell adhesion by the micropatterns of elasticity, we are also very interested in the dynamic mechanosensing processes leading to the eventual accumulation of the cells on the stiffer areas of the surface.

That's why we have also performed cell migration experiments. From the tracking of several individual cells the preference for the stiffer lanes has been confirmed. In Figure 7(a), a few of such

trajectories are overlaid onto the optical micrograph and the correlation of the cells tracks with the pattern is evident; cells prefer to migrate on top of or along the stiffer lanes. Only occasionally do they move on the softer background, but they immediately either revert to the initial stiff lane or move to the closest stiff lane. Moreover, this feature occurs in all the regions of the substrate as shown in Figure 7(b) in which the vast majority of cells move along the stiffer lanes. These preliminary studies indicate the great potential of the substrate fabrication method to elucidate the background of substrate stiffness dependent cell behavior. We present a new platform technology to fabricate patterns of elasticity, with tailored geometrical parameters to study cell adhesion and migration in a systematic way (e.g. by variations in size, shape, and periodicity of the pattern).

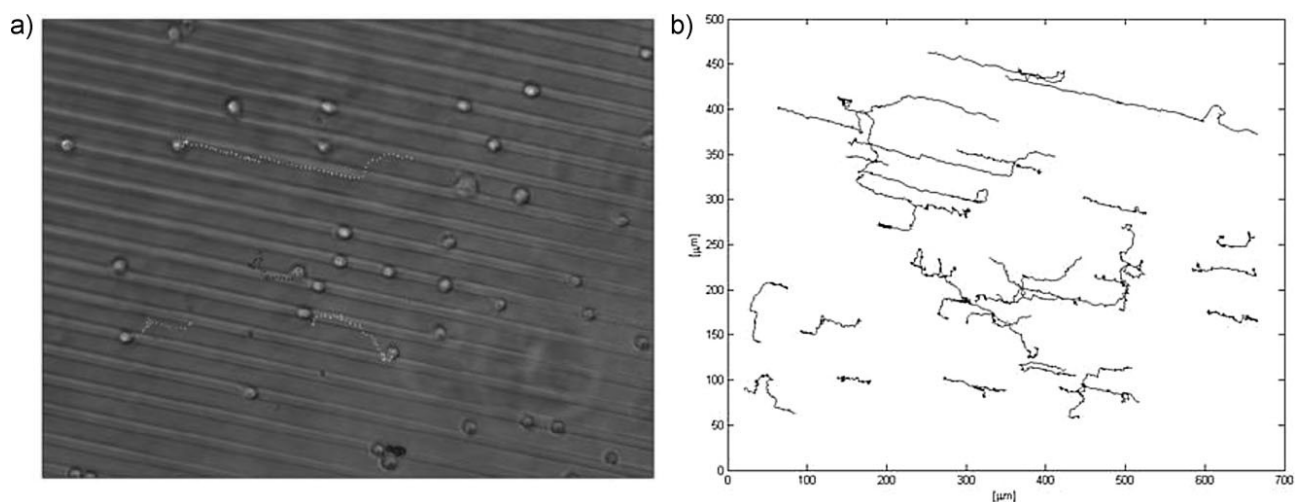


Figure 7: a) Optical micrograph of fibroblasts (L929) on hybrid hydrogels with 10 μm wide stiff and 20 μm wide soft lanes; the preferred adhesion to the narrower stripes is evident. Superimposed on the image are the migration trajectories of six individual cells over 24 h of observation. b) Composition of 30 cell trajectories (collected from 5 areas on the sample shown on the left; each following 6 individual cells). Cells tend to migrate on top of or along the stiffer stripes.

2.4 Conclusions

In this study we have demonstrated the fabrication of a robust 2D polymer composite in which hydrogels with diverse elasticity are exposed in parallel micro-lines on an otherwise smooth surface. To that end, we have described a versatile lithographic technique combining a soft lithography method (i.e., micro-molding in capillaries) with the novelty that the mold belongs to the final substrate, in this specific case a hybrid hydrogel. FIMIC (Fill-Molding In Capillaries) is a straightforward, affordable, bench-top method that permits the control of localized elasticity

patterning on hydrogel surfaces in which the effect of stiffness and pattern motif on cell behavior can be both explored simultaneously. The final substrate is a robust, transparent film with a periodic microelasticity pattern clearly distinguished on its surface.

The surface as prepared is quite smooth (the measured unevenness was only tens of nm) and the filled lines are neatly kept in place, although delamination of some individual lanes was observed as well. Besides the advantages of using a hydrogel as substrate material with elasticity variation in a wide range, the FIMIC method also permits biofunctionalization of the micropatterned surface, i.e. one of the two components of the hybrid construct can be enriched with biofunctional molecules, such as cell adhesion mediating proteins or growth factors.

The microelasticity-patterned substrates were employed in cell culture with fibroblasts and it was found that cells strongly react to the design on the surface, accumulating preferentially and strikingly selectively on the stiffer regions independently of line width, which ranged from 5 to 50 μm .

Although the cells were tightly enough adherent so that they were not washed off the surface in fixation and drying procedures, they displayed a round shape and did not spread.

Cell migration experiments confirmed the preference for the stiffer lines, as the cells were observed to migrate almost exclusively on top of or along the lines with higher stiffness. A more detailed analysis of the dynamic processes involved in the stiffness sensing mechanism is currently in progress, e.g. by employing systematic variations of pattern dimensions and periodicities, and exploring a larger variety of stiffness contrasts by using new hydrogel formulations. The goal of these investigations is not only to increase our fundamental understanding of cell-material interactions and mechanotransduction phenomena, but also to achieve better spatial and temporal control of cell movement on biomaterial surfaces for the eventual purpose of optimizing tissue engineering constructs.

2.5 References

- [1] D. E. Discher, P. Janmey, Y. L. Wang, *Science* 2005, 310, 1139.
- [2] A. J. Engler, S. Sen, H. L. Sweeney, D. E. Discher, *Cell* 2006, 126, 677.
- [3] N. W. Karuri, S. Liliensiek, A. I. Teixeira, G. Abrams, S. Campbell, P. F. Nealey, C. J. Murphy, *J. Cell Sci.* 2004, 117, 3153.
- [4] L. S. Chou, J. D. Firth, V. J. Uitto, D. M. Brunette, *J. Cell Sci.* 1995, 108, 1563.
- [5] J. Y. Lim, H. J. Donahue, *Tissue Eng.* 2007, 13, 1879.
- [6] A. S. H. Ngalim, G. Le Saux, J. J. Gooding, K. Gaus, *J. Oncol.* 2010, DOI: 10.1155/2010/363106.
- [7] G. Schlunck, H. Han, T. Wecker, D. Kampik, T. Meyer-Ter-Vehn, F. Grehn, *Invest. Ophth. Vis. Sci.* 2008, 49, 262.
- [8] J. Spatz, *Soft Matter* 2007, 3, 261.
- [9] B. G. Chung, L. F. Kang, A. Khademhosseini, *Exp. Opin. Drug Discovery* 2007, 2, 1653.
- [10] V. A. Schulte, M. Diez, M. Moller, M. C. Lensen, *Biomacromolecules* 2010, 11(12), 3375.
- [11] E. Kim, Y. N. Xia, G. M. Whitesides, *J. Am. Chem. Soc.* 1996, 118, 5722.
- [12] Y. N. Xia, E. Kim, G. M. Whitesides, *Chem. Mater.* 1996, 8, 1558.
- [13] M. C. Lensen, P. Mela, A. Mourran, J. Groll, J. Heuts, H. T. Rong, M. Moller, *Langmuir* 2007, 23, 7841.
- [14] D. Y. Pilnam Kim, A. Khademhosseini, R. Langer, K. Y. Suh, *Unconventional Nanopatterning Techniques and Applications*, John Wiley & Sons, Inc, Hoboken, NJ 2008.
- [15] Y. Xia, G. M. Whitesides, *Annu. Rev. Mater. Sci.* 1998, 28, 153.
- [16] T. Y. Yu, C. K. Ober, *Biomacromolecules* 2003, 4, 1126.
- [17] Y. Hong, P. Krsko, M. Libera, *Langmuir* 2004, 20, 11123.
- [18] M. Arnold, E. A. Cavalcanti-Adam, R. Glass, J. Blummel, W. Eck, M. Kantelehner, H. Kessler, J. P. Spatz, *Chemphyschem* 2004, 5, 383.
- [19] A. Revzin, R. J. Russell, V. K. Yadavalli, W. G. Koh, C. Deister, D. D. Hile, M. B. Mellott, M. V. Pishko, *Langmuir* 2001, 17, 5440.
- [20] S. Nemir, H. N. Hayenga, J. L. West, *Biotechnol. Bioeng.* 2010, 105, 636.
- [21] A. Kidoaki, T. Matsuda, *J. Biotechnol.* 2008, 133, 225.
- [22] Y. I. Guoping Chen, Yoshihiro. Ito, *Macromolecules* 1998, 31, 4379.

- [23] B. Cortese, G. Gigli, M. Riehle, *Adv. Funct. Mater.* 2009, 19, 2961.
- [24] D. S. Gray, J. Tien, C. S. Chen, *J. Biomed. Mater. Res, A* 2003, 66A, 605.
- [25] R. Dong, T. W. Jensen, K. Engberg, R. G. Nuzzo, D. E. Leckband, *Langmuir* 2007, 23, 1483.
- [26] R. J. Pelham, Y. L. Wang, *Proc. Natl. Acad. Sci. USA* 1997, 95, 12070.
- [27] W. H. Guo, M. T. Frey, N. A. Burnham, Y. L. Wang, *Biophys. J.* 2006, 90, 2213.
- [28] K. Y. Suh, J. Seong, A. Khademhosseini, P. E. Laibinis, R. Langer, *Biomaterials* 2004, 25, 557.
- [29] C. M. Lo, H. B. Wang, M. Dembo, Y. L. Wang, *Biophys. J.* 2000, 79, 144.
- [30] H.-B. Wang, M. Dembo, S. K. Hanks, Y.-L. Wang, *Proc. Natl. Acad. Sci. USA* 2001, 98, 11295.
- [31] S. S. K. Brandon, V. Slaughter, O. Z. Fisher, A. Khademhosseini, N. A. Peppas, *Adv. Mater.* 2009, 21, 3307.
- [32] D. W. G. M. C. Rivest, B. Ni, J. Rubin, A. M. V. Yadav, J. M. Karp, A. Khademhosseini, *J. Mech. Mater. Struct.* 2007, 2.

Chapter 3

Influence of nanotopography on focal adhesions, cytoskeleton assembly and nuclear shape

More than 15 years ago, Chen and co-workers elegantly demonstrated the powerful effects of cell shape on its fate and functions [1]. From this landmark study onwards, many others brought in evidences that focal adhesions and cytoskeleton mediated signalling are potent regulators of cell behaviour and fate and such signalling are now recognized as the fundamental elements of Mechanobiology. For example, McBeath et al. [2] seeded mesenchymal stem cells (MSC) on micropatterned adhesive islands and cell shape was critical regulating adipogenic-osteogenic switch and that such a commitment switch was regulated through ROCK induced cytoskeletal tension. Similarly, Kilian and coworker [3] plated MSC on adhesive islands whose shapes was able to either promoting or suppressing cytoskeletal generated contractile forces. They reported that increased myosin contractility enhanced osteogenesis through MAP kinase pathways and Wnt signalling, as demonstrated by microarray analyses. Engler et al. [4] showed the mechanical properties of the culturing substrate were a powerful cue in specifying MSC lineage towards, neurons, myoblasts and osteoblasts. In particular, stiff matrices lead to enhanced cytoskeletal tension and osteogenesis while compliant matrices directed MSCs towards neurogenesis and myogenesis. This example proved that cytoskeletal generated force is a powerful regulator of stem cell fate *per se*, irrespective of the way that is exploited to modulate intracellular tension, i.e. using micropatterns or mechanical cues. Although a general, unifying model that correlates cytoskeletal generated forces with genetic events is still far to come, some evidences reports that cell contractility is sufficient to deform the nucleus and such a deformation alters gene expression [5]. Altogether these data demonstrate that environmental signals, in the form of biochemical and biophysical cues, which impact on cell adhesion-cytoskeleton-nuclear shape have a profound effect on cell fate. Focal adhesions (FAs) play an important role in this process being the mechanical link between the cytoskeleton and the extracellular environment. Forces that are exchanged by substrates and cells necessarily pass through FAs. These are constituted by hundreds of proteins which form multilayer plaques that stabilize the transmembrane integrin clusters and connect them

to the cytoskeleton [6]. Several proteins that take part in the formation of FAs are implicated in numerous signalling pathways, act as mechanosensors and bind to actin fibres. FAs are not static entities, but rather change their size and dimension according to the forces that are exerted on them. Similarly, cytoskeleton changes its configuration according to the spatial arrangement of FAs. Hotulainen and Lappalainen [7] described the existence of three different types of fibres constituting the actin cytoskeleton. Transverse arcs, are not directly associated to FAs, are contractile curved arcs which forms by the peripheral membrane and move centripetally upon contraction. Dorsal fibres are small fibre bundles that originate from the interaction of moving transverse arcs with FAs. Ventral stress fibres are contractile actin bundles that are connected to FAs at both termini. These are formed by the fusion of two dorsal stress fibres and a transverse arc located in between. Several strategies have been developed in the past years to affect cell adhesion, FA assembly and cytoskeletal structures consequently, with the common aim of controlling cell functions. Among these, the use of topographic patterns, proved to be very effective in controlling FAs arrangement and cytoskeletal assemblies and, consequently, in impacting on cell behaviour. In more details, topographic patterns affect, cell adhesion, polarization and migration [8]. These constitute an immediate evidence of the influence of topography on FAs and cytoskeleton, however topographic patterns may play more subtle effects. For example, Dalby et al. [9] demonstrated that topographic signals alone, in the form of a slightly irregular pattern of nanopits, were sufficient to induce osteogenic differentiation of MSC [10]. More recently, the same group reported that ordered arrays of nanopits allowed MSC to retain a stem cell phenotype in vitro, up to eight weeks. These and other studies demonstrated that topographic signals may have regulatory effects as powerful as those exerted by chemical signals, i.e. growth factors and drugs. Furthermore, topographies might be embossed on a large variety of material surfaces: metals, elastomers, polymers, hydrogels. Several technologies have been developed for the dual purpose of patterning sufficiently large surface areas with high spatial resolution and great reproducibility. Among these, there are soft lithography, electron beam or ion beam lithography, nano imprinting lithography [11]. Therefore, beside its bioactive properties, topography also possess numerous technological advantages that make it a valuable candidate for the functionalization of bioactive materials for implantology and for the production of devices for biotechnological applications. Many works stemmed in the last decade, reporting various cell responses to the geometrical features of nanopatterns. The vast majority of these works, however, was performed by analyzing fixed cells and therefore neglecting time dependent effects or, similarly, not accounting for the effects of topography on adhesion and cytoskeleton dynamics. Compared to this abundance of results, only few works addressed the dynamics behind the cell-topography interactions.

Therefore, many aspects of the FAs/cytoskeleton/nuclear shape axis still remain unclear. Firstly, how does a cell perceive and react to a topographic pattern? What are the molecular mechanisms underlying this recognition? Can we predict FAs and cytoskeleton configuration out of a topographic pattern? Question to these answers are crucial in order to better conceive functionalization strategies with topographic patterns. Therefore, the aim of this study was to provide a comprehensive vision of cell-topography interactions at different levels: from adhesion plaques, to nuclear shape. This study wants to correlate quantitative analyses performed with high resolution microscopy with time dependent observations. To this aim, MC3T3 preosteoblasts were cultivated on nanograted polydimethylsiloxane substrates produced by means of the replica molding technique.

3.1 Experimental

Preparation of nanopatterned substrates

Patterned substrates were obtained by replica molding of PDMS (Sylgard 184, Dow Corning Corporation, Michigan, USA) on polycarbonate masters. The pattern consisted of an area of 1 cm² containing parallel and straight channels with a groove and ridge width of 700 nm and depth of 250 nm. PDMS was prepared by mixing elastomer base and curing agent at 10:1 weight ratio. The solution was degassed, poured onto the polycarbonate master and then cured at 37°C for 24 hours. Control (flat) PDMS substrates were produced by pouring the base and curing mix on a 35 mm polystyrene Petri dish (Corning, Corning, NY, USA) and curing at 37°C for 24 hours. To improve cell adhesion, PDMS substrates were treated with oxygen plasma. Briefly, the treatment was performed with a Plasma Femto (Diener, Germany) equipped with 13,56MHz 100W generator for the plasma excitation. Substrates were sterilized by UV exposure for 15 minutes and incubated with serum supplemented culture medium overnight prior to cell culturing experiment.

Cell Culture

MC3T3-E1 preosteoblasts (American Type Culture Collection, ATCC, Manassas, VA, USA) were cultured in α MEM with deoxyribonucleosides, ribonucleosides and 2 mM L-glutamine (Gibco Life, Grand Island, NY), supplemented with 10% fetal bovine serum (Gibco), penicillin (100 units/ml), streptomycin (100 μ g/ml). The cells were incubated at 37°C in a humidified atmosphere of 95% air and 5% CO₂. The culture medium was changed every two days. After 3 days of culture, cells were detached with trypsin/EDTA (0.25% w/v trypsin / 0.02 mM EDTA) (Gibco) and seeded on nanogrooved or flat substrates at a density of $5 \cdot 10^3$ cells/cm².

Immunofluorescence

Stress fibres and focal adhesion were examined by immunofluorescence confocal microscopy. Cells cultured on nanopatterned and flat substrates were fixed either at 4 or 12 hours after seeding. Cell fixation was performed with 4% paraformaldehyde for 20 min and then permeabilized with 0.1% Triton X-100 (Sigma, St. Louis, MO, USA) in PBS 1X. Samples were blocked in PBS/BSA 1% solution for 30 min, to avoid non-specific binding. Focal adhesions were recognized by incubating samples with anti-vinculin monoclonal antibody (dilution 1:200; Chemicon) for 2 hours at 20°C. After incubation substrates were washed 3 times with PBS (3 minutes per wash) and incubated with Alexa Fluor 488 conjugated goat anti-mouse antibody (Invitrogen, Carlsbad, USA) for 30 min at 20°C. Actin filaments were stained by incubating samples with rhodamine conjugated phalloidin (dilution 1:250; Sigma) for 30 minutes at 20°C. Nuclei were stained by incubating samples with DAPI for 15 minutes at 37°C.

Fluorescent images of focal adhesion and actin bundles were collected with a Leica TCS SP5 confocal microscope. Samples were excited with 488nm (vinculin) and 543nm (actin) laser lines, and the emissions were collected in the 500-530nm and 560-650nm ranges respectively. DAPI stained nuclei were visualized in two photon microscopy mode. Excitation was set at 700 nm and the emission was collected in the 400 – 450 nm range using a band pass filter.

Drug treatment

Blebbistatin (Sigma) was used to inhibit myosin II contractility. Cells grown on patterned or on flat control substrates were treated for 40 minutes with a 15 μ M solution of blebbistatin in DMSO. The treatment started either after 3 hours or 11h post seeding and lasted for 40 min. Afterwards, the samples were fixed and stained for the cytoskeleton and vinculin as described above.

Live-cell confocal microscopy

MC3T3 cells were seeded in 35mm petri dish at 80% confluency and let overnight in incubator at 37°C and 5% CO₂. Cells were then transfected with Life-Act-GFP (IBIDI) and Paxillin-RFP (EVROGEN). The transfection complex was prepared in Opti-MEM I reduced serum medium (GIBCO) and Lipofectamine 2000 (Invitrogen) was used as a transfection reagent. The amount of DNA/LIPO2000 was determined following the supplier's instruction. Briefly, after 4 h incubation with 1.5 µg of pDNA in lipoplexes, cells were incubated with a medium containing 10% FBS 100 units/mL penicillin, and 100 µg /mL streptomycin. Then, the transfected cells were replated on nanopatterned and flat substrates. Normal growth medium supplemented with 20 mM Hepes was used during the acquisition.

Time-lapse videos were acquired with a Leica TCS SP5 equipped with heated sample holder environment (37°C) and the images were collected with a 63x oil objective. Preliminary experiments were carried out to optimize confocal settings in order to minimize phototoxicity and photobleaching.

Time lapse experiments started 30 min after cell seeding on the substrates and frames were taken every 2 minutes for 12 hours.

Image analysis

Morphometric analysis (area, Feret length, major/minor axis aspect ratio) of focal adhesions was performed using ImageJ software. Confocal images in the green channel were firstly processed using blur command. Blurred image were then subtracted from the original images using the image calculator command. The images were further processed with threshold command to obtain binarized images. Pixel noise was erased using the erode command and then particles analysis was performed in order to extract the morphometric descriptors. Cell area was calculated from confocal images in the red channel (phalloidin). Cells were manually thresholded and cell area was measured with the measure command. Cell polarization was assessed from the same images using the script MomentMacroJ v1.3 (hopkinsmedicine.org/fae/mmacro.htm). Briefly, the macro calculates the second moment of grey scale images. For our purposes, we evaluated the principal moments of inertia (i.e. maximum and minimum) and the cell polarization was defined as the ratio of the principal moments (max/min). The angle of polarization was defined as the angle that the principal axes of inertia form with the reference axes. To determine actin bundle orientation, selected regions of confocal images of TRITC phalloidin stained cells were analyzed with a 2D-FFT program written in matlab. Briefly, the shape of the FFT spectrum of 2D images provides information on the

possible preferential alignments within the image. The orientation of the actin bundles was chosen as the preferential direction of alignment provided by the FFT.

3.2 Results

Topography alters cell shape and FA clustering

MC3T3 cells cultivated on nanogrooved PDMS substrates spread and acquired a polarized morphology already at 4h after seeding (fig. 1).

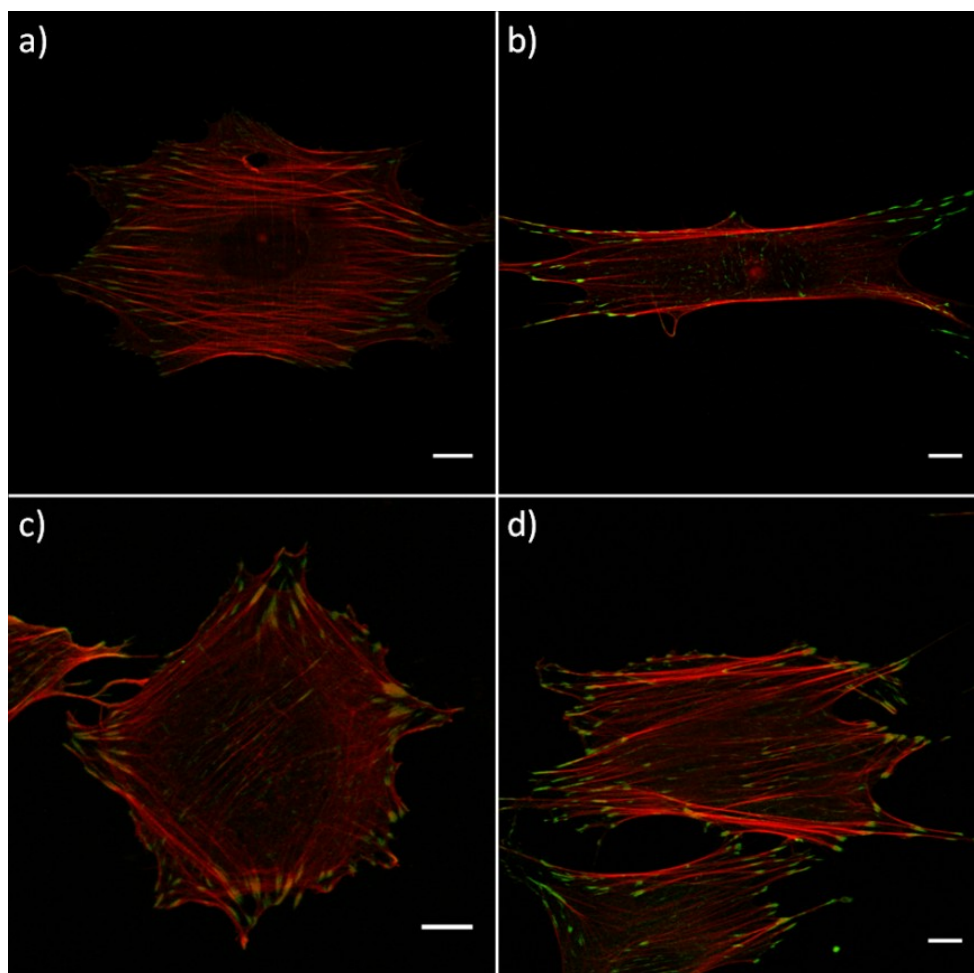


Figure 1: Spreading of MC3T3 cells on nanogrooved (a,b) and flat (c,d) substrates at 4h (a,c) and 12h (b,d) post seeding. Focal adhesion (green) and actin stress fibers (red) were visualized with anti-vinculin antibody and phalloidin respectively (Scale bar, 10 μ m).

Such a polarization, measured as the ratio of the principal moment of inertia, increased with culturing time. At 12h cells exhibited a significantly higher polarization. In both cases, the direction of polarization was coaligned with the pattern direction. On flat surfaces, we observed that cells also attained a polarized shape although to a less extent respect to that observed on the nanopatterns (fig.2a). As expected cells did not show a collective direction of alignment (fig. 2b). Furthermore, cells on nanopatterned PDMS invariably had a significantly (fig.2c) smaller projected area compared to cells on flat surfaces. To better investigate the intimate connections between actin network and cell shape, z-stacks of confocal images of actin fibres were acquired.

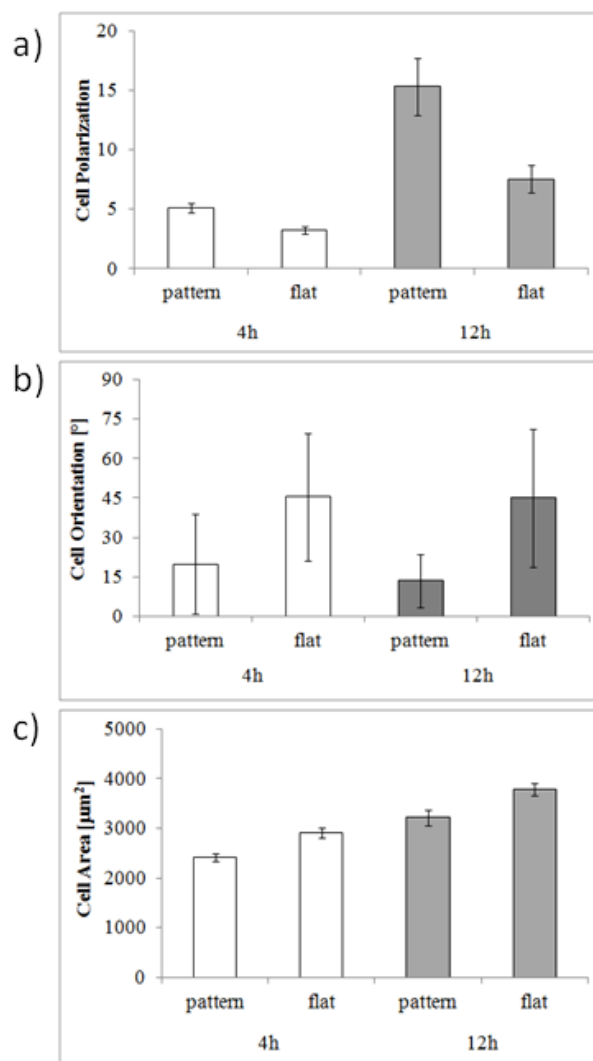


Figure 2: a) histogram of the cell polarization measured as the ratio of the principal axes of the moment of inertia. Error bars represent the standard error of the mean. b) histogram of the orientation of the cell principal axis of polarization with respect to the pattern direction. Error bars represent the standard deviation. c) histogram of the projected cell area. Error bars represent the standard error of the mean. White columns refer to data collected at 4h post seeding. Grey columns refer to data at 12h.

Images of phalloidin stained cells on nanopatterned substrates, collected at different focal planes revealed the existence of two families of fibres. The first one is composed of thin fibres, which were located on the basal plane of the cells and crossed the cell body throughout its width (fig. 3a). Invariably, these fibres were directed orthogonal to the pattern. Such a fibre assembly was observed both at 4h and 12h, although at this culturing time, basal fibres were much thinner. Fibres of the second family were anchored at both extremities on the basal plane and run along the apical surface like tent braces. Furthermore, a considerable fraction of these fibres is positioned above the nucleus (fig. 3b). This observation is consistent to what observed by Kim et al. [12] in different cell types cultivated on glass. Cells on flat PDMS displayed a cytoskeleton with very different morphology. Here, basal fibres appeared more disordered and did not cross the whole cell body but were bound in the region underneath the nucleus (fig. 3c). Apical fibres kept the coalignment with the direction of cell polarization (fig. 3d). Then, we wanted to quantify the mutual orientation of basal and apical fibres in order to establish whether a specific shifting angle existed between the two families of fibres. To this aim, we transformed the images in the frequency domain, with a 2D FFT algorithm, and calculated the angle of preferential alignment of the actin fibres below and above the nucleus. Interestingly, the FFT analysis revealed that basal fibres of cells on nanopatterns are always orthogonal the apical ones, with a very narrow distribution, whereas the orientation of the basal fibres of cells on flat surfaces did not display any relationship with that of the apical fibres and, consequently with the cell polarization axis (fig 3e).

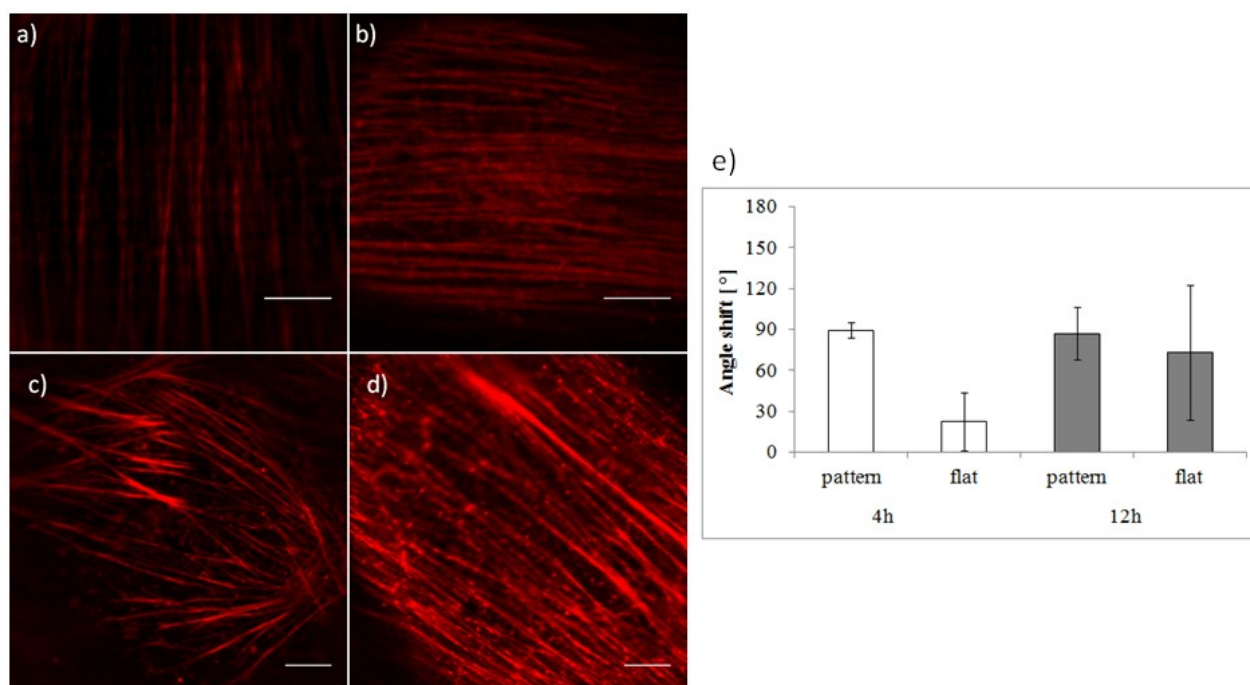


Figure 3: Confocal microscopy sections on the actin filament network at the basal plane (a,c) and apical plane (b,d) of MC3T3 cell on nanograted substrate (a,b) and flat control substrate (c,d) at 4 hours post seeding (Scale bar, 5 μ m). e, Angle shift between the preferential direction of alignment of actin fibres on the basal plane and apical plane. White and grey columns refer to the data collected at 4h and 12h post seeding respectively. Error bars represent the standard deviation.

Since stress fibres terminated, with at least one end, on focal adhesions, we asked whether the differences that were observed in cytoskeletal assemblies also reflected differences in focal adhesion clustering and morphology.

Quantification of the geometrical features of the focal adhesions revealed that FA area, of cells cultivated either on patterned or flat substrates, increased significantly from 4h to 12h. In particular, cells on flat substrates at 12h displayed more extended FAs respect to cells on nanopatterns (fig. 4a). Similarly, FA also grew significantly from 4h to 12h culture, however at 12h FA measured on nanopatterns were significantly longer respect to the flat case (fig. 4b). The presence of the pattern did not affect the FA aspect ratio at short times, i.e. no differences on patterned and flat substrates; however, they were significantly more polarized at 12h post seeding (fig. 4c). Altogether these data demonstrated that the presence of nanogrooves not only limited the overall FA area, but also forced their growth in a specific direction.

Moreover, peripheral FA which possessed higher width and length were connected to stress fibres directed along the pattern direction. FA connected on stress fibres oriented in different directions were shorter or dashed, suggesting the existence of multiple adhesions connected to the same stress fibre (data not shown).

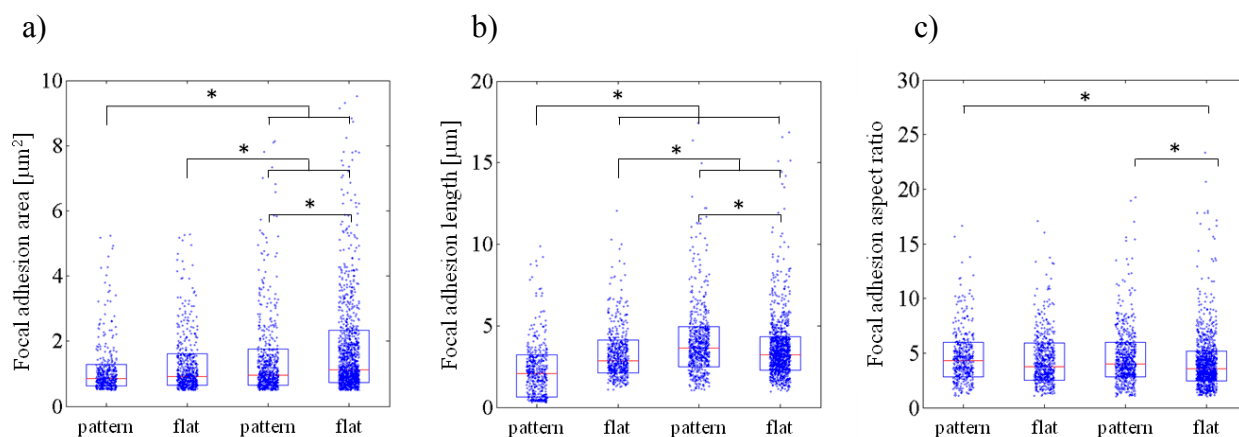


Figure 4: Box plots of the focal adhesion area (a), Feret's length (b) and aspect ratio (c) of cells cultivated on patterned and flat substrates. Individual data points are represented by blue circles. Boxes enclose the data between the 25th and 75th percentile and the red segment denotes the median values of the distribution. Statistically significant differences are marked with the asterisk ($p < 0.05$).

Nanopattern affects actin dynamics and cell polarization

To gain a better insight into the spatio-temporal evolution of the cytoskeleton, time lapse videos of z-stacks of cells transfected with GFP-lifeact and RFP-paxillin were performed. According to the images of fixed and stained cells, basal fibres assembled and were visible already at 1 hour post seeding. On nanopatterned surfaces, basal fibres were directed orthogonal to the pattern direction and were connected with several small paxillin spots (fig. 5a). Interestingly, these fibres were dynamic in nature, i.e. as the cell changed its morphology, basal fibres changed their length accordingly. Basal fibres of cells on control flat substrates displayed a very different morphology as they were thicker and connected to bright and large FAs at their extremities. As the cell spread and moved, basal fibres contracted and eventually disappeared. Occasionally, some fibres fused together to create longer fibres, others could come in close contact creating a Y shaped structure (fig 5b). This assembly was instable and one branch of the Y disassembled quickly, thus recreating a single and straight element.

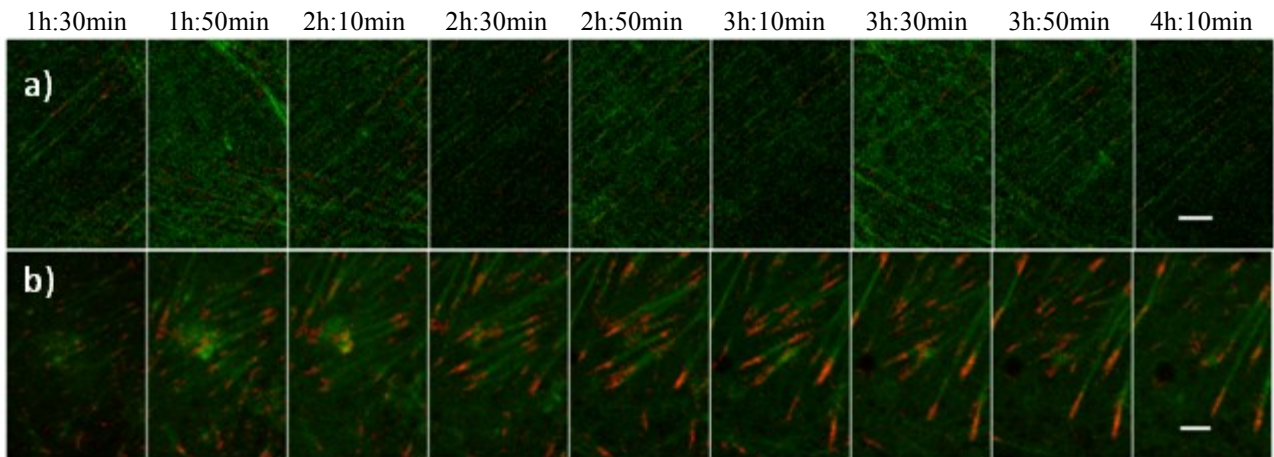


Figure 5: Basal stress fibres dynamics. Time-lapse images of MC3T3 cell seeded on nanograted (a) and flat control substrate (b) expressing Life Act-GFP (green) and Paxillin-RFP (red). Scale bar 5 μm .

The collection of z-stacked images, gave us the opportunity to investigate the dynamics of stress fibre coalignment and cell polarization. In particular we were interested in understanding how the nonograting affected stress fibres formation along with their spatial arrangement. Stress fibres were not fixed entities but moved extensively throughout the time lapse videos. In the early stages post seeding (from 1h up to 4h) whiskers of actin, reminiscent of dorsal stress fibres formed at both cell poles and were mostly aligned along the pattern. The centripetal motion of transverse arcs was particularly evident on the cell's lateral edges

During their motion, transverse arcs merged with the actin whiskers located at the front/rear poles of the cells, thus creating individual stress fibres which passed throughout the cell body and that were almost all aligned with the pattern direction. Especially at the cell periphery, fibres that were not perfectly coaligned with the pattern, terminated with dashed adhesions formed by two or three paxillin rich spots located on the top of adjacent ridges. Such an assembly proved to be unstable as the fibres invariably pivoted around one adhesion towards the pattern direction (fig. 6) This motion ended up with the disappearance of multiple adhesions in favour of a single one on the ridge. Stress fibre rotation was not observed in cells on flat substrates. The formation of dorsal and ventral stress fibres basically followed the pathway described by Hotulainen and Lappalainen [7].

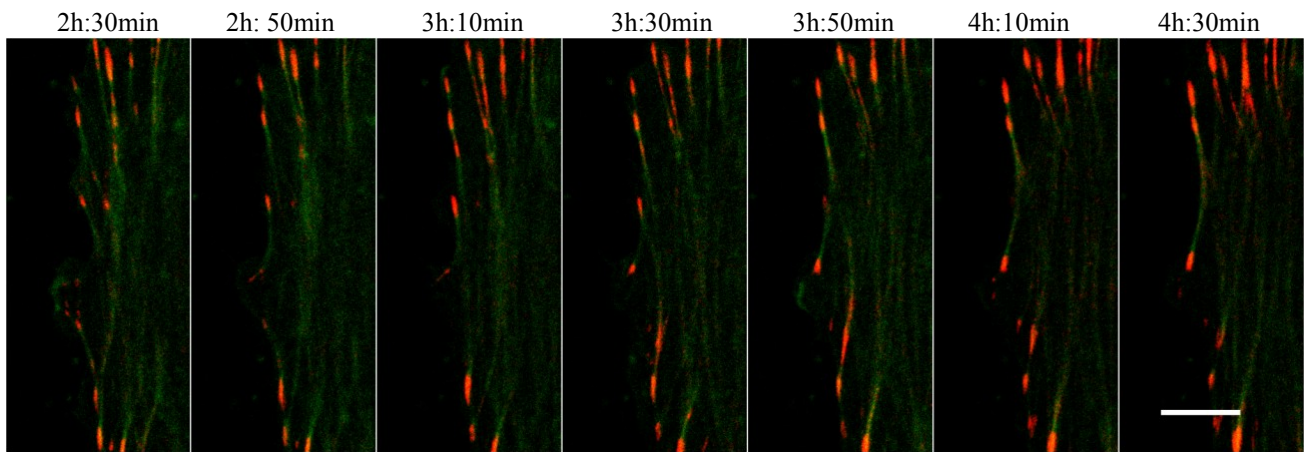


Figure 6: Stres fiber-pattern coalignment. Time-lapse images of MC3T3 cell seeded on nanograted expressing Life Act-GFP (green) and Paxillin-RFP (red). Scale bar 5 μm

The process of stress fibre-pattern coalignment was observed predominantly in the early stages of cell spreading. During this timeframe, we observed an extensive nuclear mobility. In fact, up to 1 hour post seeding nuclei had an oblate shape. As the actin centripetal motion started and the stress fibres came in close contact with the nuclear membrane, we observed a simultaneous nuclear rotation and polarization (fig. 7)

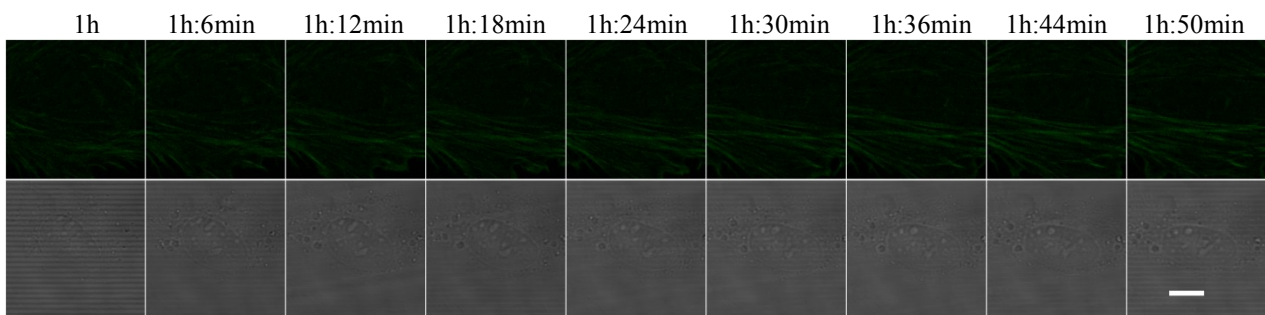


Figure 7: Nucleus Rotation on nanograted substrate. Nucleus (bright field) of MC3T3 cell seeded on nanograted substrate expressing LifeAct-GFP. Scale Bar 5 μm

Once the nucleus rotated and elongated it remained almost stationary. Quantification of nucleus stretching showed that no significant differences were observed in nuclear aspect ratio from 4h to 12h (fig. 8) suggesting that polarization occurred in the early stages after seeding, whereas polarization of the cell body proceeded over 12h. Significantly rounder nuclear shapes were visible in cells seeded on flat substrates. Also in this case, nuclear aspect ratio did not change from 4h to 12h post seeding. To investigate whether apical fibres exerted an increased normal compression on the nucleus, we calculated nucleus thickness of MC3T3 at 12h both on nanopatterns and flat substrates. Thickness did not change significantly between the two cases suggesting that the nucleus deforms in way similar to a confined compression. In particular, nucleus thickness was $5.61 \pm 0.62 \mu\text{m}$ on nanopatterned substrates and $5.85 \pm 1.09 \mu\text{m}$ on control surfaces.

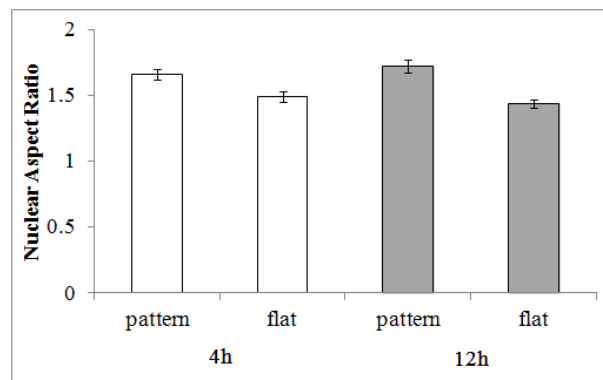


Figure 8: Histogram of the aspect ratio of cell nuclei. Error bars represent the standard error of the mean. White columns refer to data collected at 4h post seeding. Grey columns refer to data at 12h.

Basal stress fibres do not affect nuclear polarization.

Fluorescent stains and time lapse videos highlighted that, two different actin assemblies wrap the nucleus around. To understand whether these two structures behaved in concert we performed a blebbistatin treatment. Blebbistatin inhibits myosin II generated contractility and consequently has a profound influence on stress fibers assembly and FA turnover [13]. After treatment with (15 μM) blebbistatin, MC3T3 displayed a dendritic morphology with a significant number of tails (fig 9 a,b). In particular cells seeded on nanopatterned substrate possessed a disorganized cytoskeleton and stress fibers were only occasionally observed. FAs assumed a dot-like configuration and they were located mainly at cell periphery and in the far end of the tails. Surprisingly, basal (stress) fibers were still detectable, although with a wavy morphology, both at 4h and 12h post seeding. Cell

seeded on flat control and treated with blebbistatin substrates also displayed a non organized actin meshwork and peripheral FAs.

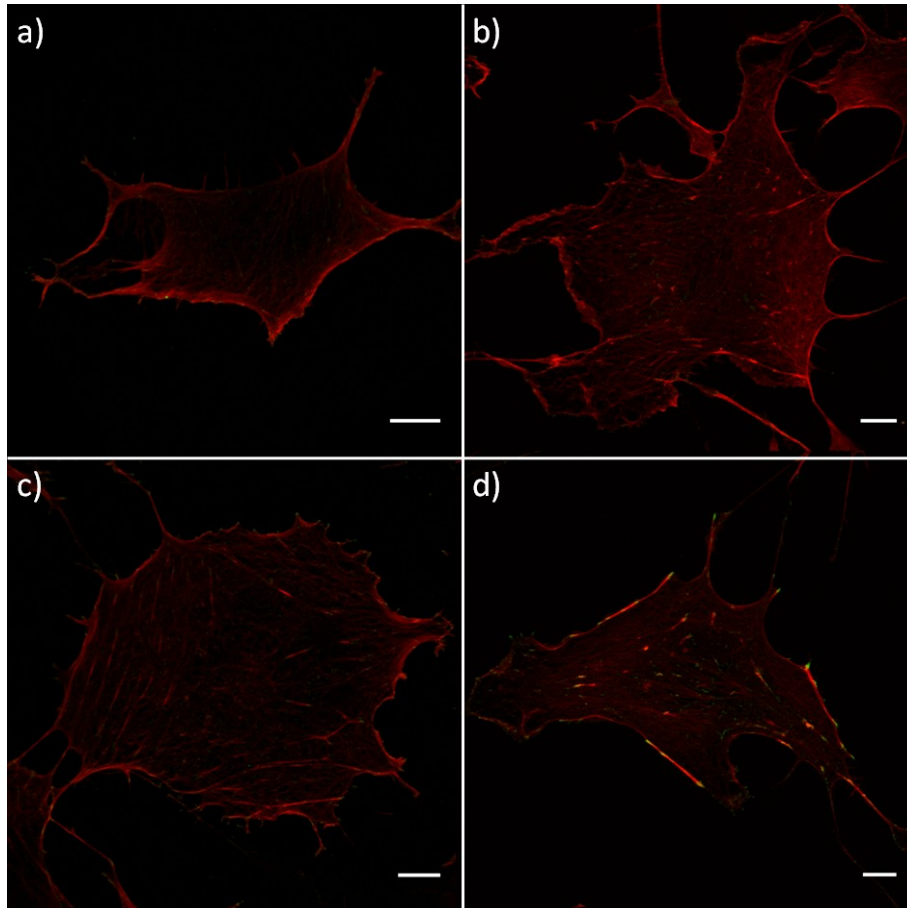


Figure 9: Effect of blebbistatin treatment on actin fiber and focal adhesion assembly. MC3T3 seeded on nanogated (a,b) and flat control (c,d) substrates. Focal adhesion (green) and actin stress fibers (red) were visualized with anti-vinculin antibody and phalloidin respectively at 4 hours (a,c) and 12 (b,d) hours post seeding. Scale bar 10 μ m

However, few basal fiber fragments connected at both ends with FA were still visible together with basal thin fibers, whose morphology was very similar to those detected on nanopatterned substrates (fig 9 c, d). We then wanted to quantify to what extent actomyosin contractility influenced cell and nucleus polarization. Cell polarization, measured as the ratio of the moment of inertia, was unchanged for all the experimental setups except for cell cultivated on nanopatterns for 12h. In this case a 48% loss in polarization respect to untreated cells was recorded. Conversely, nuclear shape, in terms of aspect ratio, proved to be more sensitive to myosin inhibition respect to the cell polarization. In particular, the nucleus of cells cultivated on nanopatterns exhibited a significant rounding after blebbistatin treatment both at 4h and 12h (fig 10). In contrast the nucleus of cells on control surfaces possessed a morphology that remained nearly unchanged with the drug treatment.

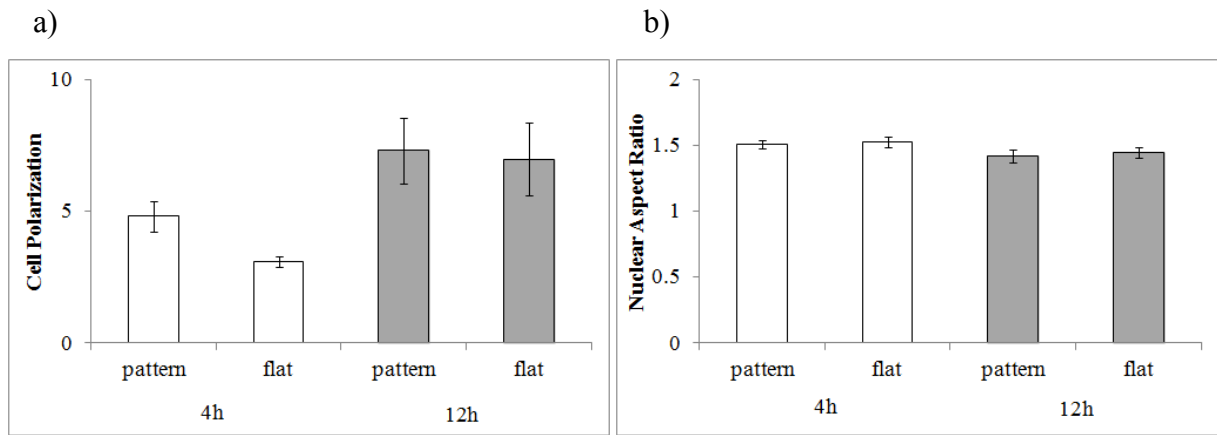


Figure 10. a, histogram of the cell polarization after treatment with blebbistatin for 1h. The polarization was measured as the ratio of the principal axes of the moment of inertia. b, histogram of the aspect ratio of cell nuclei after blebbistatin treatment for 1h. Error bars represent the standard error of the mean. White columns refer to data collected at 4h post seeding. Grey columns refer to data at 12h.

3.3 Discussion and conclusions

Focal adhesion and cytoskeleton mediated signaling are emerging as potent regulators of cell fate and functions [3, 14.] Several strategies have been developed in order to control adhesion processes and modulate cell contractility. Among these, nanotopographies proved to be very effective in doing so. However, the intimate interactions between topographic patterns and cells have not been thoroughly deciphered. Therefore, in order to define the optimal topographic features to govern cell behavior and fate, it is crucial to deeply understand the interplays occurring along the FAs-cytoskeleton-nuclear shape axis.

FAs are the first players that are involved in the process of substrate recognition and force exchange. Furthermore, FAs have often been presented as dynamic entities, owing not only to the fact that they increase their length from dot-like to mature plaques, but also because they have the ability to ‘slide’ in a threadmill-like fashion under the effect of contractile forces [15]. Stress fibres, in turn, change their morphology and potency if they are connected to small or large FAs [16]. Such a dynamic interplay between FAs and stress fibres is expected to be markedly affected by the presence of topographic patterns. In particular, grooves and pits may set constraints over FA dynamics, which impairs stress fibre formation consequently. In this work we investigated, the

interactions between MC3T3 preosteoblasts and topography in the form of nanogratings, in terms of morphological changes and spatial arrangements of FAs and the cytoskeleton. We found that nanotopography affects cell behavior at different levels. Firstly, FAs on conventional flat surfaces can grow and “slide” under the action of stress fibres. However, on nanogrooves, their growth and maturation is hindered since the space available for integrin clustering and engagement on extracellular ligands is limited. This was confirmed by the quantification of FA morphological features of fixed cells. On average, FAs grown along the ridge had a more prolate shape respect to that observed on flat surfaces, whereas FAs located at cell lateral edges were fragmented. This had a profound impact on the cytoskeleton assembly. In more details, stress fibres which were not oriented along to the pattern direction were anchored to FAs that appeared as dashed lines whose discontinuities were produced by the grooves. Such an assembly proved to be unstable and the instability might be explained with simple mechanical considerations. At equilibrium, the pulling force exerted by stress fibres is balanced at both end by the reaction of the FAs connected to the substrate. The area of FAs is adjusted according to the magnitude of the shear force acting on them, so that the shear stress on the FA attains a constant and optimal value, of approximately $5.5 \text{ nN} \cdot \mu\text{m}^2$ [17]. In the case of one of the two fibres extremities terminates with a dashed focal adhesion, the stress exerted on this could be much higher than the optimal value, since the total area of the FA is considerably lower with respect of the average value that is attained along the pattern direction. We observed that in correspondence to the dashed adhesions, fragments vanished except one that grew on the ridge in the direction of the pattern. Presumably, the component of force exerted on the FA along the pattern direction is responsible for this growth. The macroscopic effect of such a rearrangement is a stress fibre rotation around a FA spot which ultimately coaligns along the pattern.

Secondly, we revealed the existence of a subset of actin fibres that followed a different dynamics with respect of stress fibres that are commonly observed on flat substrates [7]. These fibres were found only on the basal plane of cells cultivated on nanogratings which were thin and associated with a sequence of paxillin rich spots. These fibres appeared both at short (4h) and long (12h) culturing times and were always directed across the pattern direction. Moreover, time lapse videos did not reveal any kind of contractility but rather these basal fibres were accommodating cell shape changes by either elongating or shortening. All these features were markedly different from what observed on flat surfaces. Here, basal fibres were predominantly confined in the zone beneath the nucleus and were characterized by a specific turnover: fibre formation and FAs maturation at both ends, contraction and then fibre collapsing. Furthermore, basal fibres of cells seeded on nanopatterns are scarcely affected by myosin II since its inhibition with blebbistain did not affect

their morphology significantly. Altogether these observations suggest a regulatory mechanism of the nanopattern on the spatial arrangement and maturation of the cytoskeleton. Transverse basal fibres remain thin probably because their maturation must be accompanied by the growth of larger focal adhesions. This, however, appears to be hindered on nanogrooved surfaces, which limits stress fibre maturation and hence contractility. On flat surfaces, on the other hand, focal adhesion can grow extensively and this allows the basal stress fibre to generate contractile forces that are responsible for the observed FA sliding (fig 5). A question may arise on why basal fibres on nanopatterned surfaces are always orthogonal to the pattern direction. We have observed basal transverse fibres even in the early periods after seeding (1h and 2h). Therefore, it is likely that basal fibre formation is one of the first events occurring during cell spreading on a nanogrooved surface. At the very beginning the formation of nascent adhesions and focal complexes is a stochastic event which might occur anywhere in the cell membrane contacting the grooved surface. The maturation of the complexes requires actin generated forces, in particular the drag forces exerted by transverse arcs is responsible for the adhesion maturation and the establishment of stress fibres (dorsal stress fibres). If a transverse arc during its centripetal flow engages an adhesion and drags it parallel, or nearly parallel, to the pattern, then the adhesion grows and eventually a stress fibre forms. Conversely, if the drag force is perpendicular, or nearly perpendicular, focal adhesion cannot grow, remaining punctate, and the actin fibre does not mature accordingly and it is not able to generate extensive contractile forces. However the weak forces here generated are sufficient to maintain basal fibres in the orthogonal direction.

The mutual orientation of FAs/actin fibres with the nanopattern dictates the assembly and maturation of the cytoskeleton. This becomes very relevant when considering the interactions between the cytoskeleton and the nucleus. Actin fibres morphology and actin generated forces are directly related to nuclear positioning and shape which ultimately affect gene expression and cell fate [18,19]. Versavel and coworkers [20] observed that lateral compression generated by peripheral stress fibres, regulated the nuclear shape whereas normal compressive forces generated by apical fibres constrained the nuclear height. This work, however, was focused on cells confined on adhesive islands with selected geometrical features. Instead we observed that even the spontaneous polarization of cells on nanopatterned substrates strongly was sufficient to affect nuclear shape. In particular, we found significantly more squeezed nuclei with respect to cells on flat surfaces and such a squeezing was caused by increased myosin generated forces as blebbistatin treatment cancelled the effect of the topographic signal. Taken together these data suggest that a threshold level of intracellular tension, generated by actomyosin contractility, has to build up in order to deform the

nucleus. Nanogratings may have a direct effect on nuclear squeezing, by inducing specific cytoskeletal assemblies and possibly modifying the intracellular stress state.

In conclusion this work report novel findings on the complex topography-FAs-cytoskeleton crosstalk and these might be relevant both in in vivo and in vitro contexts. Firstly, since in vivo most of the cells, are in close contact with tissues which display topographic patterns (e.g. bundles of juxtaposed collagen fibrils, basement membranes) it might be that the peculiar cytoskeletal assemblies that we observed may also occur in vivo and may have a physiologic relevance. Finally, a deeper understanding of the cell-topography interactions is necessary for a rational design of biomaterials surfaces which are able to promote specific cytoskeletal configurations and ultimately nuclear shapes.

3.4 References

- [1] Chen CS, Mrksich M, Huang S, Whitesides GM, Ingber DE. Geometric control of cell life and death. *Science* 276, 1425-1428, 1997
- [2] McBeath R, Pirone DM, Nelson CM, Bhadriraju K, Chen CS. Cell shape, cytoskeletal tension, and RhoA regulate stem cell lineage commitment. *Developmental Cell* 6, 483-495, 2004
- [3] Kilian KA, Bugarija B, Lahn BT, Mrksich M. Geometric cues for directing the differentiation of mesenchymal stem cells. *Proceedings of the National Academy of Science USA* 107, 4872-4877, 2010
- [4] Engler AJ, Sen S, Sweeney HL, Discher DE. Matrix elasticity directs stem cell lineage specification. *Cell* 126, 677-689, 2006
- [5] Thomas CH, Collier JH, Sfeir CS, Healy KE. Engineering gene expression and protein synthesis by modulation of nuclear shape. *Proceedings of the National Academy of Science USA*. 99, 1972-1977, 2002;
- [6] Kanchanawong P, Shtengel G, Pasapera AM, Ramko EB, Davidson MW, Hess HF, Waterman CM. Nanoscale architecture of integrin-based cell adhesions. *Nature* 468, 580 – 584, 2010
- [7] Hotulainen P, Lappalainen P. Stress fibers are generated by two distinct actin assembly mechanisms in motile cells. *J Cell Biol.* 173, 383-394, 2006
- [8] Ventre M, Causa F, Netti PA. Determinants of cell-material crosstalk at the interface: towards engineering of cell instructive materials. *Journal of the Royal Society Interface* 9, 2017-2032, 2012
- [9] Dalby MJ, Gadegaard N, Tare R, Andar A, Riehle MO, Herzyk P, Wilkinson CD, Oreffo RO. The control of human mesenchymal cell differentiation using nanoscale symmetry and disorder. *Nature Materials* 6, 997-1003, 2007
- [10] McMurray RJ, Gadegaard N, Tsimbouri PM, Burgess KV, McNamara LE, Tare R, Murawski K, Kingham E, Oreffo RO, Dalby MJ Nanoscale surfaces for the long-term maintenance of mesenchymal stem cell phenotype and multipotency. *Nature Materials* 10, 637-644, 2011
- [11] Bettinger CJ, Langer R, Borenstein JT. Engineering substrate topography at the micro- and nanoscale to control cell function. *Angew Chem Int Ed Engl.* 48, 5406-5415, 2009
- [12] Dong-Hwee Kim, Shyam B. Khatau, Yunfeng Feng, Sam Walcott, Sean X. Sun, Gregory D. Longmore, and Denis Wirtz. Actin cap associated focal adhesions and their distinct role in cellular mechanosensing. *Sci Rep.* 2012; 2: 555.
- [13] Ana M. Pasapera, Ian C. Schneider, Erin Rericha, David D. Schlaepfer, and Clare M. Waterman: Myosin II activity regulates vinculin recruitment to focal adhesions through FAK-mediated paxillin phosphorylation. *J Cell Biol.* 2010 March 22; 188(6): 877–890.

- [14] Mathieu PS, Lobo EG. Cytoskeletal and focal adhesion influences on mesenchymal stem cell shape, mechanical properties, and differentiation down osteogenic, adipogenic, and chondrogenic pathways. *Tissue Eng Part B Rev.* 2012 Dec;18(6):436-44.
- [15] D. Raz-Ben Aroush , R. Zaidel-Bar , A. D. Bershadsky and H. D. Temporal evolution of cell focal adhesions: experimental observations and shear stress profiles. *Soft Matter*, 2008, 4, 2410-2417.
- [16] Goffin JM, Pittet P, Csucs G, Lussi JW, Meister JJ, Hinz B. Focal adhesion size controls tension-dependent recruitment of alpha-smooth muscle actin to stress fibers. *J Cell Biol.* 2006 Jan 16;172(2):259-68.
- [17] Balaban NQ, Schwarz US, Rivelino D, Goichberg P, Tzur G, Sabanay I, Mahalu D, Safran S, Bershadsky A, Addadi L, Geiger B. Force and focal adhesion assembly: a close relationship studied using elastic micropatterned substrates. *Nat. Cell Biol.* 3, 466–472.
- [18] Khatau SB, Hale CM, Stewart-Hutchinson PJ, Patel MS, Stewart CL, Searson PC, Hodzic D, Wirtz D. A perinuclear actin cap regulates nuclear shape. *Proc Natl Acad Sci U S A.* 2009 Nov 10;106(45):19017-22.
- [19] Gupta S, Marcel N, Sarin A, Shivashankar GV. Role of actin dependent nuclear deformation in regulating early gene expression. *PLoS One.* 2012;7(12):e53031.
- [20] Versaevel M, Grevesse T, Gabriele S. Spatial coordination between cell and nuclear shape within micropatterned endothelial cells. *Nature Communications* 3 671, 2012.

Chapter 4

Microtopographies to control cell migration by interfering with surface probing and focal adhesion assembly

Biological tissues display a vast variety of topographies such as fibrils, fibre bundles, pits and protrusions, whose characteristic dimensions span from tens of nanometers up to the micronscale [0-0]. It is therefore reasonable to expect that the presentation of topographic signals is one of the strategies that Nature adopts to impart cells with specific orders which eventually dictate their behaviour. In fact, many works demonstrated that patterned substrates strongly influence cell adhesion, migration and differentiation, suggesting that the use of topographic signals might be a potent strategy to control and guide cell functions [0-0]. These studies show novel routes to design bioinspired surfaces for in vivo applications and several techniques proved to be adequate to produce micro and nano-patternes with high precision and long range order [0,0]. Yet, the implementation of such technologies for the production of biomedical devices is still in its infancy. This limitation is mainly caused by our incomplete knowledge on how cellular interactions with topographic signals develop. To make things more complicated, cell responses vary enormously according to topographic features and dimensions, which make it difficult to identify those characteristic dimensions which are relevant in biomedical applications.

In an in vivo context, it is desirable to control specific cell processes like migration, proliferation and tissue biosynthesis. Despite the large numbers of works that have been developed so far on cell-topography interactions, a consensus on which settings of topographic features elicit specific cell functions has not been reached yet. For example, while certain combination of topographies promote cell alignment and migration, others report a different trends [0,0].

This raises the fundamental question on how cells perceive topographies. Many studies pointed out that filopodial probing and focal adhesion formations are key steps in the recognition of and reaction to material surface characteristics. Filopodia are thin (0.1-0.3 μm) and few micron long protrusive processes that are constituted by parallel bundles of filamentous actin [0]. Their tips

display molecular receptors like integrins and cadherins, making filopodia the tactile sensors for the establishment of contacts in the extracellular space. Cell adhesions are dynamic molecular complexes for which formation, maturation and disassembly phases can be distinguished [0]. Nascent adhesions initiate with the binding of integrins to extracellular ligands. Under adequate conditions, integrins and additional intracellular proteins are recruited to the adhesion site, creating macromolecular complexes referred to as focal adhesions. These can be several micron long and are responsible to transmit cell generated forces to the extracellular space, thus enabling cell adhesion and migration. Therefore, the dynamics of filopodial probing and subsequent adhesion formation and maturation, ultimately govern cell-material crosstalk. Accordingly, changes in the spatial arrangements and dimensions of adhesion sites may interfere with the probing and cell adhesion mechanisms, eventually altering cell behaviour.

Along this line, topography might provide cells with preferential zones for attachment while making others inaccessible. This notwithstanding, the presentation of a topographic signal cannot prescind from the chemical characteristic of the surface, which is known to affect adhesion formation and maturation. In particular, surface hydrophilicity alters the presentation of ligands on the surface and indeed changes in material wettability have a profound effect on focal adhesion assembly [0]. The vast majority of studies on topographic signals, mainly dealt with the geometrical features of the signal itself. Conversely, only few studies investigating the synergistic effect of topographic patterns and hydrophobic/hydrophilic properties of the surface have been reported so far.

Therefore the use of ordered structures whose characteristic dimensions and chemical surface properties perturb probing and adhesion formation, might give novel insights into cell-material interaction thus providing important elements for tailoring biomaterial surfaces with cell-instructive commands.

In this study we investigated the synergistic effect of topographic signals and chemical characteristics on cell adhesion and migration. To this aim, we used micrograted polydimethylsiloxane (PDMS) substrates having feature dimension that might in principle interfere with the cell probing machinery, whereas surface chemical modifications were performed to modulate hydrophobic / hydrophilic properties by means of oxygen plasma treatment in order to affect focal adhesion formation and maturation. Our data demonstrate that a strong guidance in cell migration arises either when a 5 micron gap between adjacent ridges exists or when ridge width is smaller than mature focal adhesions length. In the first case, filopodial probing is the mechanism that is hindered causing the cell to not perceive adjacent ridges. In the second case, focal adhesions growing across the pattern cannot withstand the contractile forces of the cytoskeleton and collapse.

These results might provide an opportunity to modulate topographic features and surface properties in order to control cell dynamics, i.e. random vs directed migration, on biomaterial surfaces.

4.1 Experimental

Preparation of micropatterned substrates

Patterned substrates were obtained by replica molding of PDMS (Sylgard 184, Dow Corning Corporation, Michigan, USA) on silicon masters provided by Scriba Nanotecnologie (Bologna, Italy). The patterns consists of an area of 1 cm² containing parallel and straight channels having ridge to groove width ratio of 1:1. Two pattern features were used, either 2 μm or 5 μm wide and depth of 1 μm for both patterns. PDMS was prepared by mixing elastomer base and curing agent at 10:1 weight ratio. The solution was degassed, poured onto the Si master and then cured at 60°C for at least 2 hours. Control (flat) PDMS substrates were produced by pouring the base and curing mix on a 35 mm polystyrene Petri dish (Corning, Corning, NY, USA) and curing at room temperature for 24 hours.

For cell culture experiments, PDMS samples were either treated with oxygen plasma or left untreated. Plasma treatment was performed with a Plasma Femto (Diener, Germany) equipped with 13,56MHz 100W generator for the plasma excitation.

Untreated substrates were sterilized in autoclave while plasma treated samples were sterilized under UV for 10 minutes. Both substrates were incubated with serum supplemented culture medium (10%) overnight prior to cell culturing experiment. Geometrical features, processing and sample designation are reported in Tab. 1.

Designation	O ₂ plasma treatment	groove width [μm]	ridge width [μm]	feature depth [μm]	sterilization method
2 μm noPT	×	2	2	1	autoclave
5 μm noPT	×	5	5	1	autoclave
flat noPT	×	-	-	-	autoclave
2 μm PT	✓	2	2	1	UV
5 μm PT	✓	5	5	1	UV
flat PT	✓	-	-	-	UV

Table 1. Summary of the substrates used in the study, reporting geometrical features, surface treatment and sterilization method

Cell Culture

MC3T3-E1 preosteoblasts (American Type Culture Collection, ATCC, Manassas, VA, USA) were cultured in α MEM with deoxyribonucleosides, ribonucleosides and 2 mM L-glutamine (Gibco Life, Grand Island, NY), supplemented with 10% fetal bovine serum (Gibco), penicillin (100 units/ml), streptomycin (100 μ g/ml). The cells were incubated at 37°C in a humidified atmosphere of 95% air and 5% CO₂ and the culture medium was changed every two days. After 3 days of culture, cells were detached with trypsin/EDTA (0.25% w/v trypsin / 0.02 mM EDTA) (Gibco) and seeded on microgrooved or flat substrates at $2 \cdot 10^3$ cells/cm² density.

Spreading Area and Immunofluorescence analysis

Actin bundles of cells cultured on noPT and PT substrates were stained with TRITC conjugated phalloidin at specified time points. In particular, cell cultures were fixed at 5, 30, 60, 90, 120 minutes and 24 hours after seeding. Cell fixation was performed with 4% paraformaldehyde for 20 min and then permeabilized with 0.1% Triton X-100 (Sigma, St. Louis, MO, USA) in PBS 1x. Actin staining was done by incubating samples with TRITC phalloidin (Sigma) in PBS for 30 min at room temperature. Images of fluorescent cells were collected with a fluorescence inverted microscope (IX81, Olympus, Tokyo, Japan) equipped with an ORCA 2.8 digital camera (Hamamatsu Photonics,

Japan). Cell area was evaluated with the command Analyze Particles of ImageJ (vers. 1.44). At least 15 cells were collected and analyzed for each time point and each substrate.

Immunofluorescence staining was carried out as follows. Cells were fixed and permeabilized as described above at 2 and 24 hours after seeding on noPT and PT substrates. Samples were blocked in PBS/BSA 0.5% solution for 10 min, and then were rinsed twice in PBS. Vinculin was first recognized by anti-vinculin monoclonal antibody (Sigma) overnight at 4°C, followed by labeling with anti-mouse IgG-FITC antibody (Alexa Fluor® 488 Goat Anti-Mouse IgG, Invitrogen, Carlsbad, USA) for 30 min at room temperature. Actin staining was performed as described above. Samples were thoroughly rinsed in PBS and mounted on glass slides. Images of fluorescent cells were collected as previously described. On these images, the focal adhesion and filopodia length were measured with the command “measure” of ImageJ software. Concerning focal adhesions, only those extending in the longitudinal direction of the patterned substrates were taken into consideration for the length assessment, whereas only those filopodia not displaying visible vinculin spots were measured.

Time Lapse experiments

Cell migration experiments started 6h after cell seeding on the substrates. Briefly, preosteoblasts were cultured on PT or noPT substrates. Afterwards, at least 6 representative regions per substrate were acquired in bright field each 10 minutes for 18 hours. Time-lapse videos were analyzed with Metamorph (ver 6.1) in order to extract cell trajectories. Winderose plots of each experiment were plotted. Quantitative data on cell motility were calculated from individual cell displacements. Instantaneous cell speed was defined as:

$$v = \left\langle \frac{\sqrt{[(x_{t+\Delta t} - x_t)^2 + (y_{t+\Delta t} - y_t)^2]}}{\Delta t} \right\rangle$$

in which x_t and y_t are the position of cell centroid at time t , Δt is the time interval and the operator $\langle \cdot \rangle$ denotes the average on all time points and cells.

Directionality was assessed by evaluating the total movement of each cells along and across pattern direction in an analogous manner as described by Biela et al. [0] in symbol,

$$M_x = \sum_t \sqrt{(x_{t+\Delta t} - x_t)^2} , \quad M_y = \sum_t \sqrt{(y_{t+\Delta t} - y_t)^2}.$$

If the directional index M_y/M_x is close to one, cells perform a perfect random walk. In the case of $M_y/M_x < 1$ cells migrate preferentially along pattern direction.

4.2 Results

Early events in cell adhesion

Few minutes after seeding, cells were predominantly round in shape and extensive membrane ruffling occurred all around cell periphery. Small membrane processes were continuously projected out and retrieved, but only a limited number of these became well defined, growing in width and length. Once these stabilized, ruffling was observed exclusively on the outermost edge. A round to polarized transition of cell shape usually occurred within 90 minutes (Fig. 1). In particular, cell polarization was anticipated by an abrupt, transverse cell contraction. On flat substrates, as expected, cells polarized in random directions. Conversely, almost all the cells elongated along the 5 micron wide pattern with the cell body being suspended on the top of the ridges. On the 2 micron patterns, cells tended to polarize along pattern direction initially, however a considerable fraction of them did so randomly. Membrane ruffling of polarized cells was predominant at the leading and trailing edge, whereas minor membrane activity was observed along cell body. Moreover, during the late stages of the adhesion and spreading, polarized cells kept elongating along their major axis and only a modest cell body translocation was observed.

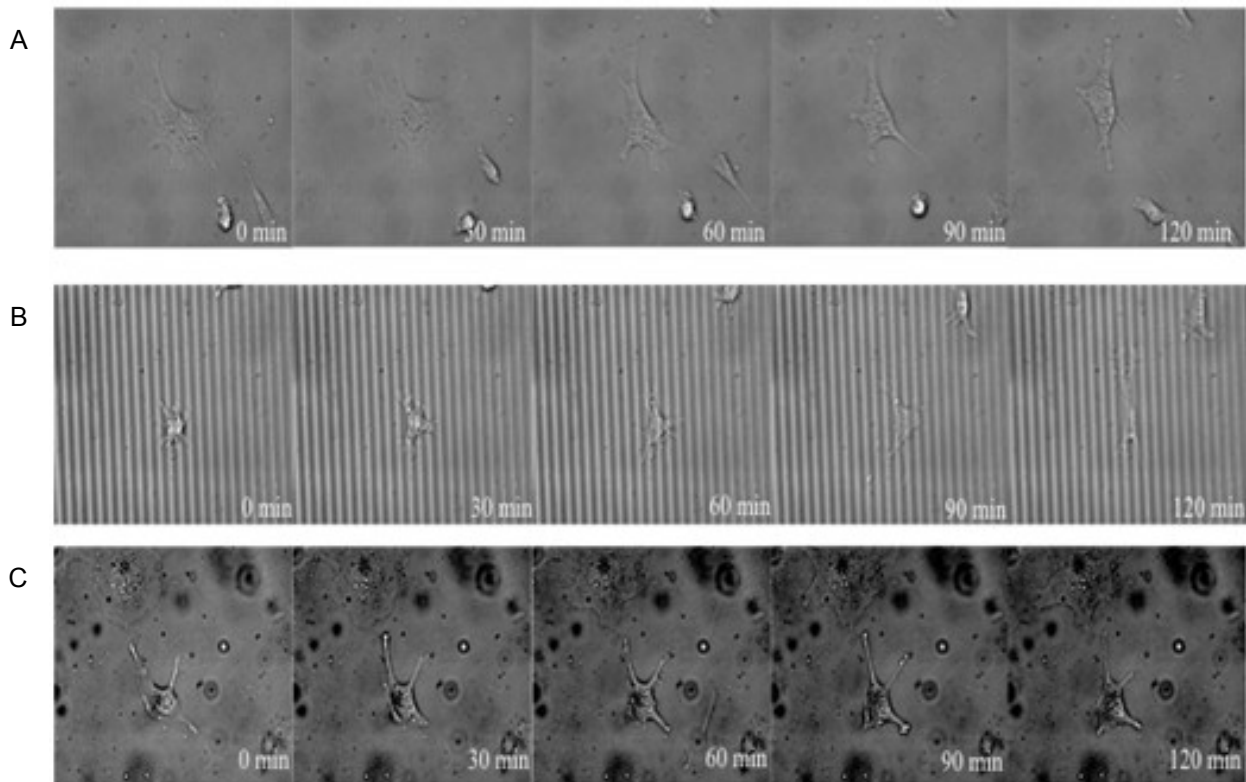


Figure 1. Bright field images of MC3T3 on the substrates, acquired every 30 minutes. (A) 2 μm noPT. (B) 5 μm noPT. (C) Flat noPT.

In order to quantify the kinetics of cell spreading, MC3T3 were stained with phalloidin and observed in fluorescence at different time points. Cell on untreated surfaces underwent spreading soon after seeding. Cell area reached a plateau value within 90 minutes after plating. After this period cell area oscillated around a mean value, indicating extension/retraction events. Such a mean value does not depend on the presence of the pattern. However, cells on flat surface were characterized by a faster spreading rate than cells on 5 micron, whereas cells on 2 micron displayed an intermediate behaviour (Fig. 2A). Plasma treatment had a profound effect on the plateau area value, which was higher and faster respect to that measured on untreated surface (Fig. 2B).

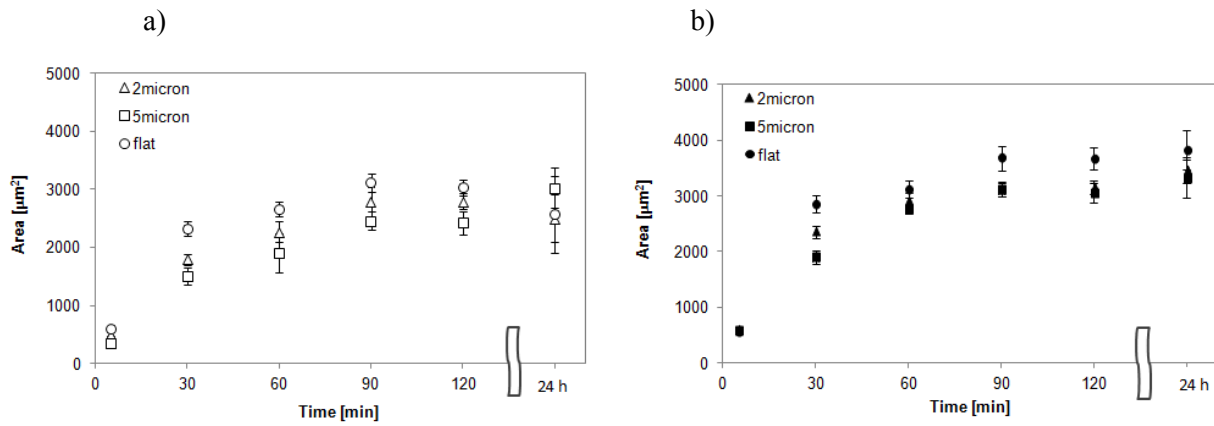


Figure 2. Cell spreading kinetics evaluated as time evolution of the cell projected area. (A) Untreated substrates. (B) Plasma treated substrates.

Long times cell migration analysis

The trajectories described by MC3T3 cells migrating on untreated substrates in 18 hour time interval are reported in the windrose plot of Fig. 3A. In the case of patterned surfaces, the horizontal axis defines the direction of the pattern. Cells on 2 μm noPT and Flat noPT substrates behaved similarly, with cell tracks distributed isotropically on the plane. A strong trajectory/pattern coalignment was observed in the case of cells on 5 micron patterns and most of the trajectories lied on a 200 μm wide horizontal stripe across the horizontal axis.

Surprisingly, cell migrating on plasma treated substrates displayed a very different behaviour both in terms of directionality and speed. As depicted in Fig. 3B, trajectories on both 2 μm PT and 5 μm PT substrates were coaligned with the pattern direction.

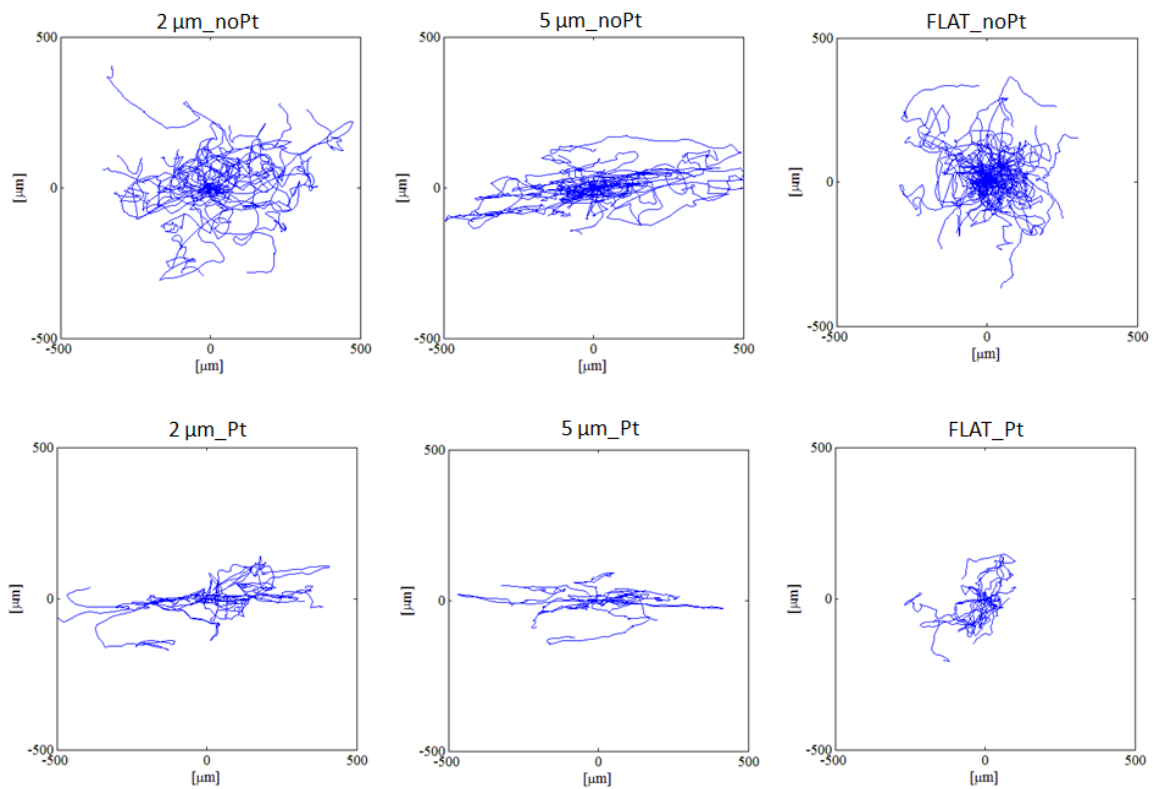


Figure 3. Windrose plots of the trajectories described by cells in 18 hours. (A) untreated substrates. (B) Oxygen plasma treated substrates.

Accordingly, the quantitative analysis of alignment of cell migration through the evaluation of the directional index, revealed a high trajectory pattern coalignment in the case of 5 μm , both PT and noPT, whereas only the tracks of 2 μm PT exhibited a considerable alignment with the pattern direction (Fig. 4). As expected, the directional index value 2 μm noPT showed a modest alignment, whereas the corresponding value of flat substrates is close to 1, reflecting an isotropic movement. Migration analysis also revealed higher instantaneous speed of cells migrating on untreated surfaces respect to plasma treated ones. Furthermore, cells migrating on flat substrates, either PT or noPT, invariably displaed a slower speed (Fig. 4).

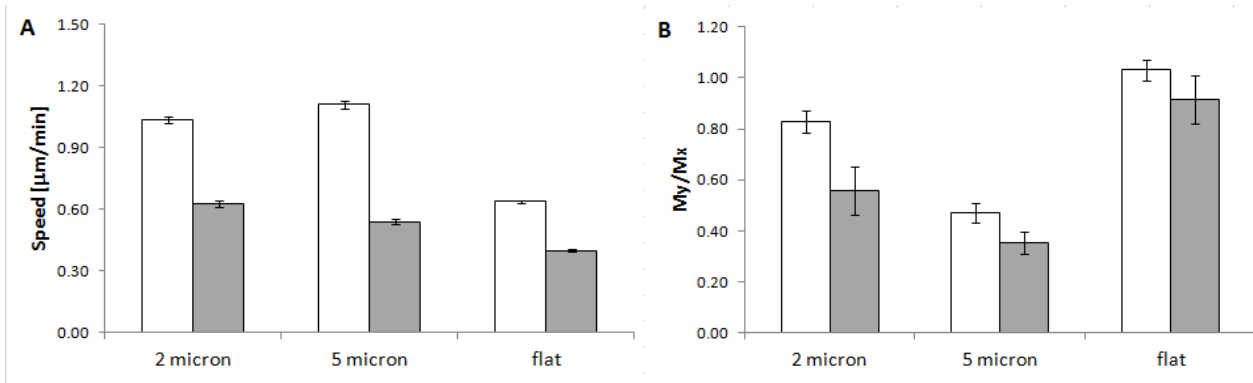


Figure 4. Instantaneous cell speed (A) and directional index (B). White bars represent cells on untreated substrates. Grey bars represent cells on plasma treated substrates

Adhesion and Cytoskeleton assemblies

Figure 5 shows images of cells cultivated on untreated substrates at 2 and 24 hours after seeding. Cells displayed cytoplasmic vinculin after 2 hours post seeding. Small focal adhesions were localized predominantly in the peripheral areas of cells cultivated on 2 μm, 5 μm and Flat noPT substrates. In particular, vinculin clusters of cells on 5 μm noPT were mostly present at the tip of the cell processes, which extended on the top of the ridges. Vinculin spots were invariably colocalized with the distal extremities of actin bundles. Actin bundles were readily observable on the three substrates. Cell contour and intracellular structures mostly lied on the same focal plane suggesting that cells adhered on the pattern ridges and membrane did not come in conformal contact with substrate recesses. No fibres-pattern coalignment was observed on 2 μm noPT, whereas arrays of parallel stress fibres traced out pattern direction in cells on 5 μm noPT, especially within peripheral cell processes protruding on the ridges. At 24 hours post seeding, vinculin spots were still localized in the peripheral region of the cells and at the end of stress fibres. However, cells on 2 μm noPT and Flat noPT samples displayed more defined vinculin spots with respect to those observed at 2 hours. Conversely, cells on 5 μm noPT patterns possessed a higher amount of diffused cytoplasmic vinculin. Actin bundles of cells on 5 μm noPT were predominantly coaligned with pattern direction and conferred cells with a spindle like structure. On 2 μm noPT, cells had a polarized morphology with mature stress fibres and transverse arcs, yet no fibres-pattern coalignment was observed. A similar cytoskeleton is observed in cells cultivated on flat substrates.

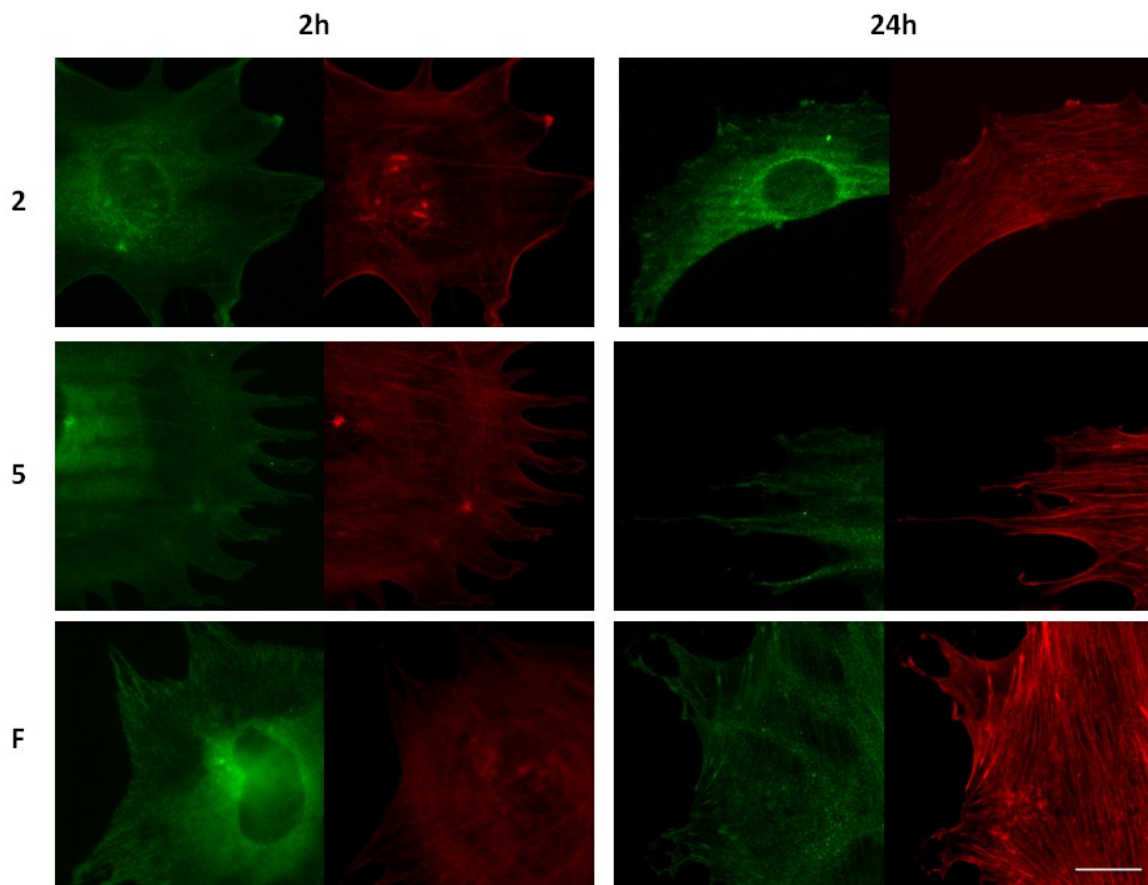


Figure 5. Immunofluorescence stain for vinculin (green) and actin (red) performed after 2 hours (A) and 24 hours post seeding of cells on untreated substrates. Bar is 20 μm .

Immunofluorescence images and cytoskeleton assemblies of cells cultivated on plasma treated substrate are reported in Fig. 6. Cells invariably showed more defined focal adhesion plaques, even at 2 hours post seeding. Most of them resided in the cell periphery, whereas additional focal adhesions became evident beneath the central part of the cell body.

Cytoskeletal assemblies also displayed marked differences respect to the noPT substrates with thick and mature stress fibres, both at 2 and 24 hours post seeding. In this case, however, a good pattern/stress fibre coalignment was observed for both 2 μm PT and 5 μm PT. Also in this case, cells were anchored on the top of the ridges.

Focal adhesion lengths for cells cultivated on PT and noPT substrate are reported in Fig. 7. Focal adhesions of cells on noPT substrates were significantly shorter and thinner respect to those observed in cells on PT substrates. Moreover, cells on 2 μm PT and 5 μm PT exhibited longer focal adhesions respect to those measured on Flat PT.

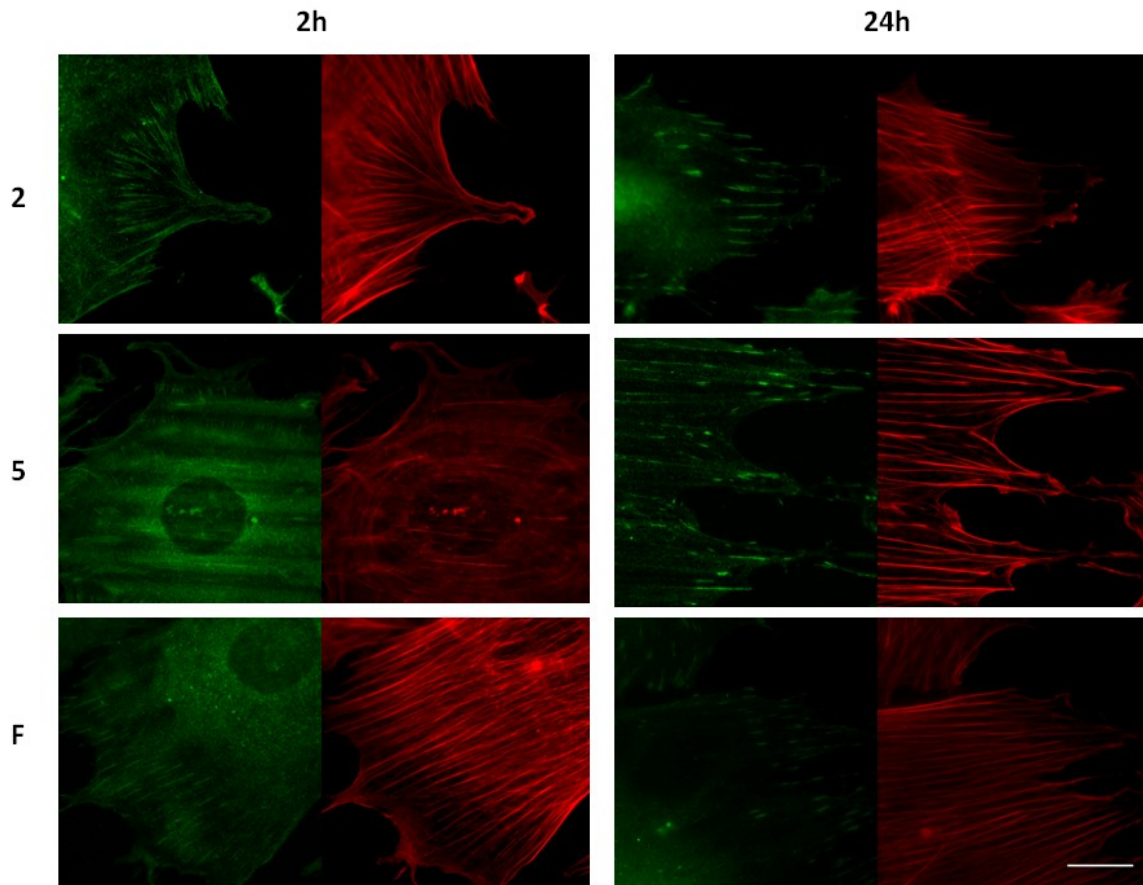


Figure 6. Immunofluorescence stain for vinculin (green) and actin (red) performed after 2 hours (A) and 24 hours post seeding of cells on plasma treated substrates. Bar is 20 μm .

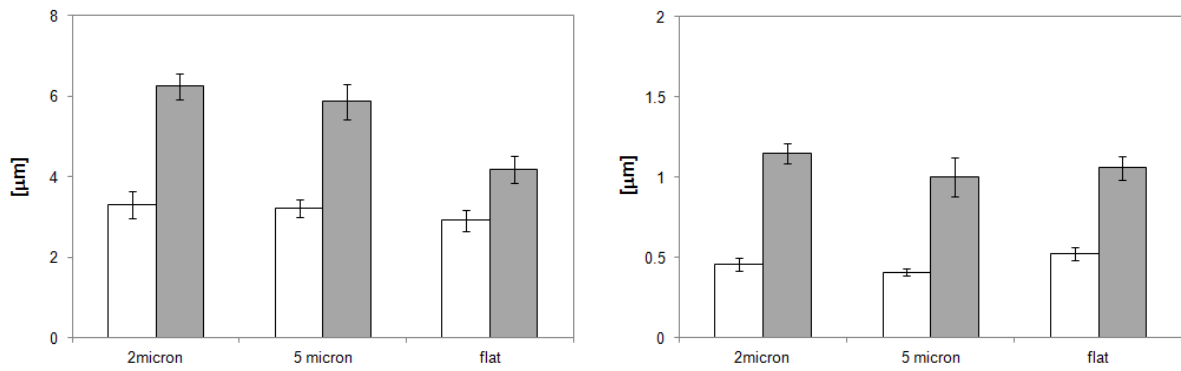


Figure 7. Focal adhesion length (A) and width (B) of cells cultivated on patterned and flat substrates. White bars refer to untreated substrates. Gray bars refer to plasma treated substrates.

Filopodia length at 2 and 24 hour after seeding was measured on phalloidin stained cells cultivated on patterned and flat substrates. Filopodia were mostly straight in shape and only occasionally branches were observed. The distribution of lengths was contained within the 1 to 6 micron range and most of the observed filopodia had length comprised within the 2 to 5 micron range (Fig. 8A-B). This occurs on all the substrates, independently from the surface treatment.

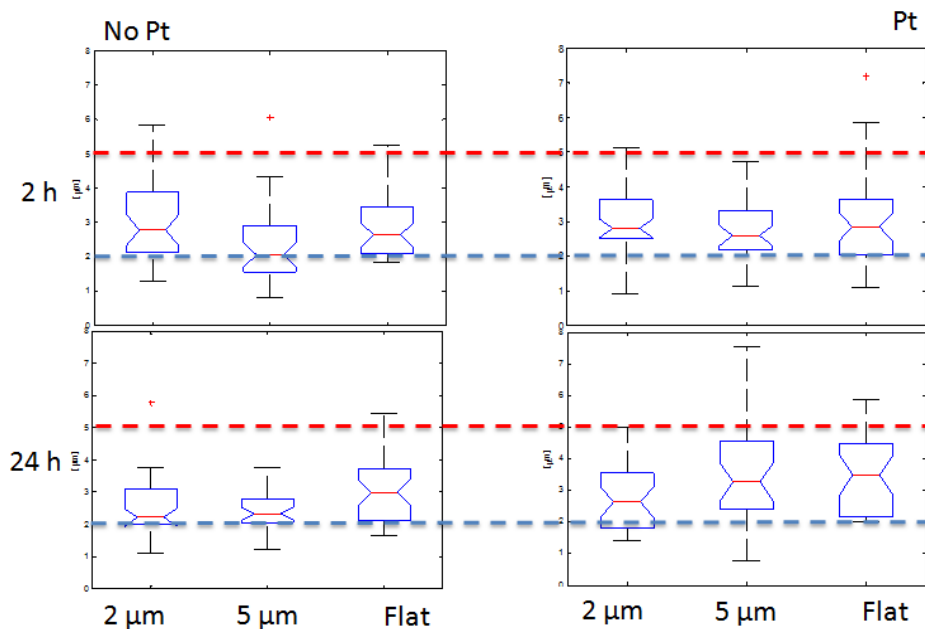


Figure 8. Filopodia length of MC3T3 after 2 hours post seeding (top) and 24 hours post seeding (bottom). The length assessment refers to cells cultivated on untreated substrates (left) and plasma treated substrates (right).

4.3 Discussion

Adequate integration and cellular colonization of biomaterials is a central aspect to improve functionality and long term stability of implants. To date, various strategies exploiting different arrays of stimuli, have been pursued in order to guide cells to the implant site and controlling their behaviour therein. However, the optimal set of stimuli that is able to elicit the desired cell response has not been identified yet. Topography is a potent signal that proved to be very effective in affecting cell adhesion, proliferation and migration. Topographic patterns can be embossed on

artificial surfaces great accuracy. Owing to these advantages, several types of devices, presenting patterned surfaces have been fabricated and tested for various applications. For example Curtis et al. proposed a micropatterned PDMS sheath for in situ tendon repair which proved to be very effective in guiding collagen biosynthesis and assembly with normal histology [0]. More recently, Divya Rani et al. [0] reported improved in vivo osteointegration of specific nanopatterned titanium implants. Taken together these data demonstrate the effectiveness of topography in *in vivo* settings, where the spatial and temporal stability of the presented signals is key central. Yet, the best way to present topographies, in order to elicit the desired cell functions, has not been defined. This limitation mainly arises from our modest understanding of the basic principles that regulate cell-topographic pattern interactions. In order to gain a better understanding on the way cells perceive and react to topographies, we used micrograted substrates with features having characteristic lengths that interfere with cell filopodial probing and focal adhesion establishment and growth. These sequential processes are known to play a central role in the recognition of the extracellular space.

In conventional cell culture experiments, topographic patterns are known to alter surface wettability and to adsorb serum proteins non uniformly [0]. This creates preferential zones for the adhesion plaques to establish and grow. The cell traction machinery constituted by actin stress fibres, which is responsible for cell polarization and migration, is also affected by the geometrical features of the adhesion plaques and hence by the spatial distribution of adsorbed proteins. In the long run, ordered topographic patterns, in the form of gratings and grooves, might produce pathways for the cell adhesion plaques, thus altering spreading and cell migration [0,0].

In fact, the presence of microtopography significantly alters the spreading kinetics (Fig. 2a) and improves the directionality of cell motion (Fig 3a). In particular, cells on 5 μm noPT describe trajectories that are highly coaligned with the pattern direction and only occasionally cell translocations across the pattern occur. 2 micron patterns affect direction of motion to a much less extent, yet a certain degree of pattern-trajectories coalignment is observed (Fig. 4). These results, however, become very different in the case of improved surface hydrophilicity through oxygen plasma treatment. In particular, spreading rate is faster and mean cell area values are higher with respect to untreated surfaces (Fig. 2b). Most surprisingly, the confinement of cell migration, i.e. coalignment of cell translocations with pattern direction, is largely improved when plasma treatment is performed (Fig. 3b). In fact, cells on 2 μm PT display a migratory behaviour which shares many similarities with what observed on 5 μm PT (Fig. 4). This remarkable change in pattern recognition and response suggests that modifications in the filopodial probing mechanism or focal adhesion formation may occur when ligand presentation is altered. From our results, filopodial

length is not significantly affected by the chemical modification of the surfaces, being the distribution of lengths always enclosed within a 1 to 6 micron range (Fig. 8). This characteristic length defines the size of the pericellular space in which new contacts can be formed. On the contrary, large differences in cytoskeleton assemblies and focal adhesion length are observed when plasma treatment is performed. In particular, focal adhesions are short and thin on hydrophobic surfaces and, if there is enough space available, they can grow up to 3 microns in length (Fig. 7a). On plasma treated surfaces, instead, focal adhesions are longer and wider and can reach 6 microns in length wherever possible (Fig. 7b). These adhesion plaques are only visible either on flat surfaces or on the patterned substrates along the ridge direction. The different assemblies of focal adhesions reflect also differences in motility. In particular, cells exhibiting small adhesions, as observed on noPT, migrate with higher speed compared to PT substrates. This arises from the extended lag times cell have to spend to build and disassemble large macromolecular adhesion complexes, which results in a slow migration speed [0]. Interestingly, cells on Flat noPT substrates possess a slower speed respect to 2 μm noPT and 5 μm noPT, even though their focal adhesions have comparable lengths. This is probably due to the increased number of focal adhesions that are usually observed on flat surfaces compared to textured ones [0]. Moreover, the differences in adhesion dimensions that we have observed are consistent with the results of Llopis-Hernández et al. [0] who reported enhanced focal adhesion formation on more hydrophilic surfaces, which is explained by an increased availability of binding domains of the physisorbed protein layer. Several straight but dashed adhesions are found in the transverse direction of 2 μm PT. Interestingly, these peculiar assemblies are connected by thick isolated actin bundles, suggesting that dashed adhesion indeed might belong to the same entity (Fig. 9). According to Balaban et al. [0], actin generated forces regulate focal adhesion area in order to maintain shear stress at adhesion site at constant value (5.5 $\text{nN}\cdot\mu\text{m}^{-2}$). If focal adhesions growth cannot keep up with increasing tensile forces, being geometrically constrained, the resistance in the transverse direction is reduced owing to a less extended contact area, In fact, we measured that the total length of a fragmented focal adhesion is 3.73 ± 0.31 . Therefore, adhesion sites in the transverse direction have a higher probability of disassembling, whereas longer and mature adhesions that elongate along the ridges are more stable. This results in polarization of cells along the pattern direction with an increased polarization of migration.

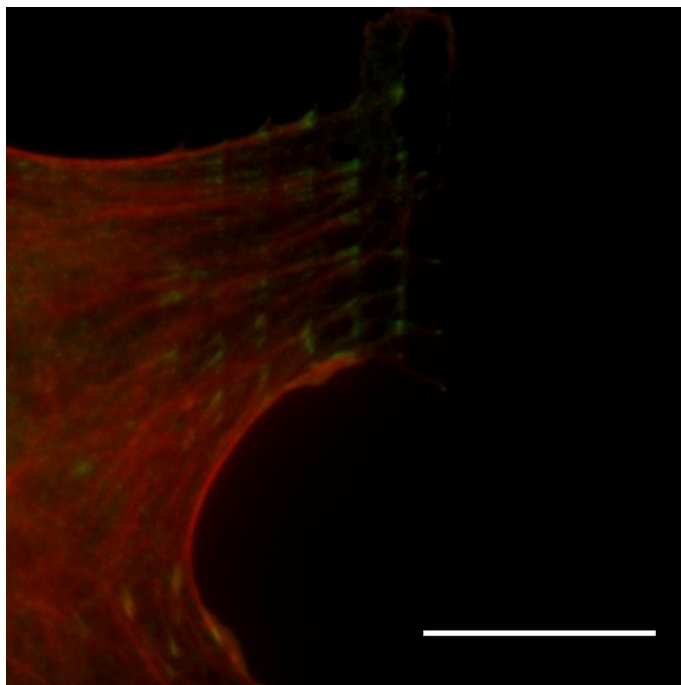


Figure 9. Detail of focal adhesion, stained with FITC labelled vinculin in green, growing perpendicularly to the pattern. Actin bundles are visualized in red. Bar is 20 μm .

The results presented so far allow us to propose a two-step model in which both topographic features and chemical properties play a synergistic role in regulating cell adhesion and migration (Fig. 10). Firstly, filopodial probing dictates the spatial configuration of cell adhesion sites after each and every extension/retraction cycle. Newer adhesions can form only on those zones that are readily accessible by filopodia and, as such, cannot be farther than 5-6 micron from the cell periphery. This process is not affected by chemical characteristics of the surface and explains why cells migrating on 5 micron patterns display a considerable degree of alignment irrespective of the surface treatment, since the probability that a filopodium might extend enough to contact an adjacent ridge is low. The second step comprises adhesion turnover. Once formed, focal adhesions may grow and their dimension will depend on the space available and the presence of ligands. If topographic features have characteristic dimensions that hinder adhesion growth, then cell adhesion and polarization might be altered. Non perturbed focal adhesions, i.e. those growing on flat surfaces or parallel to ridges, possess lengths depending on the chemical properties of the substrate. Therefore, the characteristic dimension of features that can block focal adhesion growth is not a fixed and absolute value, but it will depend on chemical properties as well. On untreated 2 micron patterns, focal adhesions can reach 3 micron in length which is not much dissimilar from the ridge extension. Therefore adhesion can form almost in all directions and limited guidance is observed. On 2 μm PT, however, adhesions can potentially attain lengths that surpass ridge dimension (6

microns). Transverse adhesions grow fragmented in order to balance traction generated forces, but such a growth is eventually unstable owing to reduced contact area. Thus protrusions extending across the patterns and which are anchored on the substrate by dashed adhesions are short lived, whereas those parallel to the pattern are more stable and govern cell polarization and migration.

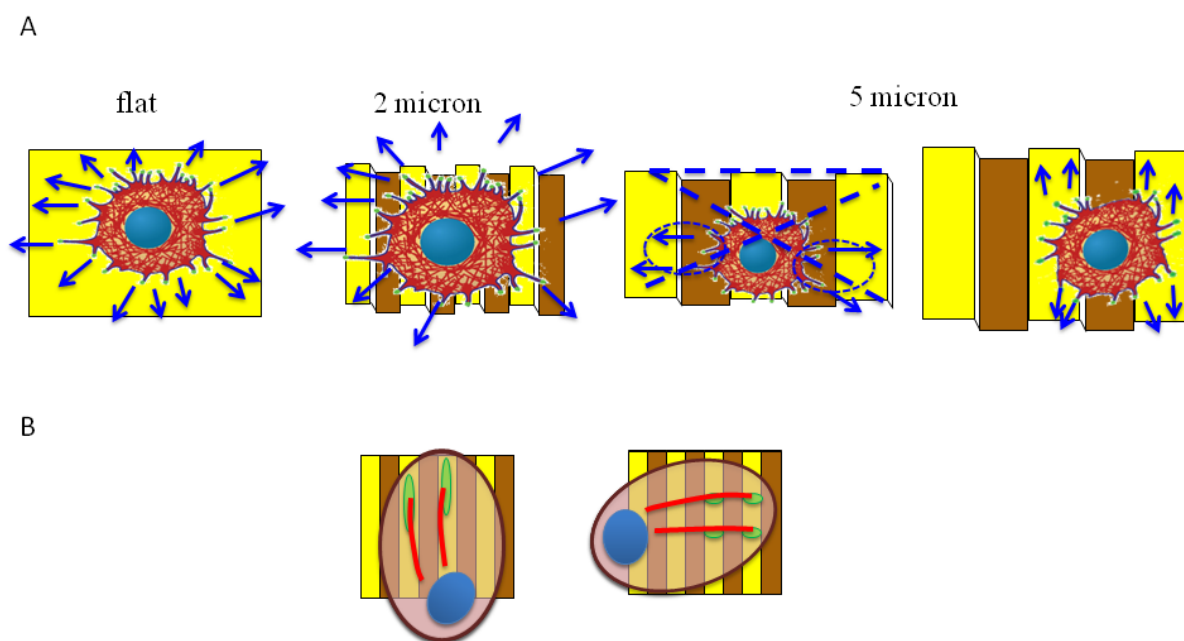


Figure 10. Model of topographic pattern recognition and migration. Early mechanisms involve filopodia probing (A). If the separation of adhesive sites, i.e. feature pitch, is smaller than the characteristic dimension of filopodia, cells perceive the substrate as, almost, isotropic. In case of large pitches, filopodia cannot bridge several ridges and cell body polarizes only on a limited number of them. This mechanism occurs irrespective of surface treatments. (B) On hydrophilic surfaces, focal adhesion can grow considerably and their length surpass ridge dimension. In this case, focal adhesions are observed in a dashed and unstable conformation, favouring cell polarization along the pattern direction.

4.4 Conclusions

This work investigated the combinatorial effects of micron scale topography and chemical characteristics of the surface on the adhesion and migratory behavior of MC3T3 cells. Our results suggest the existence of two characteristic lengths of the topographic features, according to which cells may react differently. In the context of topographies with long range order and specifically of

microgratings, cells are not able to perceive ridges that are placed farther than the length of filopodia, whose dimension span in the 2-5 micron range. Secondly, as soon as ridge dimensions are such that interfere with focal adhesion maturation, strong effects on cell polarization and migration are observed. In particular, focal adhesion growth is intimately connected to ligands availability and conformation, which in turn are strongly affected by the chemical properties of the surface. Thus, different chemical surface properties induce different focal adhesion dynamics and therefore alter the way cells perceive the topography. This suggests that probably topography is not a signal per se, but the way it is perceived is strongly mediated by proteins that are absorbed on the surface and hence by the spatial positioning of ligands. Therefore we would expect very similar results in the case of biochemical patterns constituted by micrometric stripes of adhesive proteins, separated by antiadhesive regions. This does not necessarily mean that topographic signals can always be substituted by biochemical patterns. In fact, topographic signals are easier to encode on synthetic surfaces, can be reproduced with a high consistency and are very stable under harsh processing conditions and also in in vivo settings.

4.5 References

- [1] Last JA, Liliensiek SJ, Nealey PF, Murphy CJ. Determining the mechanical properties of human corneal basement membranes with atomic force microscopy. *Struct Biol*. 2009 Jul; 167(1):19-24.
- [2] Liliensiek SJ, Nealey P, Murphy CJ. Characterization of endothelial basement membrane nanotopography in rhesus macaque as a guide for vessel tissue engineering. *Tissue Eng Part A*. 2009 Sep; 15(9):2643-51.
- [3] Gutschmann T, Fantner GE, Kindt JH, Venturoni M, Danielsen S, Hansma PK. Force spectroscopy of collagen fibers to investigate their mechanical properties and structural organization. *Biophys J*. 2004 May; 86(5):3186-93.
- [4] Liliensiek SJ, Campbell S, Nealey PF, Murphy CJ. The scale of substratum topographic features modulates proliferation of corneal epithelial cells and corneal fibroblasts. *J Biomed Mater Res A*. 2006 Oct; 79(1):185-92.
- [5] Vandrovцова M, Hanus J, Drabik M, Kylian O, Biederman H, Lisa V, Bacakova L. Effect of different surface nanoroughness of titanium dioxide films on the growth of human osteoblast-like MG63 cells. *J Biomed Mater Res A*. 2012 Apr; 100(4):1016-32.
- [6] Lamers E, van Horsen R, te Riet J, van Delft FC, Lutttge R, Walboomers XF, Jansen JA. The influence of nanoscale topographical cues on initial osteoblast morphology and migration. *Eur Cell Mater*. 2010 Nov 9; 20:329-43.
- [7] Yim EK, Pang SW, Leong KW. Synthetic nanostructures inducing differentiation of human mesenchymal stem cells into neuronal lineage. *Exp Cell Res*. 2007 May 15; 313(9):1820-9.
- [8] Dalby MJ, Gadegaard N, Tare R, Andar A, Riehle MO, Herzyk P, Wilkinson CD, Oreffo RO. The control of human mesenchymal cell differentiation using nanoscale symmetry and disorder. *Nat Mater*. 2007 Dec; 6(12):997-1003.
- [9] Yang Y, Leong KW. Nanoscale surfacing for regenerative medicine. *Wiley Interdiscip Rev Nanomed Nanobiotechnol*. 2010 Sep-Oct; 2(5):478-95.
- [10] Kim HN, Kang DH, Kim MS, Jiao A, Kim DH, Suh KY. Patterning methods for polymers in cell and tissue engineering. *Ann Biomed Eng*. 2012 Jun; 40:1339-55.

- [11] Pot SA, Liliensiek SJ, Myrna KE, Bentley E, Jester JV, Nealey PF, Murphy CJ. Nanoscale topography-induced modulation of fundamental cell behaviors of rabbit corneal keratocytes, fibroblasts, and myofibroblasts. *Invest Ophthalmol Vis Sci*. 2010 Mar; 51(3):1373-81.
- [12] Loesberg WA, te Riet J, van Delft FC, Schön P, Figdor CG, Speller S, van Loon JJ, Walboomers XF, Jansen JA. The threshold at which substrate nanogroove dimensions may influence fibroblast alignment and adhesion. *Biomaterials*. 2007 Sep; 28(27):3944-51.
- [13] Mattila PK, Lappalainen P. Filopodia: molecular architecture and cellular functions. *Nat Rev Mol Cell Biol*. 2008 Jun; 9(6):446-54.
- [14] Parsons JT, Horwitz AR, Schwartz MA. Cell adhesion: integrating cytoskeletal dynamics and cellular tension. *Nat Rev Mol Cell Biol*. 2010 Sep; 11(9):633-43.
- [15] Keselowsky BG, Collard DM, García AJ. Surface chemistry modulates fibronectin conformation and directs integrin binding and specificity to control cell adhesion. *J Biomed Mater Res A*. 2003 Aug 1; 66(2):247-59.
- [16] Biela SA, Su Y, Spatz JP, Kemkemer R. Different sensitivity of human endothelial cells, smooth muscle cells and fibroblasts to topography in the nano-micro range. *Acta Biomater.*, 2009 Sep; 5(7):2460-6.
- [17] Curtis AS, Wilkinson CD, Crossan J, Broadley C, Darmani H, Johal KK, Jorgensen H, Monaghan W. An in vivo microfabricated scaffold for tendon repair. *Eur Cell Mater*: 2005 May 11;9:50-7; discussion 57.
- [18] Rani VV, Vinoth-Kumar L, Anitha VC, Manzoor K, Deepthy M, Shantikumar VN. Osteointegration of titanium implant is sensitive to specific nanostructure morphology. *Acta Biomater*. 2012 May;8(5):1976-89.
- [19] Papenburg BJ, Rodrigues ED, Wessling M and Stamatialis D. Insights into the role of material surface topography and wettability on cell-material interactions. *Soft Matter*, 2010, 6, 4377–4388.
- [20] von Recum AF, van Kooten TG. The influence of micro-topography on cellular response and the implications for silicone implants. *J Biomater Sci Polym Ed*. 1995;7(2):181-98.
- [21] den Braber ET, de Ruijter JE, Ginsel LA, von Recum AF, Jansen JA. Orientation of ECM protein deposition, fibroblast cytoskeleton, and attachment complex components on silicone microgrooved surfaces. *J Biomed Mater Res*. 1998 May; 40(2):291-300.
- [22] Lauffenburger DA, Horwitz AF.. Cell migration: A physically integrated molecular process. *Cell* 1996 Feb 9; 84: 359–369.

[23] Meredith DO, Eschbach L, Riehle MO, Curtis AS, Richards RG. Microtopography of metal surfaces influence fibroblast growth by modifying cell shape, cytoskeleton, and adhesion. *J Orthop Res*. 2007 Nov; 25(11):1523-33.

[24] Llopis-Hernández V, Rico P, Ballester-Beltrán J, Moratal D, Salmerón-Sánchez M. Role of surface chemistry in protein remodeling at the cell-material interface. *PLoS One*. 2011 May 9; 6(5):e19610.

[25] Balaban NQ, Schwarz US, Riveline D, Goichberg P, Tzur G, Sabanay I, Mahalu D, Safran S, Bershadsky A, Addadi L, Geiger B. Force and focal adhesion assembly: a close relationship studied using elastic micropatterned substrates. *Nat Cell Biol*. 2001 May; 3(5):466-72.

Chapter 5

Build up order tissue

During the past years the fabrication of functional tissues and organs was considered the ultimate goal in Tissue Engineering [1]. Tissue functionality necessarily requires that the biological and mechanical properties match those observed *in vivo*. These, however, strongly depend on the spatial arrangement of their microconstituents.

Connective tissue consists of cells embedded in an extracellular matrix, organized in a complex architecture which is optimized to fulfill specific functions. In tendon, for example, parallel collagen fibrils are packed together and spindle-shaped fibroblasts are aligned longitudinally along the fibers direction [2]. This organization is adequate to accomplish tendon function. Another example is the precise spatial arrangement of the collagen fibers within the cornea, which is necessary for its optical functions [3].

The way specialized cells create highly well-organized collagen rich tissues is still unclear. Several studies started to unravel the interplay between the cytoskeleton machinery and collagen deposition. Canty et al. [4] described an interesting correlation between fibropositors and actin filaments. Fibropositors are membrane protrusions which actively deposit collagen fibrils in the extracellular environment. [5]. Spatial arrangement of actin fibers and fibropositor were strictly correlated suggesting that cell cytoskeleton could be involved in the spatial organization of extracellular collagen fibrils [6].

Classical Tissue Engineering approaches have been resulted non effective in controlling spatial ECM synthetic scaffolds arrangement since do not provide the necessary information to guide tissue deposition. Although the optimal set to do so is still obscure, cell polarization emerges as a tool to control collagen deposition. As previously described, nanopatterned substrate has been used in order to orient cell body through cytoskeleton actin filament reassembly [7]. This suggests that the *novo* synthesized matrix might follow a similar arrangement. However the effect of nanograted substrate on long time culture was not analyzed. Futhermore ECM producing cells invariably migrate onto/within the substrate and the effect of migration on tissue assembly has not been thoroughly investigated.

The hypothesis underlying this work is that tissue polarity and development are regulated by the dynamic and reciprocal interactions of cell migration and matrix deposition. Therefore, the control over cell migration/adhesion dynamics should lead to the production of an ordered tissue. The

objective is to verify that spatial deposition of collagen is affected by cell migration: random migrating cells produce disordered tissues, whereas a polarized migration leads to an aligned tissue. To this aim, we used nanogrooved silicone substrates and MC3T3 cells were cultured on patterned or flat substrates up to two weeks. Cell migration analysis was performed by time lapse microscopy of low density and high density cultures. At longer times, cells produce a dense multilayered collagen matrix, whose orientation was observed under polarized light. Cell migration experiments and microstructural characterizations show that cells and tissue alignment is not limited to the proximity of the pattern but extends several layers above it.

5.1 Experimental

Preparation of nanopatterned substrates

Patterned substrates were obtained by replica molding of PDMS (Sylgard 184, Dow Corning Corporation, Michigan, USA) on polycarbonate masters. The pattern consists of an area of 1 cm² containing parallel and straight channels with a groove and ridge width of 700 nm and a depth of 250 nm. PDMS was prepared by mixing elastomer base and curing agent at 10:1 weight ratio. The solution was degassed, poured onto the polycarbonate master and then cured at 37°C for 24 hours. Control (flat) PDMS substrates were produced by pouring the base and curing mix on a 35 mm polystyrene Petri dish (Corning, Corning, NY, USA) and curing at 37°C for 24 hours. Substrates were autoclaved and then incubated with serum supplemented culture medium (10%) overnight prior to cell culturing experiment.

Cell Culture

MC3T3-E1 preosteoblasts (American Type Culture Collection, ATCC, Manassas, VA, USA) were cultured in α MEM with deoxyribonucleosides, ribonucleosides and 2 mM L-glutamine (Gibco Life, Grand Island, NY), supplemented with 10% fetal bovine serum (Gibco), penicillin (100 units/ml), streptomycin (100 μ g/ml). The cells were incubated at 37°C in a humidified atmosphere of 95% air and 5% CO₂ and the culture medium was changed every two days. After 3 days of culture, cells were detached with trypsin/EDTA (0.25% w/v trypsin / 0.02 mM EDTA) (Gibco) and seeded on nanogrooved or flat substrates at 2·10⁴ cells/cm² density. Cell culture medium was supplemented with ascorbic acid 25 μ g/mL and cell medium was changed every 3 days a week. MC3T3

multilayered cell sheets were obtained after 2 weeks of culture respectively both on nanopattern and flat control substrate.

ECM characterization and Confocal microscopy

Collagen spatial assembly was assessed from picosirius red-stained samples with polarized light microscopy. Picosirius red is a collagen-specific stain that also enhances the natural birefringence of collagen fibrils under polarized light [8]. Briefly, multilayered cell sheet samples were cultured for two weeks and they were fixed in formalin and then stained with picosirius red solution (0.1 g Direct-red 80 in 100 ml saturated aqueous picric acid) for 1 hour. Then samples were washed with acidified water. Immediately after staining, polarized light images of samples were acquired with an inverted microscope (BX53; Olympus) equipped with a digital camera (Olympus DP 21). A linear polarizer was placed between the light source and the specimen, while the analyzer was installed in the light path between the specimen and the camera.

Collagen type I and actin stress fibers were examined by immunofluorescence confocal microscopy. Multilayered cells sheet cultured on nanopatterned and flat substrates were fixed after two weeks of seeding. Cell fixation was performed with 4% paraformaldehyde for 20 min and then permeabilized with 0.1% Triton X-100 (Sigma, St. Louis, MO, USA) in PBS 1X. Samples were blocked in PBS/BSA 1% solution for 30 min, to avoid non-specific binding. Collagen type I were recognized by incubating samples with anti-collagen monoclonal antibody (dilution 1:200; BD) for 2 hours at 20°C. After incubation, substrates were washed 3 times with PBS (3 minutes per wash) and incubated with Alexa Fluor 488 conjugated goat anti-mouse antibody (Invitrogen, Carlsbad, USA) for 30 min at 20°C. Actin filaments were stained by incubating samples with rhodamine conjugated phalloidin (dilution 1:250; Sigma) for 30 minutes at 20°C. Images of stained multilayered cell sheets were collected with a LSM Zeiss 510 Confocor confocal microscope. Samples were excited with 488nm (collagen) and 543nm (actin) laser lines, and the emissions were collected in the 500-530nm and 560-650nm ranges respectively.

Time Lapse experiments

Cell migration experiments started 6h after cell seeding both on the nanograted and flat control substrates. At least 6 representative regions per substrate were acquired in bright field each 10 minutes for 24 hours. Videos of migrating cells were obtained using a Olympus IX 50 optical microscope (Olympus Co., Tokio, Japan) equipped with a mini-incubator mounted on an automated stage (PRIOR, Rockland, MA) and a CoolSnap Camera (Photometrics, Tucson, AZ).

In order to evaluate single cell migratory behavior within cell sheet, we labeled MC3T3 cell with PKH26 (Sigma PKH26-GL, St. Louis, MO), a fluorescent membrane intercalating dye, following the supplier's suggested instruction. After staining, labeled cells were seeded on the top of the cell sheet obtained on the nanopattern and flat control substrates. Cell migration experiments started 1 hour after cell seeding. Images were acquired both in fluorescence and in bright field each 10 minutes for 12 hours using a fluorescence inverted microscope (IX81, Olympus, Tokyo, Japan) equipped with a mini incubator stage (Okolab) and a digital camera (Olympus, Japan). Time-lapse videos were analyzed with Metamorph (ver 6.1) in order to extract cell trajectories. Windrose plots of each experiment were plotted using Matlab.

5.2 Results

Nanogrooved substrate effects on cell migration

Nanogrooved PDMS substrates are effective in providing isolated cells with an initial guidance that promotes polarized adhesion (cap2). In order to gain a better insight into the migratory behavior of cell seeded both on nanogrooved and flat substrates, time lapse video were collected. Figure 5.1 reports the windrose plot of cell trajectories.

A preferential direction of migration is clearly observed when cells are grown on nanogrooved substrates. Only occasionally they moved across pattern direction but when this occurred, they eventually reverted to the groove line. We also observed that after cell division daughter cells were uniformly elongated in shape and coaligned with pattern direction. Conversely cells on flat surfaces exhibited a random migration.

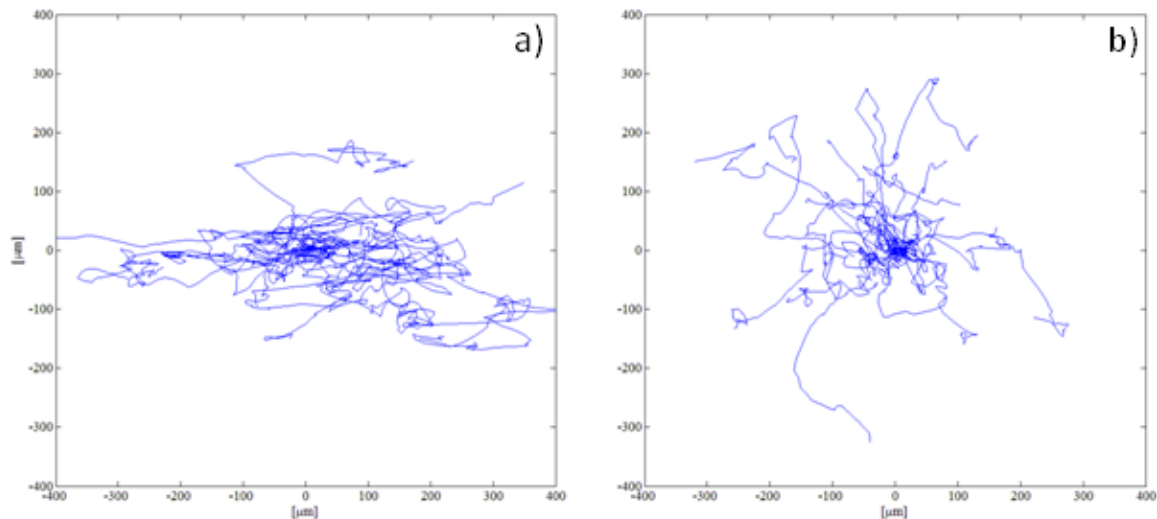


Figure 5.1: Cell migration trajectory of cell seeded on a) nanopatterned substrate b) flat control substrate

Nanograted PDMS substrate influences collagen deposition

MC3T3 were cultured for long time frames in presence of ascorbic acid both on the nanograted and control substrates in order to verify if cell alignment was kept also in a confluent state. Cells reached confluence within 3 days of culture after which cells began to form a multilayered, highly cellularized tissue. Microscopic images in fig. 5.2 show that multilayer tissue was still aligned along nanopattern direction two weeks after seeding. Conversely, on flat control substrates no macroscopic orientations were observed.

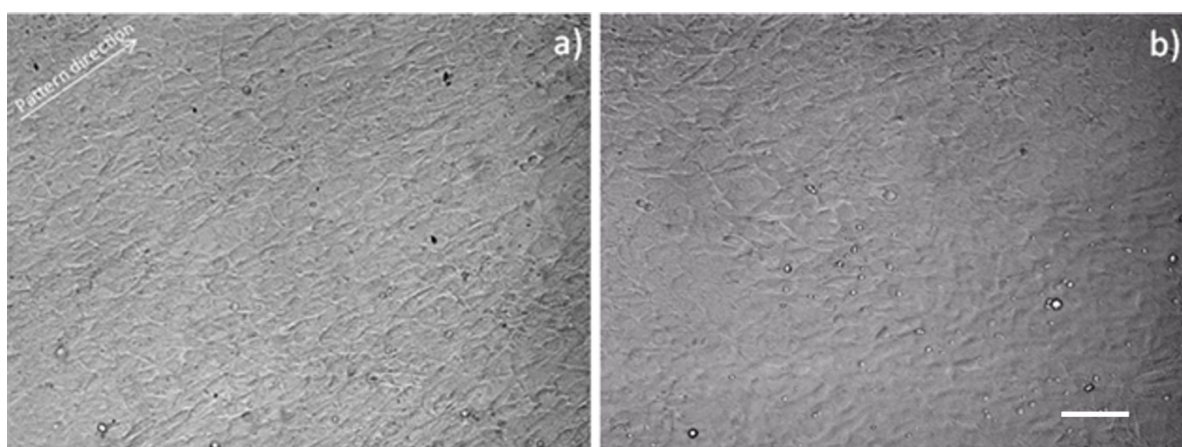


Figure 5.2: multilayered cell sheet cultured for two weeks on a) nanograted substrate and b) flat control substrate (scale bar 100 μm)

Nanopatterned substrate resulted effective in orienting cell body by a rearrangement of cytoskeleton components. As observed in chapter 3, stress fibres-pattern coalignment occurs already in the early stages of cell spreading. Cells polarized along the nanograted substrate, rearranging actin stress fibres. We performed phalloidin staining on multilayered cell tissue in order to evaluate actin bundles coalignment to nanopattern direction also when cells reached a confluent state. Z-stack confocal images showed that in each layer cells organized actin bundle mostly along the pattern direction (fig. 5.3). Instead no coalignment was observed on flat control substrates where only local patches of aligned actin bundles were observed (data not shown).

In order to evaluate the orientation of ECM deposited by cells, immunostainings of type I collagen was performed. Confocal images showed that on nanopatterned substrate collagen type I was mostly distributed along cell actin filaments. In contrast, no significant co alignment was observed on control flat substrate (data not shown).

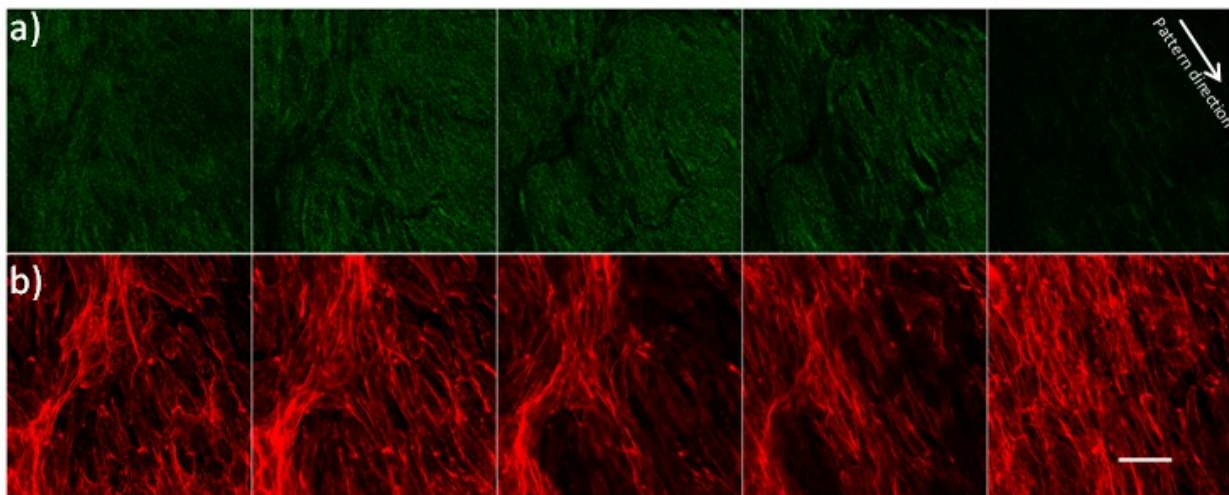


Figure 5.3: z stack confocal images of a) collagen type I and b) actin filament. Z step was 25 μm (scale bar 50 μm)

Multilayered cell sheet as a guidance for cell migration

In order to gain a better inside into the collagen spatial arrangement, multilayered cell sheet were stained with picrosirius red. Microscopy observation in bright field revealed that MC3T3 cells after 3 days of culture on both the nanograted and flat control substrates produced a visible layer of ECM. Preosteoblast MC3T3 cells indeed are known to produce great amounts of collagen in culture [9]. To visualize collagen fibers and to assess their alignment, stained samples were observed under

polarized light. On nanograted PDMS, thick collagen bundles were detected and they appeared highly oriented along pattern direction. On the contrary, only limited patches of aligned collagen were observed on flat surfaces, but no long range order was observed.

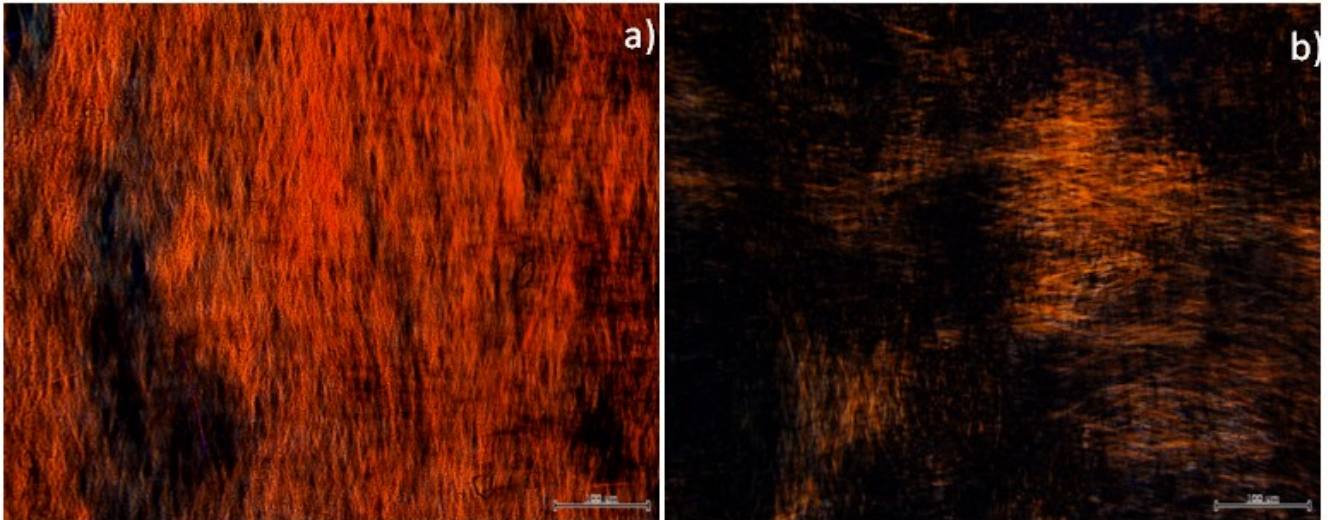


Figure 5.4: Picosirius red-stained multilayered cell sheet obtained two weeks post seeding on a) nanopatterned and b) flat control substrates (scale bar 100 μ m)

To prove that the neo-formed tissue had a guidance effect on cell migration process, MC3T3 cells were stained with the red fluorescent vital dye PKH26 and then they were seeded on the top of multilayered cell sheet. Time lapse videos of fluorescent cells were collected and cell trajectories were reconstructed as described above. Fluorescent cells quickly adhered on the top of multilayered cell sheet and their migratory behavior was profoundly affected by ECM spatial arrangement. As show in fig. 5.5, on ordered cell sheet fluorescent cells migrated with a preferential direction, while on control tissue no preferential direction of migration was observed.

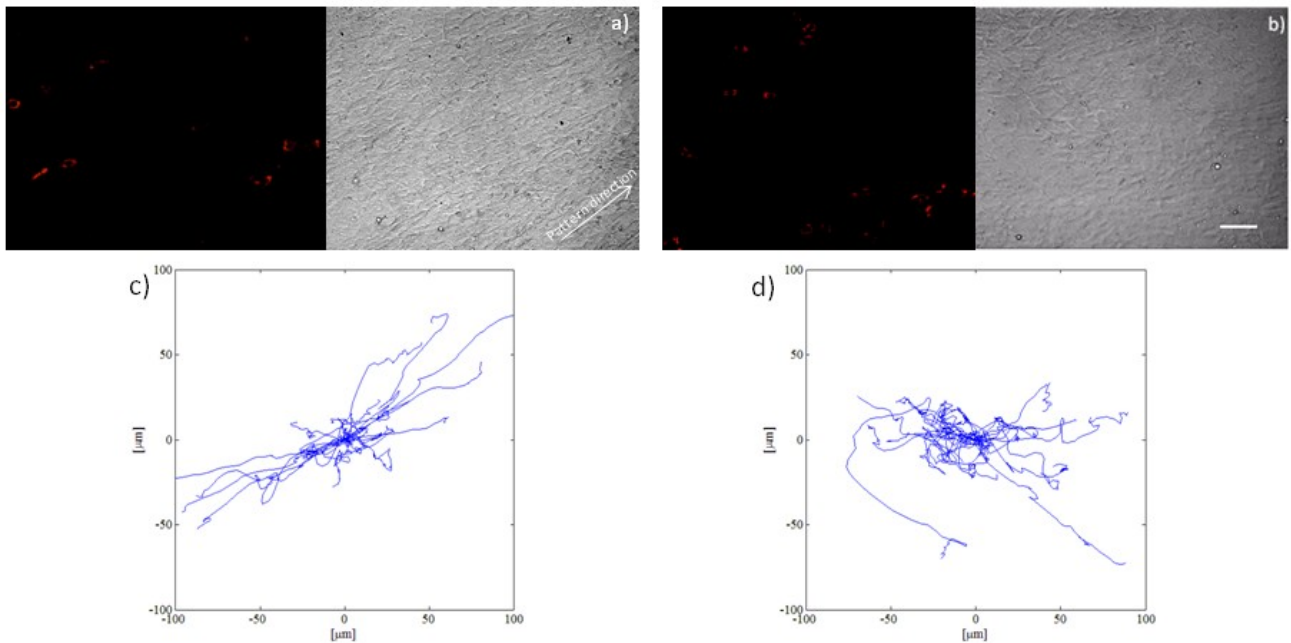


Figure 5.5: MC3T3 fluorescent cells cultured on multilayered cell sheet grown on a nanogrooved substrate for 2 wk on a) nanopattern and b) flat control substrate. Migration trajectory of cell seeded on c) nanopatterned substrate d) flat control substrate (scale bar 100 μm)

5.3 Discussion

Topography represents a powerful tool by which it is possible to modulate cellular behaviour in terms of adhesion and migration. In fact, the use of nanogrooved substrate allows cells to effectively elongate along pattern direction. Many authors [10-15] illustrated that microgrooved elastomeric membranes can be used to orient cells along pattern direction as a result of geometrical confinement of cell body. In chapter 2, we described the possibility to modulate cellular polarization using nanogrooved PDMS substrate by controlling FA/cytoskeleton dynamics. Such a modulation of focal adhesion/cytoskeleton interplay affected cell migratory behaviour making nanogrooved substrate a perfect device to control cell motion.

In this study we described the possibility to control spatial arrangement of ECM microconstituents by modulating cell migratory behavior. In particular nanogrooved substrates were used to produce a multilayered cell sheet whose extracellular components displayed a predefined spatial arrangement. We did not use collagen reconstituted as scaffold in which cells proliferate and migrate, but we control collagen assembly by promoting cell elongation and migration. In this way we tried to reproduce a more representative *in vivo* environment in which cells do not remodel a pre existing

matrix, but they produce and organize ECM microconstituent according to a predetermined orientation. To this aim, nanogrooved silicone substrates were used as platform to produce a multilayer cell sheet and MC3T3 cell line were cultured on it according to their ability to produce an abundant collagen matrix.

Our results showed that nanogrooved PDMS substrates were effective in providing isolated cells with an initial guidance that promotes polarized adhesion and migration. In particular surface topography promoted cell elongation both on low and high density cultures. In contrast, no preferential direction of migration/alignment was evident on flat substrates.

During this culture time cells produced an abundant collagen matrix and the spatial arrangement presented substantial difference between two substrates. A macroscopic co alignment between fibers and cell was observed on nanogrooved substrate while multilayered cell sheet grown on flat substrates showed only local patches of cell/collagen coalignment although no macroscopic orientation was observable.

Aligned collagen fibers formed a provisional scaffold in which the same cell migrate and subsequently remodeled ECM environment. In fig 5.6, a schematic representation of the hypothesized mechanism of multilayered tissue development and assembly is shown.

Growing on nanopattern substrate cells adopt the orientation of the underlying topography. Once cell proliferated and become confluent, collagen was deposited stabilizing the first cell layer. Collagen fibers were coaligned to the pattern direction and they became a guidance to the cell migration and matrix deposition process of the newly formed cell layer. This layer resulted aligned in the direction of nanogrooved pattern even it was not in direct contact with it. This ends up in the production of a multilayer tissue whose aligned collagen fibers act as guidance for the production of cell layers.

Future studies will be carry out in order to unequivocally demonstrate the correlation between cell migration and matrix deposition on nanopatterned substrate and is efficient for the production of a functional multilayered cell sheet. Mechanical and biochemical constitution of cell sheet have to be determined in order to better characterize “tissue” properties. These informations may reveal the potential of nanogrooved substrate to serve as biomedical devices in ligament and tendon repair.

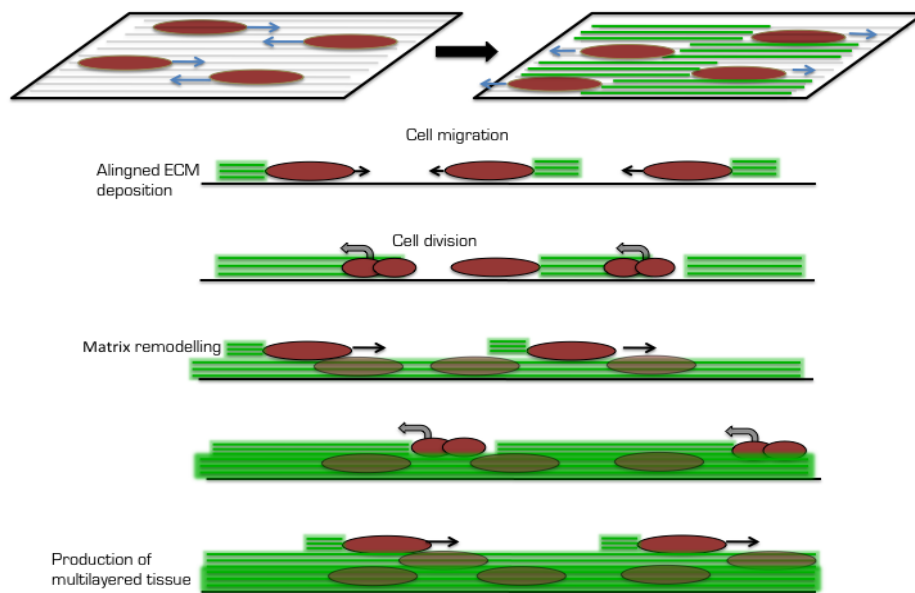


Figure 5.6: Schematic representation of the hypothesized mechanism of multilayered tissue development and assembly

5.4 Conclusion

We have provided collagen secreting cells with an initial guidance to the processes of adhesion and migration, by using topographic cues. Cells are able to self sustain these processes by secreting aligned ECM thus forming a provisional scaffold on which cells migrate and pile up newly synthesized aligned tissue. This ends up in the production of a tissue whose microarchitecture is reminiscent of the underlying pattern.

These preliminary results pave the way to exploit topographic instruction to control cell dynamics and possibly producing tissues having microarchitecture defined *ab initio*.

The experimental setup might be a starting platform to explore different topographic patterns and to assess the optimal condition to generate tissues with predetermined orientations.

5.5 References

- [1] Langer R, Vacanti JP. Tissue Engineering. *Science* 1993;260:920-926
- [2] Franchi M, Trirè A, Quaranta M, Orsini E, Ottani V. Collagen structure of tendon relates to function. *ScientificWorldJournal*. 2007; 7: 404-20
- [3] Keith M. Meek. Corneal collagen—its role in maintaining corneal shape and transparency. *Biophysical Reviews* 2009, Volume 1, Issue 2, pp 83-93.
- [4] Canty EG, Starborg T, Lu Y, Humphries SM, Holmes DF, Meadows RS, Huffman A, O'Toole ET, Kadler KE. Actin filaments are required for fibroblast-mediated collagen fibril alignment in tendon. *J Biol Chem*. 2006; 281(50): 38592-8.
- [5] Canty EG, Kadler KE. Procollagen trafficking, processing and fibrillogenesis. *J Cell Sci.*, 2005; 118(Pt 7):1341-53
- [6] Olsen, B. R. (2004) *Matrix Biol.* 23, 73–74
- [7] Yim EK, Darling EM, Kulangara K, Guilak F, Leong KW. Nanotopography-induced changes in focal adhesions, cytoskeletal organization, and mechanical properties of human mesenchymal stem cells. *Biomaterials* 2010; 31(6):1299-306
- [8] Rich L. and Whittaker P. Collagen and picrosirius red staining: a polarized light assessment of fibrillar hue and spatial distribution. *J. morphol. Sci*, 2005; 22(2), 97-104
- [9] Ecarot-charrier B., Glorieux F.H., van Der Rest M. and Pereira G. Osteoblasts isolated from mouse calvaria initiate matrix mineralization in culture. *The journal of cell biology*, 1983; 96: 639-643.
- [10] Curtis, A., Wilkinson, C. Topographical control of cells. *Biomaterials*, 1997 18 (24), 1573–1583.
- [11] Qu, J., Chehroudi, B., Brunette, D.M.,. The use of micromachined surfaces to investigate the cell behavioural factors essential to osseointegration. *Oral Diseases*, 1996; 2 (1), 102–115 6
- [12] van Kooten, T.G., Whitesides, J.F., von Recum, A., 1998. Influence of silicone (PDMS) surface texture on human skin fibroblast proliferation as determined by cell cycle analysis. *Journal of Biomedical Materials Research*, 1998; 43 (1), 1–14
- [13] Walboomers, X.F., Croes, H.J., Ginsel, L.A., Jansen, J.A.,. Contact guidance of rat fibroblasts on various implant materials. *Journal of Biomedical Materials Research*, 1999; 47 (2), 204–212

- [14] Wang, H., Ip, W., Boissy, R., Grood, E.S., Cell orientation response to cyclically deformed substrates: experimental validation of a cell model. *Journal of Biomechanics*, 1995; 28 (12), 1543–1552
- [15] Wang, J.H.-C., Grood, E.S., Florer, J., Wenstrup, R., Alignment and proliferation of MC3T3-E1 osteoblasts in microgrooved silicone substrata subjected to cyclic stretching. *Journal of Biomechanics*, 2000; 33 (6), 729–735
- [16] Birk, D.E., Trelstad, R.L., Extracellular compartments in tendon morphogenesis: collagen fibril, bundle, and macroaggregate formation. *Journal of Cell Biology*, 1986.103 (1), 231–240
- [17] Trelstad, R.L., Hayashi, K., Tendon collagen fibrillogenesis: intracellular subassemblies and cell surface changes associated with fibril growth. *Developmental Biology*, 1979; 71 (2), 228–242.

Chapter 6

Conclusions

This thesis highlights the possibility to exploit mechanical and topographical substrate properties in order to affect cell behaviour. This is consistent with analysis of *in vivo* microenvironment where cells are embedded in a complex microenvironment which displays a wide range of stimuli that are biochemical, structural and mechanical in nature.

Improvements in material processing and manipulation techniques enable local modifications of material chemical and physical features with a high spatial resolution. The data generated throughout this thesis are consistent with the hypothesis that cell-material crosstalk eventually dictates cell fate [1-2].

In order to study cell response to material mechanical properties we produced smooth hydrogel surfaces displaying locally varied elasticity regions using FIMIC (Fill-Molding In Capillaries) technique. Cells strongly react to the design on the surface, accumulating and migrating preferentially on the stiffer regions of the hydrogel in a highly selective manner. This occurred independently of line width. These observations corroborate the existence of a regulatory mechanism for the interplay between cytoskeleton-generated forces and the mechanical properties of materials that represent the foundation of mechanosensing [3].

Adhesion and migration are processes essential for numerous physiological and pathological processes, including embryogenesis, wound repair and metastasis [4-5]. A certain number of intracellular pathways are strictly correlated with adhesion and focal adhesion plaques formation [6]. However many aspects of the FAs/cytoskeleton/nuclear shape axis still remain unclear. Yet, it is well recognized that substrate presenting nanotopography can interfere with focal adhesion formation and stability [7]. Therefore, topographic cues might in principle be used to control intracellular signalling pathways and therefore cell behaviour.

In our work we discern two characteristic length scales of the topographic features, according to which cells may react differently. The regulation of cell behaviour via focal adhesion maturation and polarization was investigated with the use of nanograted PDMS substrates. We found that nanotopography is highly effective in altering FAs dynamics and assembly, which eventually affects cytoskeleton spatial arrangement. Furthermore, Our data show that nanograted PDMS may have a

direct effect on nuclear squeezing, by inducing specific cytoskeletal assemblies and possibly modifying the intracellular stress state. Scaling up to micrometric pattern dimension we observed that cell is not able to perceive ridges that are placed farther than the length of filopodia. Moreover, on this length scale, chemical-physical properties of the pattern, in terms of wettability, also play a major role in pattern recognition by cells. Therefore, topography emerges as powerful tool in regulating the cell–material crosstalk and in directing cellular activity and fate.

Furthermore, our preliminary results showed that nanopattern platform resulted effective also in controlling ECM microconstituent spatial arrangement via cell migratory behavior.

In particular the control of cell migration affects collagen spatial deposition: random migrating cell produced disordered tissues while a polarized migration leads to an aligned tissue.

Patterns of mechanical and topographic signals might be in principle used to functionalize synthetic scaffolds in order to control tissue deposition and assembly. Alternatively, topographic patterns might be encoded on conventional prosthetic devices to control specific functions. For example the outer surface of coronary stents might be patterned in order to guide endothelialization and to control endothelial cell behavior to reduce neointimal hyperplasia. Orthopedic implants might be encoded with patterns of topographic signals in order to improve the integration with surrounding tissues and simultaneously instruct cells to attain specific differentiation states. In conclusion, the presentation of mechanical and topographical signal on material surface represents a tool not only to analyze or alter cell behavior in and in vitro setting, but also it gives the opportunity to realize in vitro or in vivo functional tissues having microstructural features predefined ab initio.

6.1 References

- [1] Kilian KA, Bugarija B, Lahn BT, Mrksich M. Geometric cues for directing the differentiation of mesenchymal stem cells. *Proceedings of the National Academy of Science USA* 107, 4872-4877, 2010
- [2] Ventre M, Causa F, Netti PA. Determinants of cell-material crosstalk at the interface: towards engineering of cell instructive materials. *Journal of the Royal Society Interface* 9, 2017-2032, 2012
- [3] Trichet L, Le Digabel J, Hawkins RJ, Vedula SR, Gupta M, Ribault C, Hersen P, Voituriez R, Ladoux B. Evidence of a large-scale mechanosensing mechanism for cellular adaptation to substrate stiffness. *Proc Natl Acad Sci U S A*. 2012 May 1;109(18):6933-8.
- [4] Gaggioli C, Hooper S, Hidalgo-Carcedo C, Grosse R, Marshall JF, Harrington K, Sahai E. Fibroblast-led collective invasion of carcinoma cells with differing roles for RhoGTPases in leading and following cells. *Nat Cell Biol*. 2007 Dec;9(12):1392-400.
- [5] Friedl P, Wolf K. Plasticity of cell migration: a multiscale tuning model. *J Cell Biol*. 2010 Jan 11;188(1):11-9.
- [6] Wozniak MA, Modzelewska K, Kwong L, Keely PJ. Focal adhesion regulation of cell behavior. *Biochim Biophys Acta*. 2004 Jul 5;1692(2-3):103-19.
- [7] Goffin JM, Pittet P, Csucs G, Lussi JW, Meister JJ, Hinz B. Focal adhesion size controls tension-dependent recruitment of alpha-smooth muscle actin to stress fibers. *J Cell Biol*. 2006 Jan 16;172(2):259-68.